Paleo-oceanographic and -climatic reconstruction in the Southwest Pacific [ODP Site 1123] during MIS 11

Kylie Jane Christiansen

A thesis submitted in partial fulfilment of a Masters of Science degree in Geology

School of Geography, Environment and Earth Sciences

Victoria University

2012

Abstract

Marine Isotope Stage 11 [424 to 374 ka] is unique compared to most other recent Quaternary interglacial periods due to its duration and orbital geometry, both of which have previously been cited as evidence that MIS 11 may be a suitable analogue to project future climate. This study aims to evaluate this prolonged warm period at a key site in the sparsely studied Southwest Pacific Ocean at Ocean Drilling Program [ODP] 1123. This cored site, situated at 3290 m water depth on the northern flank of the Chatham Rise, straddles the northern limit of the modern Subtropical Front, 1100 km east of New Zealand, where sediments record strong subtropical and subpolar signals over interglacial to glacial cycles.

Two species of planktonic foraminifera were analysed, *Globigerinoides ruber* and *Globigerina bulloides* [*Gs. ruber* and *Gg. bulloides*], for trace elements and size-normalised test weights [SNW; *Gg. bulloides* only] in order to reconstruct ocean temperature, chemistry, structure and circulation during MIS 11. *Gg. bulloides* was found to have anomalously low SNW [~50% compared to modern specimens] implying either [i] poor calcification environment due to low CO_3^{-2} concentrations, or [ii] post-mortem alteration either in the deep water column or ocean floor environment. Traditional dissolution proxies for ODP 1123 do not indicate significant dissolution during MIS 11. Nevertheless, the inception of modern carbonate platforms and reefs at this time leads to the hypothesis that CO_3^{-2} concentrations in the surface ocean were low due to a shifting in the locus of carbonate production, and this is a potential cause, amongst other possibilities, of the low SNW in *Gg. bulloides.* However, calcification in a low CO_3^{-2} concentration ocean does not appear to have significantly affected the geochemical proxies utilised in this study [Mg/Ca-derived paleo-ocean temperatures, $\delta^{18}O$ and micro-nutrients Mn/Ca and Zn/Ca ratios as water-mass tracers] based on comparison with a similar study on younger sediments in the same core. The temperature difference between *Gs. ruber* and *Gg*. *bulloides* is the same as the modern temperature difference at ODP 1123, implying that *Gs.*

ruber was also not markedly affected by either low CO_3^{-2} concentrations during calcification or post-mortem dissolution.

Laser ablation inductively coupled plasma mass spectrometry is utalised to measure *in situ* trace element ratios [Mg, Al, Ca, Mn, Zn and Sr/Ca], and reconstruct the thermal structure of the ocean's upper 200 m. The main findings are [i] a well stratified upper ocean in warm periods punctuated by well mixed waters in cooler and presumably windier conditions; [ii] an invigorated South Pacific Gyre during the prolonged MIS 11 interglacial, resulting in a greater inflow of subtropical water to ODP 1123 as evinced by Mn/Ca and Zn/Ca ratios and supported by elevated subtropical foramiferal assemblages; [iii] paleo-ocean temperatures that indicate the mean MIS 11 sea surface temperature optimum was *ca*. 2°C warmer than present; and [iv] a spike in productivity is identified by elevated Mn/Ca and Zn/Ca ratios at *ca*. 400 ka, coinciding with a spike in eutrophic species abundance, indicating a period of significantly enhanced subtropical water influence.

Records from other New Zealand sites reveal MIS 11 as a prolonged [up to 40 kyr] interglacial period, following a rapid and pronounced 10˚C warming from the MIS 12 glacial. Deglaciation occurred 13 kyr earlier than the global benthic record. This rise was punctuated by an Antarctic Cold Reversal-like cooling confirming episodic sub-polar influences at the site. Some differences between the orbital configurations of MIS 1 and 11, particularly at the precessional scale, coupled with apparently unusual ocean chemistry [e.g., low CO_3^{-2}] during MIS 11, suggest that MIS 11 may not be an ideal analogue for the Holocene.

Acknowledgements

There are many people whom I would like to acknowledge and thank for their various academic, financial and emotional contributions, without which I would not have been able to complete this work.

Firstly, my supervisor Professor Lionel Carter. Thank you for always encouraging me and being so positive, all of those times when I was ready to give up and walk away. Professor Joel Baker supervised my laboratory work and early writing and was absolutely invaluable throughout this process.

I must also acknowledge the support of my colleagues with the completion of my lab work. Dear Pras, thank you for keeping me company during long laboratory nights and changing the gas bottles for me. This meant more to me than you probably realise and enabled me to collect my data at warp speed. John Creech, thank you for developing the magical macro that minimises data processing time. You have saved me hundreds of hours of mindless data processing and for this I will always be eternally grateful. Annette Bolton and Julene Marr, thank you for all of the technical assistance you have provided me over the course of my data acquisition.

Also, Dr Martin Crundwell at GNS, thank you for assisting me by providing pre-picked mono-specific samples. This again saved me a huge amount of time and rescued me from the evil dangers of species misidentification. Martin, you were also my guru for interpreting surface textures, and your expert eye made an invaluable contribution, leading to some of the main findings of my thesis. Dr Gavin Dunbar and Dr Helen Bostock, thank you for valuable insight into the marine carbon cycle, which turned out to be highly pertinent to my research. Dr Marc-Alban Millet, together with Professor Joel Baker helped me with Monte Carlo modelling to determine the real error associated with Mg/Ca derived temperatures from my analyses.

The Dominion Post Antarctic Research Scholarship provided me with funding for my final year, in the form of payment of my fees and a glorious stipend. Without this funding I would not have completed this degree. Antarctic-New Zealand Interglacial Climate Extremes [ANZICE] also provided support by covering analytical costs. I have also received other smaller scholarships which have made the struggles of a student so much more bearable, and I would like to thank all of the amazing donors out there who deemed me deserving of funding. These scholarships also bolstered my own confidence in my academic ability.

To Holly, Ramona, Zara, Megan, Tim, Gemma, Melissa, Kirsty and Netty. Thank you for being my friends. I couldn't have done this without your love, encouragement and support.

I have to make a special mention of my family, in particular my long-suffering mum and sister. You two have provided me with so much support over the years during my [sometimes tumultuous!] journey through academic life. The care packages, the endless patience and the never-faltering blanket acceptance

of the never-fail excuses '….I've just got too much work to do this week…' that can apply to getting out of any situation or obligation, and the '….I just need a little break from work I am so stressed…' that can apply to getting into anything or into any situation. And lastly my papé and Steve. Thank you for making me who I am. You will always live on in my heart, and knowing that you believe in me has kept me going, when every inch of me has wanted to walk away.

Finally to my Joel. You are one of the most loving, tender, caring men I have ever met, and you have been my rock through the last few months. Thank you for always making me laugh until I cry, no matter how grumpy or moan-ie I am feeling. Our little family of seven, soon to be eight, makes me so happy and excited about getting up in the morning. Thank you for giving me a beautiful baby girl, who we will get to meet in a few weeks time, thank you.

Table of Contents

Front matter

Title.....I
Abstract.....II
Acknowledgements.....IV
Table of contents.....VI
List of figures and tables.....IX
List of abbreviations.....XII

Chapter 1: Introduction

Opening remarks.....1
1.1 General background.....1
1.2 Modern oceanographic setting.....5
1.3 Quaternary climate cycles.....11
1.3.1 Marine Isotope Stage 11 ice core and marine sedimentary records.....15
1.3.2 Marine Isotope Stage 11 terrestrial records.....17
1.3.3 The latest Quaternary climate cycle.....19
1.4 Geochemical archives and proxies of past ocean temperature and global ice volume changes.....20
1.4.1 Magnesium/calcium ratios in foraminifera as a proxy of paleo-ocean temperatures.....20
1.4.2 Secondary influences on the trace element chemistry of foraminifera.....21
1.4.3 Oxygen and carbon isotopes.....25
1.4.4 Geochemical archives and proxies utilised in this thesis.....26
1.5 Thesis objectives and key research questions.....27
1.6 Thesis structure.....29

Chapter 2: Materials and Methods

2.1 ODP Site 1123 sediment core……31
2.2 Dating of the sediment core……33
2.3 Separation, preparation and cleaning of foraminifera……34
2.4 Determination of size normalised weights [SNW]……35
2.5 LA-ICPMS trace element analysis……37
2.6 Calculation of Mg/Ca paleo-ocean temperatures……39
2.7 Scanning electron microscopy [SEM] imaging……42
2.8 Stable isotope analysis……42

Chapter 3: Results

3.1 Trends in foraminiferal trace element/Ca ratios during MIS 12 to 11……44
3.2 Stable isotope data……47
3.3 Size normalised test weights……48
3.4 Mg/Ca and size normalised weight [SNW] derived temperatures……49
3.5 Trace element/Ca error determination……51
3.6 Scanning electron microscopy images……52
3.7 Timing of changes in geochemical proxies……54

Chapter 4: Discussion

4.1 Southwest Pacific marine carbonate system during MIS 11……57
4.2 Dissolution and its potential effect on geochemical proxies……62
4.3 Implications of unusual Southwest Pacific Ocean chemistry during MIS 11……70
4.4 Mn and Zn/Ca records……71
4.5 Paleo-climate reconstruction for MIS 12-11……74
4.6 Intra-test trace element convergence in Gg. bulloides……77

Chapter 5: Regional overview – MIS 11 paleo-ocean temperatures in the Southwest Pacific Ocean

5.1 Regional oceanographic response to MIS 11……..79

Chapter 6: Conclusions

6.1 Concluding remarks……..88

6.2 Suggestions for future work……..93

References……96

Appendix one

Compendium of scanning electron microscopy images

Appendix two (electronic)

Summary data tables including all geochemical data

Appendix three (electronic)

Sample size error determination for Mg/Ca-derived paleo-ocean temperatures in Gg. bulloides

Appendix four (electronic)

Age model

List of Figures and Tables

Figure 1.1	Benthic oxygen isotope record from ODP Site 849 in the eastern equatorial Pacific for the last 5 Myr. Figure modified from *Zeigler et al*. [2003].	2
Figure 1.2	Comparison between the MIS 12-11 and MIS 2-1 deglacial transitions. Figure taken from *Dickson et al.* [2009].	3
Figure 1.3	ODP Site 1123 core location and major oceanic fronts and surface currents around New Zealand. Figure modified from *Carter et al*. [1998].	4
Figure 1.4	Bathymetric map of undersea New Zealand. Figure from *Carter et al.* [1996].	6
Figure 1.5	Chatham Rise modern ocean currents. Figure modified from *Carter et al*. [1998].	9
Figure 1.6	Cenozoic climate evolution in a stacked benthic $\delta^{18}0$ record. Figure modified from *Zachos et al*. [2008].	12
Figure 1.7	Global benthic $\delta^{18}0$ stack with the mid-Pliestocene transition highlighted. Figure modified from *Lisiecki and Raymo* [2005].	12
Figure 1.8	Antarctic temperature record for the last 800 kyr. Figure modified from *Jouzel et al*. [2007].	16
Figure 1.9	Schematic illustration of a foraminifera test. Figure modified from *Kozden et al*. [2009].	22
Figure 1.10	Scanning electron microscope images of *Gg. bulloides* [*Marr et al*., 2011] and *Gs. ruber* [*Bolton et al.,* 2011].	26
Figure 2.1	Major eastern deep ocean circulation and the location of the ODP Site 1123 core in the path of the DWBC. Figure modified from *Carter et al*. [1998].	32
Figure 2.2	Age model	33
Figure 2.3	Exponential negative correlation between Mg/Ca and temperature [°C], and SNW. Figure modified from *Marr et al*. [2011].	36

Figure 2.4	Examples of ideal and non-ideal trace element depth profiles generated in this study.	38
Figure 2.5	Mg/Ca thermometry calibration for *Gg*. *bulloides* and *Gs*. *ruber*. Figure taken from *Marr et al*. [in prep].	41
Figure 3.1	Nested trace element/Ca graph for *Gg. bulloides* analysed in this study.	47
Figure 3.2	Stable isotope data for ODP 1123 MIS 12-11.	48
Figure 3.3	Relationship between size normalised test weight and Mg/Ca-derived paleo-ocean temperature in *Gg. bulloides*.	50
Figure 3.4	Mg/Ca error associated with various sample sizes.	52
Figure 3.5	Textural comparison of *Gg. bulloides* in plankton tow material and two ODP 1123 core samples.	53
Figure 3.6	Timing and magnitude of deglaciation at ODP Site 1123 in Mg/Ca-derived sub-surface temperature, Zn/Ca, Mn/Ca and $\delta^{18}O$ in *Gg. bulloides*.	54
Figure 4.1	Mg/Ca-derived *Gs. ruber* sea surface temperature and *Gg*. *bulloides* sub-surface temperature [*this study*] and ANN_{25} sea surface temperature [*Crundwell et al*., 2008] for MIS 11 at ODP Site 1123.	68
Figure 4.2	Modern upper ocean thermal structure.	69
Figure 4.3	Surface ocean Zn transect across the Chatham Rise. Figure modified from *Carter et al*. [1998] using unpublished Zn data provided by Michael Ellwood, Australia National University.	72
Figure 4.4	Zn and Mn/Ca during MIS 12-11 compared with modern subtropical and subantarctic values.	72
Figure 4.5	Zn profiles in the upper 500 m of the east Tasman Sea. Figure modified from *Carter et al*. [1998] using unpublished Zn data provided by Michael Ellwood, Australia National University.	74
Figure 5.1	Regional modern sea surface temperature map with nine sediment cores.	80

Figure 5.2	Sea surface temperature records and one sub-SST record from three sites in the New Zealand region.	86
Table 3.1	Calculated percent difference between chambers *f-2* and *f* of *Gg. bulloides* of trace element/Ca ratios.	46
Table 5.1	Regional comparison between the SSTs of seven sites.	85

List of Abbreviations

AABW	Antarctic Bottom Water
AAIW	Antarctic Intermediate Water
ACC	Antarctic Circumpolar Current
ACR	Antarctic Cold Reversal
ANN	Artificial Neural Networks
CDW	Circumpolar Deep Water
CO_3^{-2}	Carbonate ion concentration
CO_2	Carbon dioxide
DTF	Dinoflagellate transfer function
DWBC	Deep Western Boundary Current
EAC	East Australian Current
EAUC	East Auckland Current
ECC	East Cape Current
EDC	EPICA Dome Concordia
EPICA	European Project for Ice Coring in Antarctica
ETM1	Eocene Thermal Maximum 1
ETM2	Eocene Thermal Maximum 2
f	Final chamber
f-1	Penultimate chamber
f-2	Anti-penultimate chamber
GHG	Greenhouse gas
Ka	Thousands of years ago
Kyr	Thousand years duration
LA-ICPMS	Laser ablation inductively coupled plasma mass spectrometry
Ma	Millions of years ago
MAT	Modern Analogue Technique
Mbsf	Metres below sea floor
MIS	Marine Isotope Stage
Myr	Million years duration
NADW	North Atlantic Deep Water
NIWA	National Institute of Water and Atmospheric Research

ODP	Ocean Drilling Program
PETM	Paleocene-Eocene Thermal Maximum
SAF	Subantarctic Front
SAW	Subantarctic Water
SC	Southland Current
SEM	Scanning electron microscope
SMOW	Standard mean ocean water
SNW	Size-normalised weight
STW	Subtropical Water
STF	Subtropical Front
Sub-SST	Sub-surface sea surface temperature
SST	Sea surface temperature
$\delta^{13}C$	Ratio of carbon isotopes [$^{12}C/^{13}C$] normalised to a standard in per mil
δD	Ratio of hydrogen isotopes [$^{1}H/^{2}D$] normalised to a standard in per mil
$\delta^{18}O$	Ratio of oxygen isotopes [$^{16}O/^{18}O$] normalised to a standard in per mil

Chapter 1: Introduction

The primary motivation of this research was to determine the past oceanic conditions of the prolonged, interglacial period, marine isotope stage [MIS] 11 in the Southwest Pacific Ocean, and assess the potential of MIS 11 to represent an analogue to the present interglacial period [Holocene], and hence the use of MIS 11 to guide projections of the Holocene's future behaviour in a warming world.

1.1 General background

The ocean is the largest thermal reservoir on Earth and together with atmospheric processes controls the redistribution of the Sun's energy from equatorial latitudes to the poles [*Carter et al.*, 2008; *Lea*, 2003]. Debate exists as to how the ocean circulation system as a whole will respond to a warming climate in the future [*e.g., Boning et al.,* 2008*; Toggweiler and Russell,* 2008] and part of this thesis research aims to address such questions and provide insights into future environmental change in the region of study, namely the Southwest Pacific Ocean off eastern New Zealand.

MIS 11 occurred from 424–374 ka [*Lisiecki and Raymo*, 2005] and is often cited as an analogue to the present interglacial period as it is the most recent, long, stable warm period in Earth's history that resembles the Holocene [*e.g*., *Dickson et al.*, 2009; *Loutre*, 2003; *Loutre and Berger*, 2003]. During the Holocene and MIS 11, Earth's orbital configuration was characterized by a nearly circular orbit around the Sun [low eccentricity], which resulted in a similar distribution of seasonal isolation to modern values [*McManus and Tzedakis*, 2006]. Ice core

records from Antarctica show that MIS 11 atmospheric greenhouse gas levels were comparable to pre-industrial levels [*EPICA Community Members*, 2004], and benthic oxygen isotope records and climate models suggest similar global ice volumes [*Loutre and Berger*, 2003; *Pollard and DeConto*, 2009]. The deglacial transition from MIS 12 to MIS 11 was the largest amplitude [*Crundwell et al.*, 2008; *Droxler et al.*, 2003; *Lisiecki and Raymo*, 2005; *Lüer et al.*, 2008; *Zeigler et al.*, 2003] in the last 5 Myr [Fig. 1.1] and has been described as the major step in the global climate of the past 3 Myr [*Droxler et al.*, 2003]. Moreover, the timing and magnitude of the MIS 12-11 transition was similar to the MIS 2-1 transition [Fig. 1.2; *Dickson et al.*, 2009]. However, as discussed in Section 1.3, differences between MIS 11 and MIS 1 also suggest MIS 11 may not be an ideal analogue.

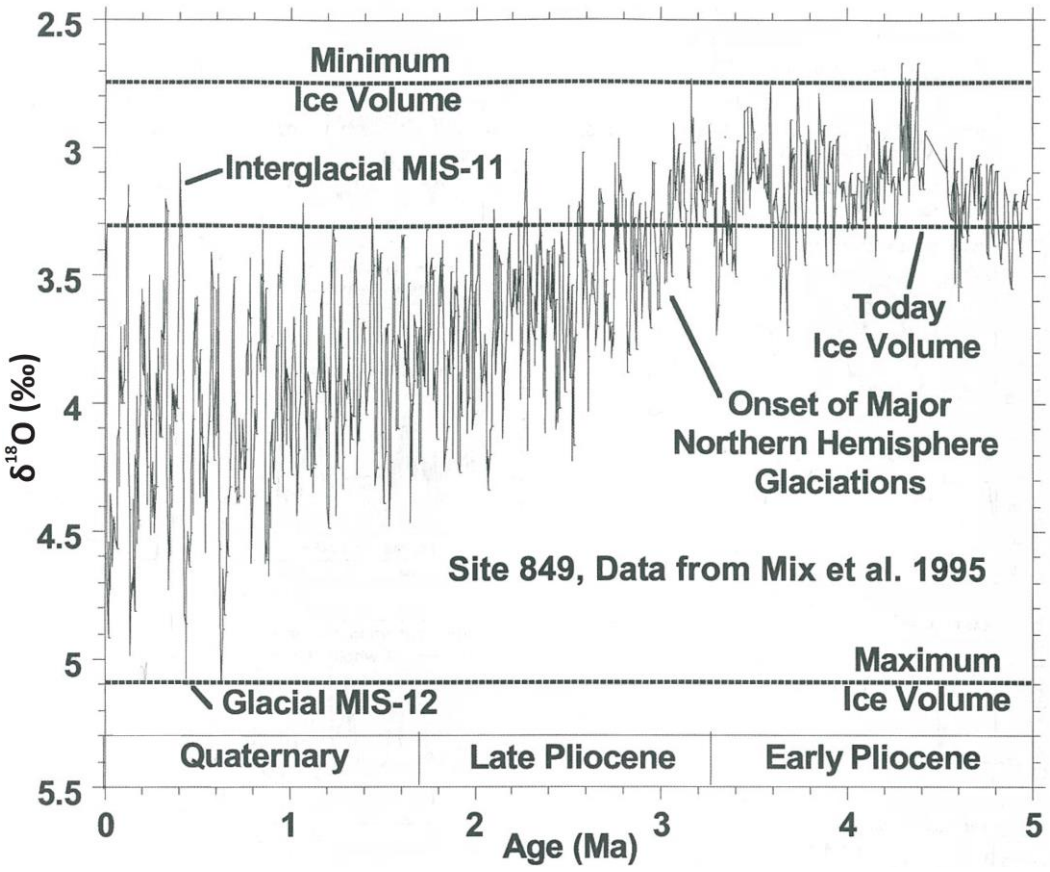

Figure 1.1. Benthic oxygen isotope record from ODP 849 in the east equatorial Pacific Ocean for the last 5 Myr showing climatic evolution over this time, and the amplitude of the MIS 12-11 deglacial transition. Figure taken and modified from *Zeigler et al.* [2003].

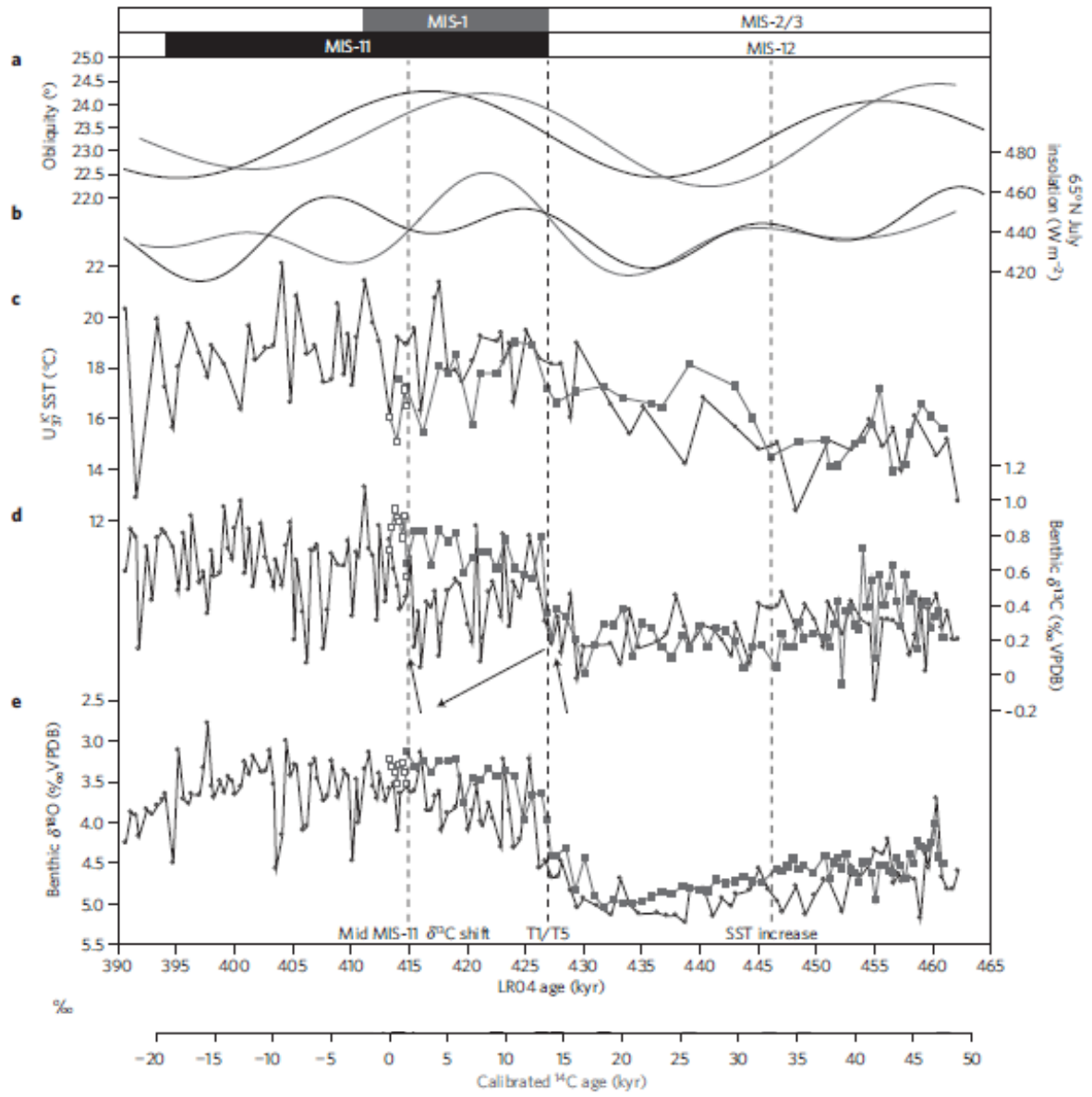

Figure 1.2. Comparison between the MIS 12-11 and MIS 2-1 transitions in the Southeast Atlantic. Solid grey squares are MIS 2-1 from GeoB1720-2; open grey squares from GeoB1720-3; black lines and circles are MIS 12-11 from ODP 1085. Colour coding: black circles = MIS 11; grey squares = MIS 1. **a**, Orbital obliquity. **b**, Insolation July 65°N. **c**, Alkenone derived sea surface temperature [SST]. **d**, **e,** Benthic derived $\delta^{13}C$ and $\delta^{18}O$. Dashed lines show the initial SST increase recorded by alkenones, termination 5/1 alignment and end of the MIS 11 carbon isotope excursion. Black arrows in **d** show benthic $\delta^{13}C$ isotope excursion at ODP 1085. Figure taken from *Dickson et al.* [2009].

The ODP 1123 sediment core studied in this thesis was drilled on the northern limit of the modern Subtropical Front [STF] and in the path of the Deep Western Boundary Current [DWBC; Fig 1.3], the largest deepwater outflow of the

Antarctic Circumpolar Current [ACC] and density driven abyssal currents [*Carter and McCave*, 1994; *McCave and Carter*, 1997; *Warren*, 1973]. As such, the ODP 1123 core is situated in a climatically and oceanically sensitive region and has the potential to reveal the oceanic response to MIS 11.

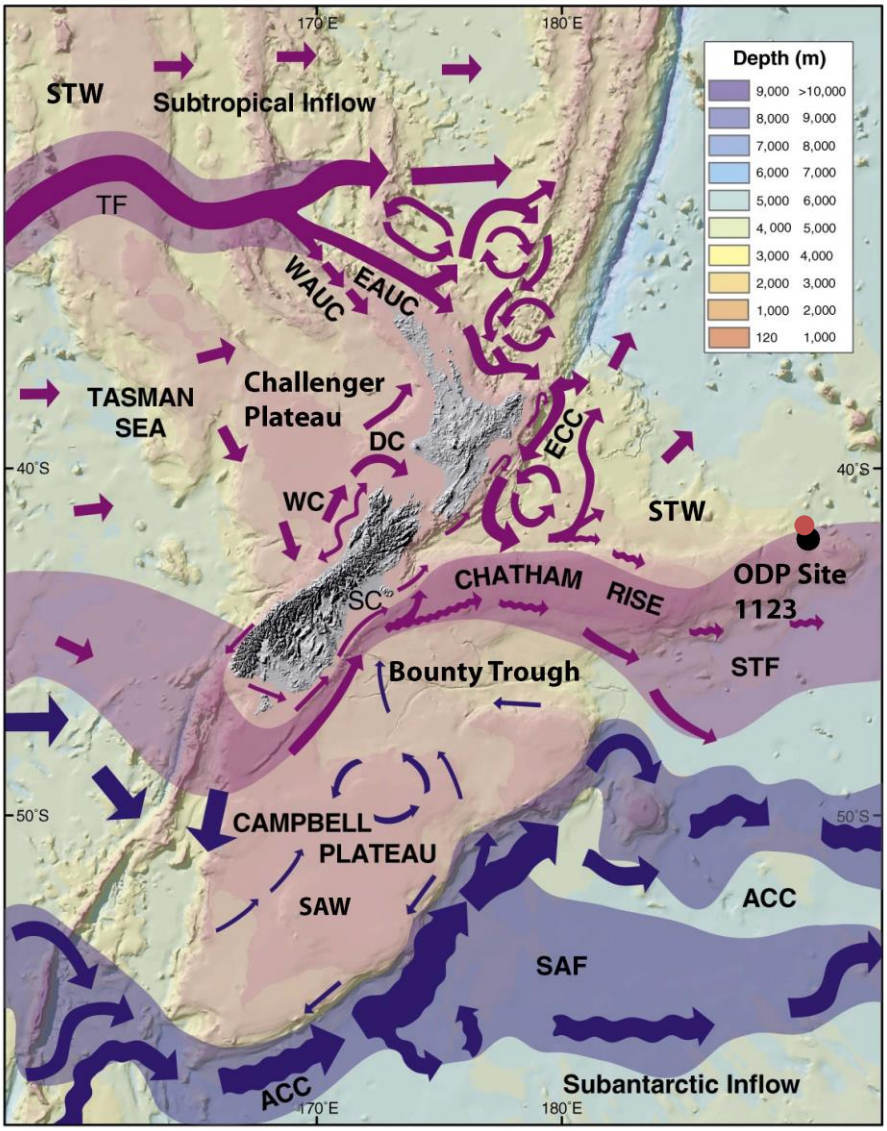

Figure 1.3. ODP 1123 [black dot] and CHAT 1K [red dot] core locations and major oceanic fronts and surface currents around New Zealand superimposed on a bathymetric chart. Gondwanic continental crust shown as warm coloured shallow plateaux, with cool colours showing relative deep water. Note the strong north-to-south water mass gradient from subtropical to subantarctic water over < 10° latitude. Figure taken and modified from *Carter et al.* [1998]. Acronyms as follows: ACC – Antarctic Circumpolar Current; EAUC – East Auckland Current; ECC – East Cape Current; DC – D'Urville Current; SAF – Subantarctic Front; SC – Southland Current; STF – Subtropical front; WAUC – West Auckland Current; WC – Westland Current.

1.2 Modern oceanographic setting

The oceans surrounding New Zealand are strongly influenced by complex regional bathymetry [Figs. 1.3 and 1.4; *Heath*, 1981]. Emergent New Zealand spans over 12˚ of latitude and makes up *ca*. 10% of the total continental landmass of Zealandia, which is a remnant of the old Gondwana supercontinent [*Mortimer*, 2004]. This old continental crustal material has cooled and subsided, while recording the tectonic history of the changing plate boundary system between this section of the Pacific and Australian tectonic plates, which are converging at *ca*. 40mm/yr [Norris and Cooper, 2000]. The tectonically dynamic setting has exerted a first order control on the bathymetry around New Zealand, and by association the regional oceanography [*Hayward et al.*, 2008; *Orpin et al.*, 2008; *Sutherland*, 1999].

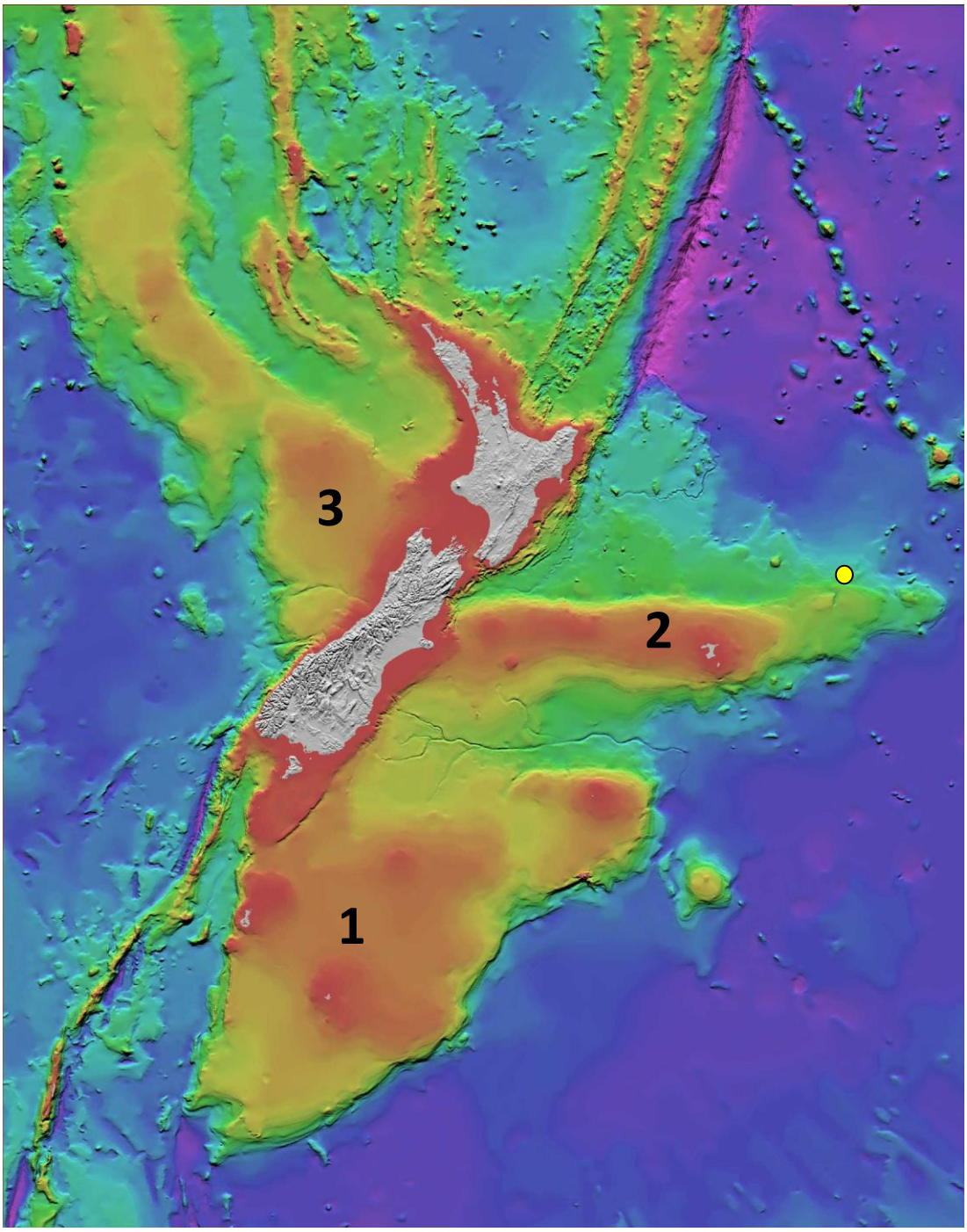

Figure 1.4. Bathymetric map of undersea New Zealand where blue to pink colours represent depths of 4000 to > 10,000 m of the SW Pacific basin and Kermadec Trench and red to yellow colours represent shallower depths of 120 to 1400 m on the 1: Campbell Plateau, 2: Chatham Rise and 3: Challenger Plateau. Yellow dot is the ODP 1123 core site. Figure taken and modified from *CANZ* [1996].

New Zealand intercepts two major oceanic fronts to the east and southeast, the Subantarctic Front [SAF] and the Subtropical Front [STF; Fig. 1.3; *McCave et al.*, 2008]. These fronts represent strong hydrographic gradients in ocean temperature, salinity and nutrient content, and define the interface between tropically- and polar-sourced water masses.

Ocean circulation to the west of New Zealand is largely wind driven and less well defined compared to east of New Zealand. In the east, the ocean is dynamically influenced by opposing inflows of tropical and polar waters particularly the South Pacific Gyre locally represented by the Tasman Front [TF], and the Antarctic Circumpolar Current [ACC; Fig 3.1]. Off eastern Australia, the TF bifurcates from the East Australian Current [EAC] and delivers warm saline STW that feeds the East Auckland Current [EAUC]. The EAUC flows southeast along the eastern continental margin of the upper North Island and continues flowing southwest as the East Cape Current [ECC], off the central and lower North Island before turning eastwards along the northern flank of the Chatham Rise. At the Chatham Rise, the ECC constrains the STF, which is dynamically positioned along the rise crest, and the southern side of the STF is mainly affected by the eastward flowing Southland Current [SC; *Carter et al.*, 1998].

Directly east of New Zealand at 45˚S, the STF is aligned with the Chatham Rise, which has a shallow crest at 250–400 m water depth [*Chiswell*, 2002; *Heath*, 1975]. The STF is a zone of intense mixing and high productivity as STW and SAW interact and mix through strong eddy activity [*Chiswell*, 2002]. This mixing is further facilitated by periodic breaches where southern- or northern-sourced water spills through relatively deep bathymetric features in the Chatham Rise, such as the Mernoo Saddle [*Greig and Gilmour*, 1992; *Murphy et al.*, 2001;

Schaefer et al., 2005]. Modern observations show that the STF may migrate seasonally by up to 2˚ of latitude between 42 and 44˚S, with the extremes occurring in late summer and autumn [*Chiswell*, 1994; 2002]. It has been postulated that the STF is dynamically constrained by the East Cape Current along the northern flank of the rise, and the Southland Current [SC] along the southern rise [Fig. 1.5; *McCave et al.*, 2008].

The STF reaches a depth of *ca*. 350 m [*Heath*, 1975] and defines a sharp gradient between relatively warm subtropical water [STW] and relatively cool subantarctic water [SAW]. STW is characterised by summer temperatures >15˚C, high salinity [*ca*. 35.7‰] and is typically macronutrient-poor [e.g., nitrate, silica, phosphorus] and micronutrient-rich [e.g., iron, manganese, zinc, barium]. SAW has relatively lower summer temperatures < 15˚C and salinity [*ca*. 34.7‰] and, in comparison with STW, is micronutrient-poor and macronutrient-rich [*Boyd et al*., 2004; *Murphy et al*., 2001]. Mixing of these two chemically distinct water masses is facilitated and enhanced by the bathymetric intrusion of the Chatham Rise and results in an area of high productivity [*Murphy et al.*, 2001].

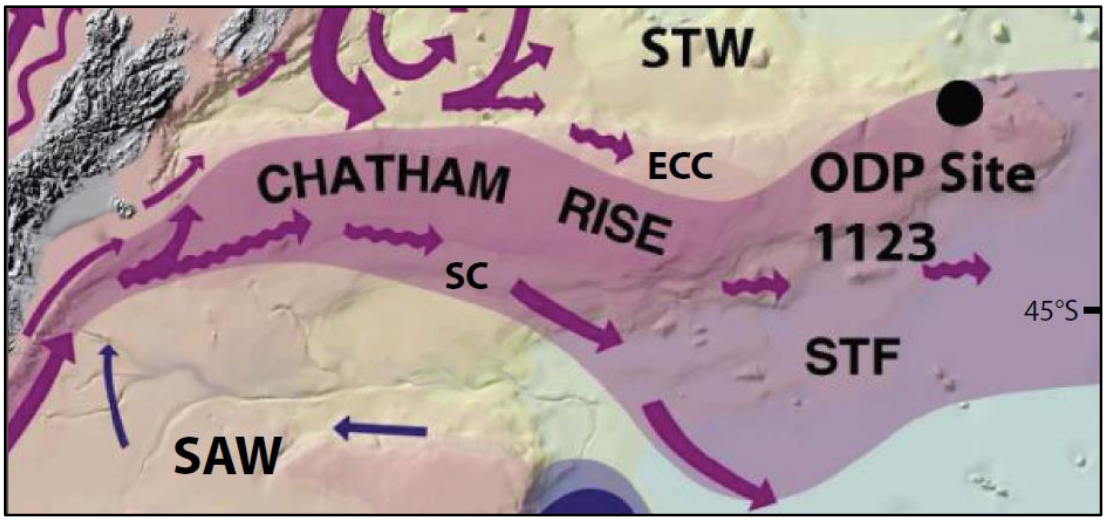

Figure 1.5. Map of modern ocean currents showing the East Cape Current [ECC] and Southland Current [SC] flow paths along the north and south of the Chatham Rise, where these currents act to constrain the STF. Figure modified from *Carter et al.* [1998].

Paleoceanographic reconstructions suggest that the restricted latitudinal migration of the frontal system was maintained throughout the Quaternary, although at the eastern and western limits of the Chatham Rise there was northward migration of the northern limit of the STF during glacial periods [*e.g., Crundwell et al.*, 2008; *McCave et al.*, 2008; *Nelson et al.*, 1993; *Weaver et al.*, 1998]. Moreover, various lines of evidence suggest that on glacial-interglacial timescales this bathymetric barrier inhibits major latitudinal migration of the frontal system beyond the observed ca. 2˚ latitude of modern migration [*Crundwell et al.*, 2008; *McCave et al.*, 2008; *Nelson et al.*, 1993 and 2000; *Weaver et al.*, 1998].

During the last glaciation [MIS 2] the SAF intensified against the western boundary presented by the Campbell Plateau. A gap in the boundary allowed SAF water to jet northeastwards and contribute to a clockwise gyre in the Bounty Trough [*e.g., Hayward et al.*, 2008; *Neil et al.*, 2004]. Where the SAF was unconstrained by the plateau it migrated north. As the STF does not appear to

have left its general position along the Chatham Rise crest, this subantarctic incursion intensified the temperature gradient across the STF from *ca*. 4 to 8˚C over just 4˚ of latitude [*Weaver et al.*, 1998]. Furthermore, *Schaefer et al*. [2005] and *Hayward et al*. [2008] suggested that during interglacial periods the STF may have periodically allowed subtropical waters to penetrate south from the Chatham Rise. This holds true for MIS 11 when modern analogue technique [MAT] paleo-ocean temperatures were similar north and south of Chatham Rise. In the open ocean away from these shallow bathymetric constraints, the STF may migrate by as much as 4 to 6˚ latitude during glacial-interglacial cycles, and is known to do so in the Indian Ocean [*Howard and Prell*, 1992] and the Tasman Sea [*Sikes et al.*, 2009].

At ODP 1123, the surface oceanography is presently dominated by the STF with modern sea surface temperatures [SST] ranging seasonally between 12.1 and 17.6°C with a mean annual average of 15.5°C [*Locarnini et al.*, 2006; *Schlitzer*, 2002]. According to the Conductivity-Temperature-Depth profiles taken just south of ODP 1123 by *McCave and Carter* [1997], the surface waters are underlain by Antarctic Intermediate Water [AAIW; *ca*. 600-1400 m water depth], Upper Circumpolar Deep Water [UCDW; *ca*. 1400-2700 m] and Lower Circumpolar Deep Water [LCDW: *ca*. 2700 m to the seabed at 3290 m depth]. This last water mass contains modified North Atlantic Deep Water [NADW] identified by its distinctive high salinity and low carbon isotope [$\delta^{13}C$] signatures. This occurrence of NADW has the potential to reveal if the nature of the meridional circulation changed during MIS 11 [*Hall et al.*, 2001]. This circulation is associated with the largest deep water offshoot of the ACC, the Pacific DWBC which passes over ODP 1123 en route to the central Pacific Ocean.

Occupying water depths of *ca*. 2000 m, the Pacific DWBC transports *ca.* 20 Sv [1 Sv = 10^6 m^3 s^{-1}] to contribute 35 to 40% of the cold deep water entering the world's ocean basins [*McCave et al.*, 2008; *Warren*, 1973].

As the DWBC passes ODP 1123, it decelerates, depositing a major sediment drift comprising alternating hemipelagites and calcareous pelagites with both foraminiferal and nannofossil assemblages [*Carter et al*., 1999]. Biogenic carbonate contents are accordingly variable ranging from 10-84%. Dissolution and diagenesis do not appear to be significant [*Hall et al.*, 2001; *Crundwell et al.*, 2008], except perhaps for MIS 11 and 9 [*Elderfield et al.*, 2010; *Greaves*, 2008], and this is explored further in Section 4.1.2.

1.3 Quaternary climate cycles

During the Cenozoic, global climate has gradually cooled from a "Greenhouse World" with no permanent polar ice to an "Icehouse World" with permanent polar ice sheets [Fig. 1.6]. The climate of the Quaternary is characterised by asymmetric glacial-interglacial climate cycles with rapid warmings from full glacial to interglacial states followed by a prolonged cooling into the next glacial period [Fig. 1.7; *Lisiecki and Raymo*, 2005; *Zachos et al.*, 2001]. These climate cycles follow changes in the orbital geometry of the Earth on its axis and annual path around the Sun [i.e., Milankovitch cycles]. Many authors agree that global glacial-interglacial climate cyclicity is most likely driven by orbital cycles, however, the lack of any direct physical linking mechanism makes it unclear whether these cycles actually drive global climate or modulate it [*e.g., Berger and Loutre,* 2003; *Howard and Prell*, 1992; *Miller et al*., 2010; *Raymo and Huybers,* 2008].

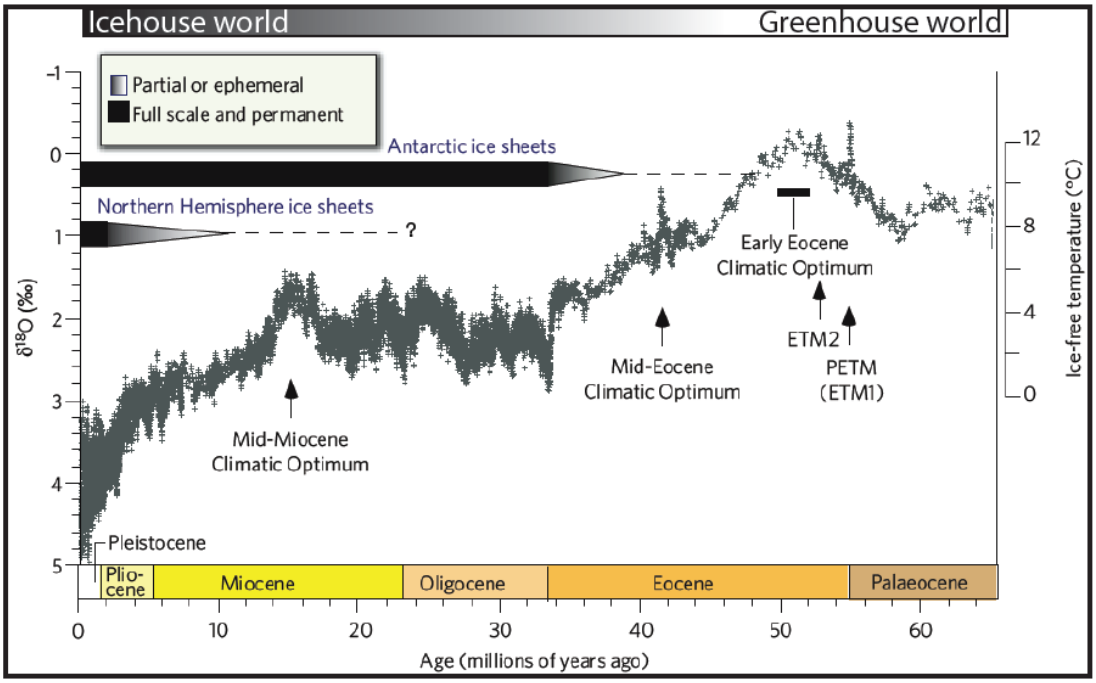

Figure 1.6. Stacked deep sea benthic global $\delta^{18}O$ curve showing the climatic evolution of the Cenozoic from a 'Greenhouse World' to an 'Icehouse World'. Superimposed on the long term cooling trend are various large magnitude transient climatic events of differing temporal and climatic magnitude, identifiable by their $\delta^{18}O$ perturbation from the mean climatic state. PETM [ETM1 – Eocene Thermal Maximum 1] refers to the short-lived and abrupt Paleocene-Eocene Thermal Maximum; ETM2 refers to the Eocene Thermal Maximum 2. Figure modified from *Zachos et al*. [2008].

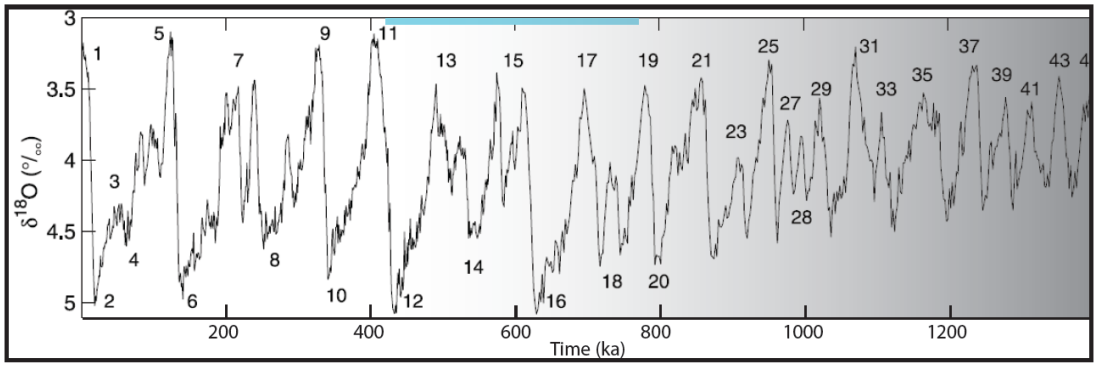

Figure 1.7. Global benthic $\delta^{18}O$ stack showing Quaternary climate cycles from 1400 ka. Blue bar shows the Mid-Pleistocene Transition after *Imbrie et al.* [1993], culminating at the mid-Brunhes event, which coincides with the MIS 12-11 transition [*EPICA Community Members*, 2004]. Grey shaded area shows 40 kyr glacial-interglacial climate cycles; white area shows 100 kyr climate cycles. Numbers refer to marine oxygen isotope stages. Figure modified from *Lisiecki and Raymo* [2005].

For most of the Quaternary until the mid-Pleistocene transition [*ca*. 0.8 to 0.4 Ma] these climate cycles show the strongest affinity with the 40 kyr obliquity frequency band [*Imbrie et al.*, 1993]. After the mid-Pleistocene transition, the climate system appears to be responding more strongly to the 100 kyr eccentricity cycle [Fig. 1.7]. However, eccentricity only has a minor control on the distribution of incoming solar radiation, and primarily modulates the 19-23 kyr precession cycle [*Imbrie et al.*, 1993; *Loutre and Berger*, 2003; *Raymo and Huybers*, 2008]. This leads to the question as to how minor and relatively insignificant changes of incoming solar radiation can cause such significant global climate changes that result in the growth and decay of massive ice sheets [*e.g., Howard*, 1997; *Imbrie et al.*, 1993; *Raymo and Huybers*, 2008]. As such, the role of internal non-linear feedbacks in the climate system [such as greenhouse gas and ice albedo feedbacks] is considered to be crucial in driving orbitally induced climate change [*Imbrie et al.*, 1993; *Prokopenko et al.*, 2010; *Raymo and Huybers*, 2008].

One significant problem with the orbital hypothesis of glaciation-deglaciation cycles is the precession signal. Precession has a marked influence on incoming solar radiation intensity compared to eccentricity and obliquity, yet glacial terminations do not appear to be caused by, or coincide with, changes in precession [*Raymo and Huybers*, 2008]. This has led to the hypothesis that rapid glacial terminations may occur at multiples of precession cycles [*Maslin and Ridgwell*, 2005] or at multiples of obliquity cycles [*Huybers*, 2007; *Huybers and Wunsch*, 2005]. *Jouzel et al*. [2007] argued that the insolation overlap between high obliquity and precession is associated with Quaternary interglacials, with the largest amplitude temperature changes occurring during deglacial

transitions in the EPICA Dome Concordia [EDC] core [e.g., MIS 1, 5, 9, 11 and 19]. Less intense interglacial periods occur when northern and southern hemisphere insolation is antiphased [e.g., MIS 13, 15 and 17].

Hall et al. [2001] performed spectral analysis of stable isotope and grain size data from the ODP 1123 core and found that upper ocean conditions and the strength of the DWBC inflow were in-phase with orbitally-induced variations in global ice volume for the last 1.2 Myr on obliquity timescales with deglaciations occurring at multiples of obliquity cycles [two or three cycles corresponding to deglaciation every 80 to 120 kyr; *Hall et al.*, 2001].

Past climatic records are important to better identify climatic forcing mechanisms, rates of change and extremes. This thesis research focuses on MIS 11 because the insolation geometry was similar to present MIS 1 conditions, with low eccentricity and precessional amplitude, and high obliquity [*Dickson et al.*, 2009; *Loutre and Berger*, 2003]. However, after the glacial termination, insolation differed for MIS 11 and MIS 1 [Fig. 1.2; *Dickson et al.*, 2009]. MIS 11 spans two insolation maxima separated by a weak minimum [July 65˚N], which is a consequence of the coincidence of the 400 kyr eccentricity cycle and maximum in Earth's axial tilt [*Tzedakis*, 2010]. In contrast, MIS 1 only spans one insolation maximum [July 65˚N]. Furthermore, all other typical interglacial periods since MIS 11 have terminated after one insolation maximum [*EPICA Community Members*, 2004; *Jouzel et al.*, 2007; *Loulergue et al.*, 2008; *Rohling et al.*, 2010; *Siegenthaler et al.*, 2005]. This raises the question as to whether the Holocene is likely to continue or enter a new glaciation in response to the coming insolation minimum in an undisturbed climate system. Ignoring any potential additional climate forcing by anthropogenic greenhouse gas [GHG]

emissions, the answer to this question depends on the temporal alignment of MIS 11 and MIS 1 and whether precession [*Loutre*, 2003; *Loutre and Berger*, 2003] or obliquity parameters are aligned [*Dickson et al.*, 2009; *EPICA Community Members*, 2004; *Masson-Delmotte et al.*, 2006]. If precession is the dominant forcing effect on climate cycles, then the Holocene interglacial period should be ending. However as low eccentricity dampens the effect of precession then obliquity alignment [which coincidentally aligns terminations I and V] may be the more dominant effect [*Masson-Delmotte et al.*, 2006]. The latter case would suggest that the Holocene may continue for another *ca*. 12 kyr in a natural world without the added complication of anthropogenic GHG emissions and attendant warming [*Tzedakis*, 2010].

1.3.1 Marine Isotope Stage 11 ice core and marine sedimentary records

While most previous studies have argued that MIS 11 was an extended interglacial compared to more recent Quaternary interglacials [*Droxler and Farrell*, 2000; *Droxler et al.*, 2003; *Lisiecki and Raymo*, 2005; *Loutre and Berger*, 2003; *McManus and Tzedakis*, 2006; *Miller et al.*, 2010; *Rohling et al.*, 2010], its magnitude of warmth [*Candy*, 2009; *Preece et al.*, 2007; *Stanton-Frazee et al.*, 1999] and sea level rise relative to the present, are widely debated [*e.g.*, *Olson and Hearty*, 2009; *Raymo and Mitrovica*, 2012].

MIS 11 also marks a fundamental change in the nature of long-term climate cyclicity, the 'mid-Bruhnes event', sometimes also called the mid-Pleistocene transition [*EPICA Community Members*, 2004] when the climate system switched to larger amplitude climate cycles and favoured an overall warmer

state [*Jouzel et al.*, 2007], which is believed to be a reflection of some change in climate forcing mechanisms or crossing of some internal threshold [Fig. 1.8].

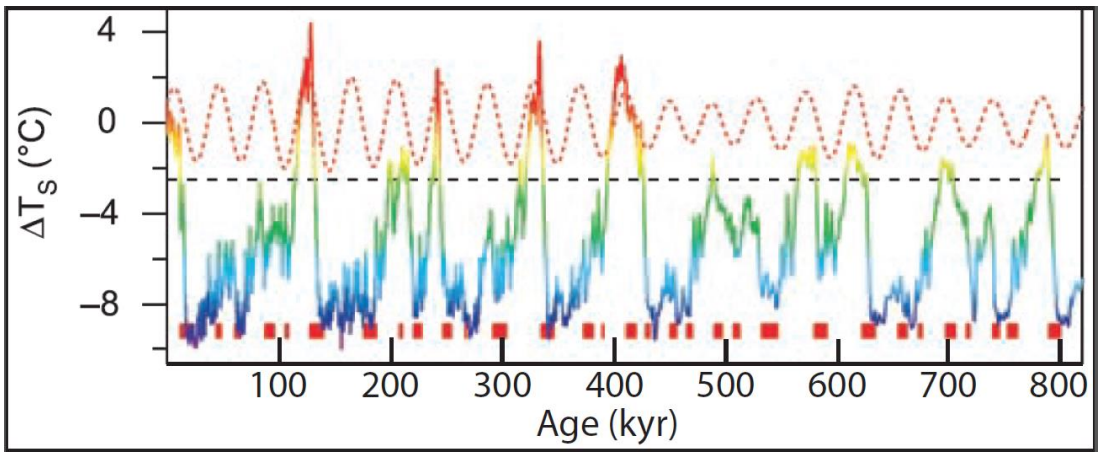

Figure 1.8. EDC δD-derived temperature with warm and cool colours representing relative temperatures, and the obliquity component extracted using a Gaussian filter within the frequency range 0.043 ± 0.015 kyr. Red blocks indicate times when precession is decreasing and obliquity is increasing. Figure taken and modified from *Jouzel et al.* [2007].

Some studies have argued for similar sea levels during MIS 11 and the present [*Bowen*, 2010], using evidence from seven different localities [*Elmejdoub and Jedoui*, 2009; *Rohling et al.*, 2010; *Zazo et al.*, 2003]. Somewhat controversially, other studies have suggested that sea level was *ca*. 20 m above present based on direct biological and sedimentological evidence from coastal shelf deposits [Hawaii and Bermuda; *Hearty*, 2002; *Hearty and Olson*, 2008; *Hearty et al.*, 1999; *Kindler and Hearty*, 2000; *Olson and Hearty*, 2009].

Such a sea level rise would require collapse of both the West Antarctic Ice Sheet and the Greenland Ice Sheet, plus a significant contribution from melting of the East Antarctic Ice Sheet. Sufficient sedimentological evidence, proximal to the southern hemisphere ice sheets, to support this high sea level hypothesis does not currently exist. Instead, an ice-rafted debris depositional anomaly favours the MIS 15-13 interval as a likely time of West Antarctic Ice Sheet collapse in the Quaternary [*Hillenbrand et al.*, 2009].

Limited evidence for an ice-free Greenland during MIS 11 has been identified, such as a 23 kyr-long ice-rafted debris depositional absence at ODP 982 and an even more substantial and longer ice-rafted debris absence at ODP 980 both from offshore Greenland in the Northeast Atlantic, implying no ice available for iceberg calving [*McManus et al.*, 1999; *Stanton-Frazee et al.*, 1999]. *Willerslev et al.* [2007] analysed ice core basal silts for DNA to reveal that a forested south-central Greenland may have existed at this time, although this event is not accurately dated. Pollen records from marine sediment core ODP 646 from the Labrador Sea, southwest of Greenland, indicate a significantly reduced Greenland ice sheet with an order of magnitude increase of *Picea* pollen, which also implies a forested southern Greenland during MIS 11 [*de Vernal and Hillaire-Marcel*, 2008].

The EDC ice core revealed that atmospheric GHG levels and deuterium [δD]-derived Antarctic air temperatures for MIS 11 were similar to pre-industrial levels [GHG] and unexceptional [air temperatures]. This ice core record does not support a warmer than present MIS 11, particularly as climate warming is generally thought to be amplified in polar regions [*Rohling et al.*, 2012].

1.3.2 Marine Isotope Stage 11 terrestrial records

Continental records have raised more questions about MIS 11 climatic conditions, with results from different proxies and locations varying. Furthermore, terrestrial records often lack the temporal resolution and continuity offered by the ice and deep marine sediment cores. Some terrestrial proxies suggest local warming, superimposed on an generally wetter climate with greater biotic diversity, perhaps owing to the extended duration of MIS 11

[*Preece et al.*, 2007]. Lacustrine sediments from Siberia also indicate generally humid and warm conditions during MIS 11, with the proportion of biogenic silica in Lake Baikal being the highest at this time in the last 450 kyr [*Mackay et al.*, 2008]. Well developed paleosols from the Chinese Loess Plateau were originally interpreted to reflect extreme semi-humid and subtropical, warm MIS 11 conditions relative to the present. However, other studies disagree that these paleosols formed under conditions that were significantly different to the modern environment [see *Wu et al.*, 2007 for a review]. More recently *Wu et al.* [2007] identified two different climatic regimes based on terrestrial molluscs in the MIS 11 paleosols of the Chinese Loess Plateau, which reflect an early climatic optimum, more humid and warmer than the Holocene optimum, that lasted *ca*. 30 kyr and was characterised by significant diagenesis, followed by cooler conditions that were similar or even cooler than the Holocene. MIS 11 appears generally to have been of extended duration relative to other Quaternary interglacials and shows regionally complex variations, with some areas showing similar temperatures and some areas appearing warmer than the present. A generally wetter trend implies warmer SST and enhanced evaporation, although marine records do not implicitly show this [*Rousseau*, 2003].

The key to reconciling the various lines of evidence for climatic variability during MIS 11 may lie in a multi-proxy approach, focusing on deep marine sediment cores with continuous resolution, and this was the aim of the research undertaken during this thesis study. However, evidence exists to suggest that during MIS 11 some perturbation occurred in the ocean carbon cycle, which led to a carbonate dissolution interval in the world's oceans [*Farrell and Prell*, 1989;

Zeigler et al., 2003]. An important question is whether this ocean carbon cycle perturbation was the result of an extreme warm period relative to the present day.

1.3.3 The latest Quaternary climate cycle

The last glacial maximum occurred between 26.5 and 19-20 ka when southern and northern hemisphere ice sheets were at their maximum extent. Sea level was approximately 120 m below the present level and as a result major reorganisation of upper ocean circulation occurred. Termination I is strongly characterised in ice and marine cores by a marked rapid increase in greenhouse gas levels in ice cores and a decrease in $\delta^{18}O$ values in foraminifera in marine cores [Fig. 1.7]. This warming was punctuated by the cooling reversals in both hemispheres, the Antarctic Cold Reversal [ACR] occurring from 14.1–12.4 ka and the Younger Dryas cooling event in the northern hemisphere occurring 13–11.5 ka [*Broecker, W.*, 2002]. As this study focuses on southern hemisphere climate, the Younger Dryas will not be discussed further.

The ACR is identified in ice and marine core records by either a full climatic reversal of ~2 degrees [e.g. the EPICA ice core record; *Jouzel et al.*, 2007] or a 'pause' in the deglacial stable isotope trend [e.g. MD97-2121 on the Campbell Plateau; *Carter et al.*, 2008]. Offshore New Zealand saw the ACR manifest as a temporary halt in the benthic $\delta^{18}O$ lightening from 14.1 ka, however this change didn't register in the upper ocean until the ACR was at its strongest at 13.5 ka. This resulted in merging of planktonic $\delta^{18}O$ profiles, interpreted as a collapse in upper ocean structure [*Carter et al.*, 2008].

1.4 Geochemical archives and proxies of past ocean temperature and global ice volume changes

Determination of Mg/Ca-derived paleo-ocean temperatures has been an area of active research for 90 years, since *Clark and Wheeler* [1922] first identified the potential of the Mg content in biogenic carbonates to reveal growth temperatures.

Urey [1947] first theorised that the fractionation of oxygen isotopes in biogenic carbonates was temperature-dependent. This was applied to natural samples by *Epstein et al*. [1953] who established the thermodynamic relationship between ocean temperature and oxygen isotope composition. The first cyclical variations in foraminiferal oxygen isotopes in a sediment core interpreted as climatic fluctuations were described by *Emiliani* [1955].

Subsequently, the potential for the accurate determination of paleo-ocean temperatures and past global ice volumes using Mg/Ca-derived paleo-ocean temperatures and oxygen isotopes on the same samples have been extensively developed [see *Lea*, 2003 for a review], and are the primary research tools utilised in this thesis study.

1.4.1 Magnesium/calcium ratios in foraminifera as a proxy of paleo-ocean temperatures

Foraminifera are unicellular protists, and in addition to temperature, other environmental conditions and biological factors also influence the biomineralization of trace elements into their tests [*Erez*, 2003; *Lea*, 2003]. Foraminifera secrete calcite tests in equilibrium with surrounding ocean water in which they inhabit and, therefore, incorporate trace elements such as Mg as

they progress through their life cycle [*Anand et al.*, 2003; *Lea*, 2003]. Mg incorporation into foraminiferal calcite is strongly dependent on temperature, hence the Mg/Ca ratio is one of the most widely studied of all trace element ratios [*e.g., Lea*, 2003; *Nürnberg et al.*, 1996; *Rosenthal and Lohmann*, 2002; *Rosenthal et al.*, 1997]. Given the temperature, salinity and CO_3^{-2} concentration ranges identified at the ODP 1123 site, temperature has been shown to be the primary control on Mg incorporation in *Gg. bulloides* and *Gs. ruber* from the Southwest Pacific Ocean [*Bolton et al.*, 2011; *Marr et al.*, 2011].

1.4.2 Secondary influences on the trace element chemistry of foraminifera

Factors other than temperature that influence trace element chemistry in foraminiferal calcite include: [1] vital effects, [2] ecology, [3] low carbonate ion [CO_3^{-2}] concentration [4] preservation, [5] growth rates and [6] salinity. All of these can cause natural chemical heterogeneity through the test wall and are now discussed sequentially.

Vital effects

As foraminifera grow they sequentially add new chambers and an extra layer of calcite to the existing chambers [Fig. 1.10]. In addition, individual test layers are comprised of a primary inner high-Mg calcite and a larger proportion of primary outer low-Mg calcite [*Anand and Elderfield*, 2005; *Eggins et al.*, 2003; 2004; *Erez*, 2003; *Sadekov et al.*, 2009]. Distribution of Mg throughout the test for the two species analysed in this study has not been well characterised, but the amount of chemical heterogeneity in the form of alternating high- and low-

Mg bands may not be as important as other species such as *Orbulina universa* or *Amphistegina lobifera* [*Eggins et al.*, 2004; *Erez*, 2003]. Furthermore, growth rates can vary over diurnal timescales, which provides an extra complication with high-Mg bands being secreted at night by certain symbiont-bearing species [*Eggins et al.*, 2004]. Another inherent complication is the biological mediation of trace element uptake related to kinetic or taxonomic effects. These vital effects cause a departure from equilibrium and are species-specific, resulting in inorganically cultured calcite and cultured foraminifera differing in their uptake of trace elements, and therefore require the development of species-specific calibration equations [*Stephenson et al.*, 2008].

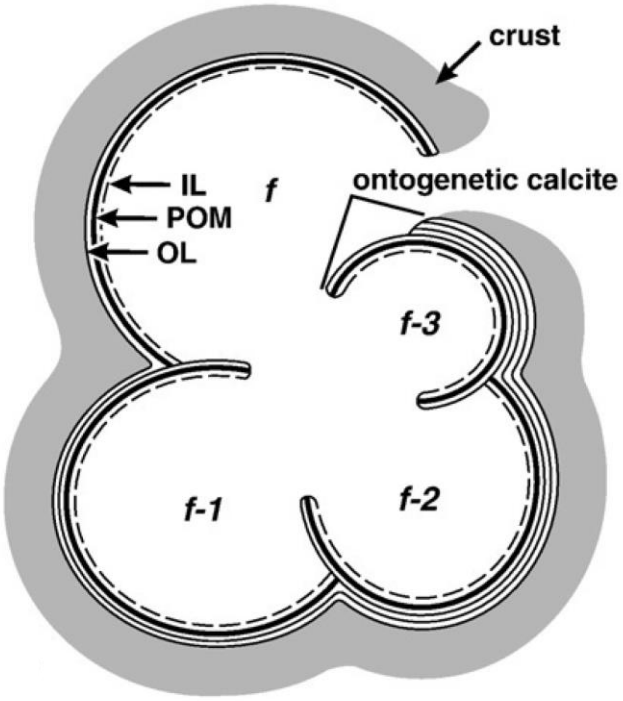

Figure 1.9. Schematic illustration showing the sequential addition of new chambers and outer ontogenetic calcite layers, and gametogenic crust layer associated with reproduction. Letters denote the chamber age, with [f] referring to the youngest and [f-3] referring to the oldest chamber. IL refers to the inside calcareous lining; POM refers to the primary organic membrane where calcification initiates and OL refers to the outer calcareous

Ecology

Some non-symbiont-bearing planktic foraminiferal species also migrate through the water column throughout their lifecycle, which results in a lower overall Mg/Ca value, reflecting cooler temperatures at depth. Similarly, the secretion of gametogenic calcite with reproduction at the end of the lifecycle at greater depth, can also cause a significant cool temperature bias [*Caron et al.*, 1990; *Eggins et al.*, 2003].

Carbonate ion concentration

Low CO_3^{-2} concentration can affect foraminifera's ability to calcify and maintain a strong healthy test, both during ontogeny and post-mortem [*Barker and Elderfield*, 2002]. The CO_3^{-2} effect is species specific and correlates with a linear decrease in Mg/Ca ratios below a threshold CO_3^{-2} concentration [*Regenberg et al.*, 2006]. The influence of low CO_3^{-2} concentration on Mg/Ca ratios in the foraminifera in this study is considered in more detail in Chapter 3.

Preservation

Post-mortem diagenetic change can also affect Mg/Ca ratios, due to the preferential dissolution of less stable Mg-rich calcite and recrystallisation at depth, biasing the calculated Mg/Ca-derived paleo-ocean temperatures towards cooler values [*Brown and Elderfield*, 1996; *Lea*, 2003; *Rosenthal and Lohmann*, 2002]. Planktic foraminifera are more susceptible to this process due to greater micro-porosity in the test compared to benthic species [*Pearson et al.*, 2001; *Sexton et al.*, 2006]. The extent to which *Gg. bulloides* and *Gs. ruber* are

susceptible to dissolution of Mg-rich portions of the test is not known. Perfect 'glassy' preservation is often found only in foraminifers recovered from clay-rich hemipelagic sediments [*Sexton et al.*, 2006]. However, the section of the ODP 1123 core studied in this thesis is foraminiferal-bearing nannofossil ooze [*Carter et al.*, 1999], which may be problematic when geochemically analysing foraminifera due to the possibility of diagenetic effects [*Pearson et al.*, 2001].

Growth rates

Variable growth rates have been suggested to affect trace element incorporation in foraminifera [*e.g., Elderfield et al.,* 1996; *Elderfield et al*., 2002], where faster growth rate equals higher trace element incorporation. However, *Erez* [2003] has shown the variable incorporation of trace elements does not vary with growth rates and instead is likely to be of biologically mediated by the organism. *Aldridge et al*. [2012] suggested that greater nutrient availability causes faster growth rates in *Gg*. *bulloides* resulting in thinner, less dense, calcite tests.

Salinity

Establishing to what extent salinity controls Mg/Ca uptake in planktonic foraminifera is important because varying salinity gradients may produce a paleotemperature bias. Due to a semi-enclosed geography, a large salinity gradient [36-40 psu] exists in the Mediterranean Sea, providing a natural laboratory to study the effect of varying salinity on Mg/Ca ratios in foraminifera. In the highly saline East Mediterranean Sea, Mg/Ca ratios in planktonic foraminifera are higher than the *in situ* ocean temperature would

suggest [*Ferguson et al.*, 2008]. However the range of salinities at ODP 1123 is not sufficiently elevated to cause significant Mg/Ca bias in foraminiferal calcite [34.7-35.7 psu; *Boyd et al.*, 2001].

1.4.3 Oxygen and carbon isotopes

The $\delta^{18}O$ signature preserved in the tests of planktic foraminifera reflects ocean temperature and the $\delta^{18}O$ composition of seawater, with the latter in turn reflecting global ice volume and local salinity [*Emiliani*, 1955; *Shackleton*, 1987; *Urey*, 1947]. $\delta^{18}O$ measurements of foraminifera are particularly useful when combined with Mg/Ca-derived paleo-ocean thermometry, which allows the identification of ocean temperature, and thus changes in $\delta^{18}O$ of seawater through time that can be related to changes in global ice volume [*Lear et al.*, 2000; *Mashiotta et al.*, 1999; *Nürnberg et al.*, 1996; *Rosenthal et al.*, 2000]. The $\delta^{18}O$ value recorded in biogenic carbonate is the most widely used paleo-climate proxy as it is relatively easy to measure accurately with modern mass spectrometry techniques [*Lea*, 2003].

Foraminifera record the ratio of $^{12}C/^{13}C$ [normalised to a standard as $\delta^{13}C$] in seawater in their calcite tests. $\delta^{13}C$ can be utilised as a productivity indicator as algal photosynthesis favours the preferential uptake of lighter ^{12}C, resulting in more positive $\delta^{13}C$ in surface waters, although this proxy is complicated by other factors, such as the pre-formed carbon signature of the water mass. The carbon isotopic signature of a water mass can also act as a circulation tracer and the inverse relationship between high productivity and lower benthic $\delta^{13}C$ [*Mackensen et al.*, 2001]. As a water mass ages, respiration liberates oxygen and releases CO_2, which causes a subsequent negative $\delta^{13}C$ signature, and this is a

first-order indicator to distinguish between Pacific and Atlantic deep water [*Kroopnick*, 1985; *Spero*, 1992].

1.4.4 Geochemical archives and proxies utilised in this thesis

Two planktic foraminiferal species, *Gg. bulloides* and *Gs. ruber* [Fig. 1.11] were analysed in this study by LA-ICPMS to determine their trace element geochemistry. The primary focus of this work was to measure Mg/Ca ratios to derive paleo-ocean temperatures, although other trace elements [Mn and Zn] were also measured to assess their potential to trace changes in water mass chemistry, paleo-productivity and ocean circulation. Recently, *Marr* [2009] analysed these elements in *Gg. bulloides* from core-top sediments in the Southwest Pacific Ocean and suggested it is possible to differentiate between modern SAW and STW based on the Mn/Ca, Zn/Ca and Ba/Ca ratios.

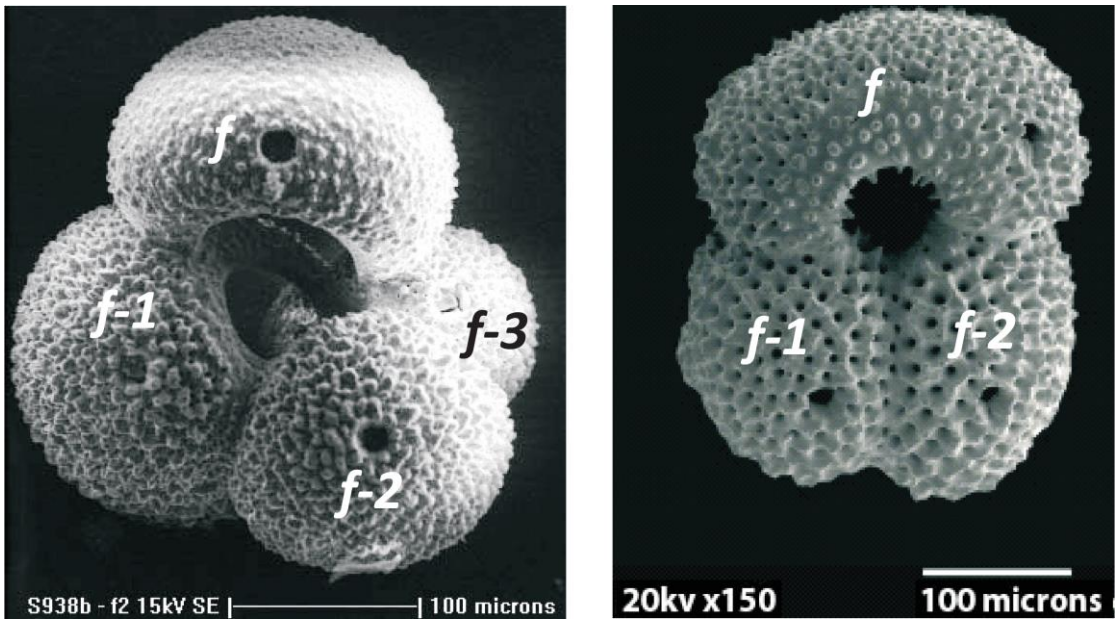

Figure 1.10. Scanning electron microscope [SEM] images of the two foraminiferal species analysed by LA-ICPMS in this study, *Gg. bulloides* [left] and *Gs. ruber* [right]. Chamber ages are annotated as in Figure 1.10, where the youngest final chamber is [*f*], and sequentially older chambers are denoted by higher *f* values [*f-1, f-2* etc.]. Left image was taken from *Marr et al*. [2011] and the right image was taken from *Bolton et al*. [2011].

The time period studied is 445–375 ka, which encompasses the deglaciation from MIS 12 through to the climatic optimum of MIS 11. *Gg. bulloides* is a eutrophic, temperate species and is relatively abundant throughout this time interval. Peak abundance precedes the deglaciation and decreases notably during the early deglacial transition at *ca*. 435 kyr [*Crundwell et al.*, 2008]. *Gs. ruber* is a tropical-subtropical species [*Crundwell et al.*, 2008] and, thus, is very low in abundance during colder environmental conditions and so was only analysed for the "warm" period from 428–394 ka.

Trace element data were complemented with previously acquired stable oxygen isotope analyses of the foraminifera [*Federici et al., unpubl. data*], in order to reconstruct changes in ocean salinity and global ice volume [$\delta^{18}O$] and identify large-scale changes in paleo-circulation, specifically the relative influence of different water masses at ODP Site 1123.

1.5 Thesis objectives and key research questions

This thesis applies geochemical proxies to determine the oceanic response to MIS 11 [*Lisiecki and Raymo*, 2005; *Rohling et al.*, 2010; *Ruddiman*, 2005]. As noted previously, debate exists as to the magnitude of warming during MIS 11 as compared to the present. MIS 11 has previously been considered to have been markedly warmer than the present [*Droxler and Farrell*, 2000; *Hays et al.*, 1976; *Lea et al.*, 2000; *McManus et al.*, 1999], although this has been challenged as subsequent research has modified this picture of extreme warmth [*e.g., Crundwell et al.*, 2008; *Kolodziej*, 2010; *Mackay et al.*, 2008; *Preece et al.*, 2007; *Wu et al.*, 2007]. These recent studies reveal MIS 11 temperatures were similar

or slightly warmer than present, and lasted *ca*. 30 kyr. Encapsulated by the fundamental question: "How did the Southwest Pacific Ocean respond to the prolonged warming associated with MIS 11?" there are several second order objectives to this thesis study.

1. Determine the timing and pattern of the MIS 11 interglacial.
2. Determine a paleo-ocean temperature record for MIS 11 using Mg/Ca based thermometry.
3. Identify changes in water masses and ocean structure from peak glacial MIS 12 conditions to the end of MIS 11 using trace element foraminiferal test chemistry.
4. Investigate the ocean carbon response to MIS 11 via analysis of size-normalised test weights of foraminiferal tests.
5. Determine New Zealand's oceanic regional response to MIS 11.
6. Compare MIS 11 to MIS 1 and assess the suitability of the former as an a analogue for the future.

In order to address these research questions, LA-ICPMS trace element analyses were complemented by previously unpublished [*Federici et al., unpubl. data*] stable oxygen isotope analyses on planktonic foraminifera species [*Gg. bulloides*] and one benthic species [*Uvigerina spp*.] from the same ODP 1123 core. These data are compared with other published information on MIS 11 [*Crundwell et al.*, 2008, *Hayward et al*. 2012; *Kolodziej*, 2010; *Prebble*, 2012], to determine the regional response to MIS 11.

1.6 Thesis structure

This thesis is structured into six chapters and a set of appendices as follows:

Chapter 1 – Introduction: This chapter presents a description of MIS 11 and the general setting of ODP 1123. A review of Quaternary climatic cycles and the geochemical proxies used to study these follow, finishing with the thesis research objectives and questions.

Chapter 2 – Materials and methods: This chapter describes the location of the sediment core and its dating. The second part of this chapter documents the sample preparation techniques and the analytical methods.

Chapter 3 – Results: This chapter presents the main results of the research carried out in this thesis.

Chapter 4 – Discussion: This chapter discusses the implications of the previous chapter.

Chapter 5 – Regional overview: MIS 11 paleo-ocean temperatures in the Southwest Pacific Ocean. This chapter synthesises available data that constrain the environmental conditions around New Zealand during MIS 11 using a range of proxies from multiple sites.

Chapter 6 – Conclusions and suggestions for future work

Appendix 1: SEM images of a selection of analysed foraminifera.

Appendix 2: A data file containing details of samples including depth/age, and all geochemical data [foraminifera test weights, stable isotopes, trace elements] and calculated paleo-ocean temperatures acquired in this thesis research.

Appendix 3: A data file containing the sample size error determinations for Mg/Ca-derived paleo-ocean temperatures.

Appendix 4: Age model data file.

Chapter 2: Materials and methods

2.1 ODP 1123 sediment core

The studied sediment core was drilled at 3290 m water depth into contourite drifts during Leg 181 of the Ocean Drilling Program in 1998. The core is situated on the northeastern edge of the Chatham Rise, 410 km northeast of the Chatham Islands [41˚47.15'S, 171˚29.94'W]. ODP 1123 is located in an oceanographically important region near the northern edge of the modern STF, and also in the path of the DWBC the main outflow, and largest offshoot of, Antarctic Bottom Water [AABW] into the Pacific Ocean via the ACC [Fig. 2.1; *Warren*, 1973]. The section of the core studied is Hole B, core 3H, section 3-2 to 3-4, 15.15 to 17.50 m below sea floor [mbsf] and is primarily cyclic alternating greenish grey clayey nannofossil ooze with white nannofossil ooze, with carbonate content oscillating around 65% [*Carter et al*., 1999].

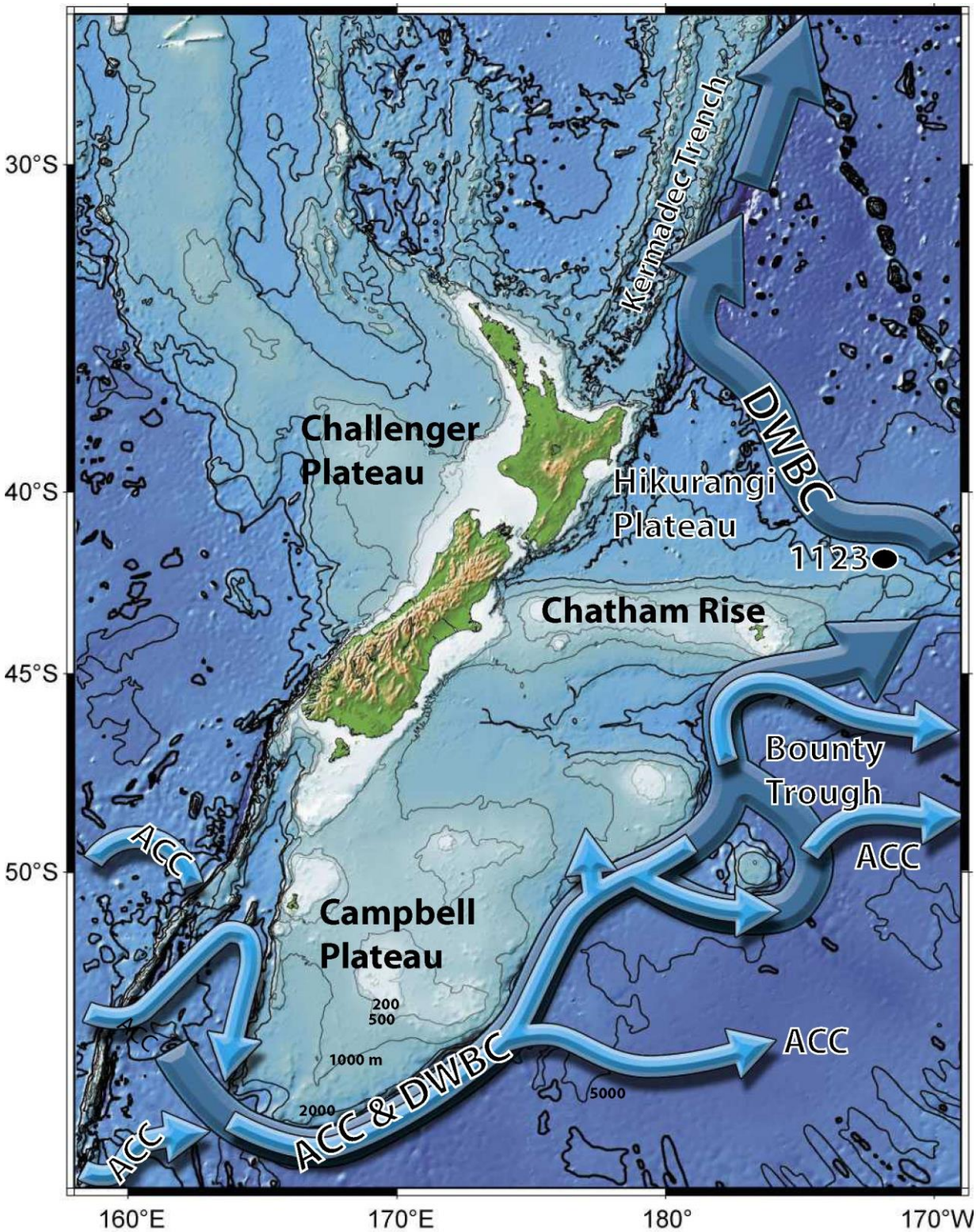

Figure 2.1. Major western boundary ocean currents including the surface to seabed ACC, underlying DWBC and the location of ODP 1123 in the path of the DWBC. Figure modified from *Carter et al.* [1998].

2.2 Dating of the sediment core

The upper 47 m of the core were initially dated by tuning a coarse resolution [1.2-2.5 kyr] stable isotope record obtained by *Hall et al*. [2001] to the ice-volume model of *Imbrie and Imbrie* [1980] using July 65˚N insolation values. This work was subsequently refined by *Elderfield et al.* [2010] by retuning the entire core to the *Lisiecki and Raymo* [2005] global benthic stack, although this only made a small difference to the earlier age model. The age model in this thesis was obtained by tuning high resolution unpublished stable isotope data [*Federici et al., unpubl. data*] on the benthic foraminifera *Uvigerina sp*. from 15.15 to 17.02 mbsf to the *Lisiecki and Raymo* global benthic stack.

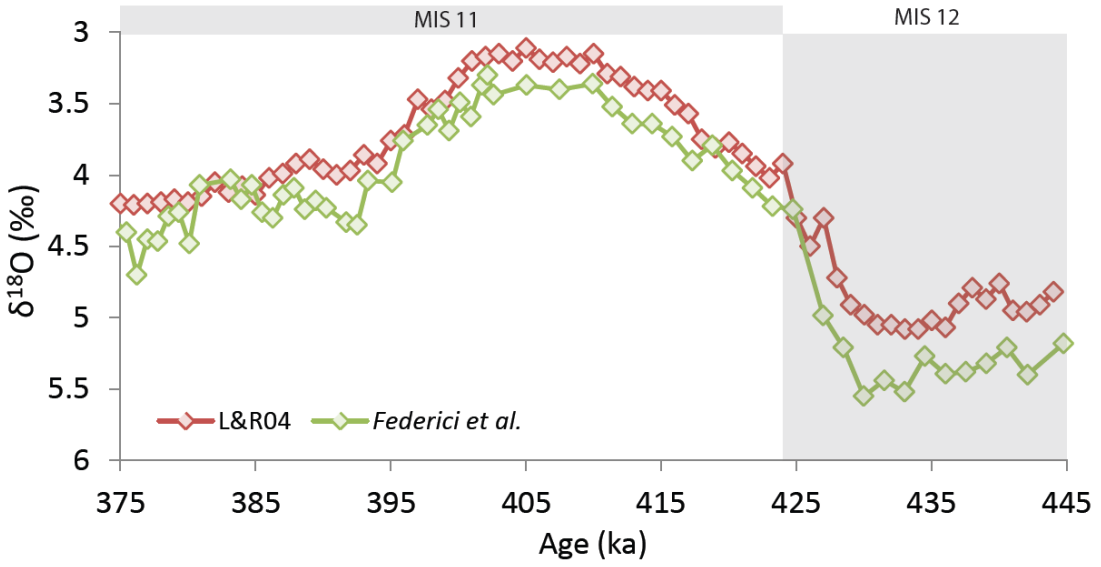

Figure 2.2. Age model constructed utilising benthic $\delta^{18}O$ measurements during MIS 12-11 for the global benthic stack [*Lisiecki and Raymo,* 2005; red] and the data used in this study [*Federici et al.*, unpublished; green]. Data included in Appendix four.

2.3 Separation, preparation and cleaning of foraminifera

Sample preparation was primarily undertaken at GNS Science. The core was sectioned into 2 cm intervals and rehydrated for 24 h, after which the sample underwent ultrasonication in *Calgon* to disaggregate any clay material. The samples were then rinsed through a 63 μm sieve to remove excess clay and silt material, and dried for 24 h at 40°C. After dry sieving, single species samples were picked from the > 150 μm size fraction. The majority of foraminifera were picked from the 212-300 μm size fraction. Two species of planktic foraminifera were separated for analysis [Fig. 1.11]; the eutrophic species *Gg. bulloides* for the entire period studied [444–374 ka] and the tropical/subtropical species *Gs. ruber* for the peak interglacial period [428-392 ka].

However, the abundance of *Gg. bulloides* and other eutrophic taxa is significantly lower during the deglacial transition [*ca*. 420 ka] at ODP 1123 and, therefore, picking a smaller size fraction [150-212 μm] was necessary to obtain enough individuals [n = 50] required for LA-ICPMS analysis.

The foraminifera cleaning procedure used prior to LA-ICPMS trace element analysis generally follows that of *Eggins et al.* [2003], except for some samples from MIS 11, which proved to be extremely fragile and could not withstand ultrasonication. The majority of the samples received ultrasonication rinses for 2-3 s in > 18.2 MΩ ultraclean water and AR-grade methanol in order to remove adhering detritus and clays. Ultrasonication proved difficult on the fragile tests frequently causing shattering and fracturing along chamber suture lines. The fragility of these samples meant that even short ultrasonication sometimes resulted in > 80% sample loss [i.e., a reduction from 50 to < 10 intact individuals], and so these samples were transferred to 1.5 mL microcentrifuge

tubes and received three 30 s vigorous agitation rinses in 1 mL of > 18.2 MΩ ultraclean water, which was allowed to settle for 3 s and then any excess fluid and contaminant phases [such as suspended clays] were removed with a pipette. The samples were then subjected to one 30 s vigorous agitation rinse in 1 mL of methanol, again followed by a 3 s settling time and removal of the supernatant. This technique is based on that of *Barker et al.* [2003]. The cleaned foraminifera samples were then dried in an oven for 24 h at 40°C. After drying, the samples were then inspected under a binocular microscope to check for any obvious signs of contaminants [e.g., Fe-Mn oxide coatings]. If contaminants were identified, the sample material was discarded.

2.4 Determination of size-normalised weights [SNW]

After cleaning and drying, *Gg. bulloides* samples were weighed using a Mettler Toledo [MX/UMX 2] ultramicrobalance, before being mounted onto an adhesive medium attached to a circular wafer of the NIST SRM 610 glass standard [*Pearce et al.,* 1997] for trace element analysis. Size-normalised weights [SNW] in core top *Gg. bulloides* follow a predictable exponential negative correlation with temperature where warmer temperatures lead to a lower test mass [Fig. 2.2], following the equation derived by *Marr et al*. [2011]:

$$T[°C] = 31.8 \times e^{-30.5 \times SNW} \; [r^2 = 0.90]$$

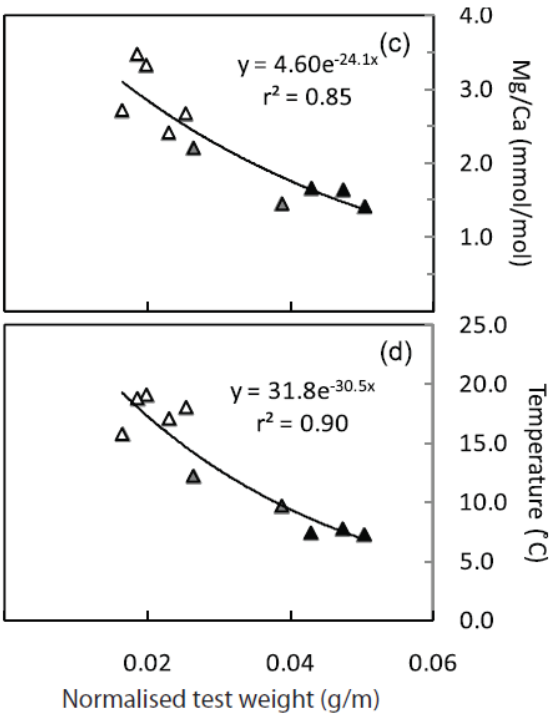

Figure 2.3. Exponential negative correlation between Mg/Ca and temperature [°C], and SNW. Symbol shading denotes sample location with open triangles representing sites bathed in warm STW and filled triangles representing SAW sites. Grey triangles represent mixed sites. Figure taken from *Marr et al.* [2011]

Following this relationship, SNW is used as a first order proxy to assess the possibility of dissolution of a given sample.

The mounted samples were then photographed using an Olympus SZX12 microscope with an Olympus DP70 camera, to provide an image to guide LA-ICPMS trace element analyses and to provide individual foraminifera images to measure test sizes using Semafore software, in order to calculate sample SNW using the equation:

$$\text{SNW} = \text{mean test weight [µg]/mean test length [µm]}$$

The mean SNW calculated for the samples analysed in this study were approximately a factor of two lighter than predicted by the Mg/Ca-derived paleo-ocean temperatures, and so further visual investigation using SEM

imaging was carried out to assess if the samples had been affected significantly by dissolution.

2.5 LA-ICPMS trace element analysis and data reduction

LA-ICPMS trace element analysis was carried out by high-resolution depth profiling utilising a New Wave deep-UV Nd:YAG [193 nm] solid state laser coupled to an Agilent 7500cs ICPMS at Victoria University of Wellington, New Zealand. A detailed description of these analytical methods is given in *Bolton et al*. [2011] and *Marr et al*. [2011]. In brief, data acquisition was achieved during ablation of a 35 µm spot for 60-120 s followed by 30 s of ablation cell washout, on both NIST SRM 610 standards and foraminifera samples. Isotopes of six trace elements [^{25}Mg, ^{27}Al, ^{43}Ca, ^{55}Mn, ^{66}Zn, ^{88}Sr] were monitored.

Mean background values were subtracted from raw data before normalising to the NIST SRM 610 values to correct for instrumental trace element fractionation effects. This raw data reduction was completed using a MATLAB script written by Prof. Euan Smith. Trace element depth profiles [Fig. 2.3] were produced automatically in Microsoft Excel using macros developed by Annette Bolton and John Creech to individually scrutinize profiles. This allowed the exclusion of outer trace-element-enriched surface veneers [*Eggins et al.*, 2003], contaminant phases inside the test cavity and altered calcite identifiable by elevated contaminant phases throughout the test [e.g., elevated Al and Mn].

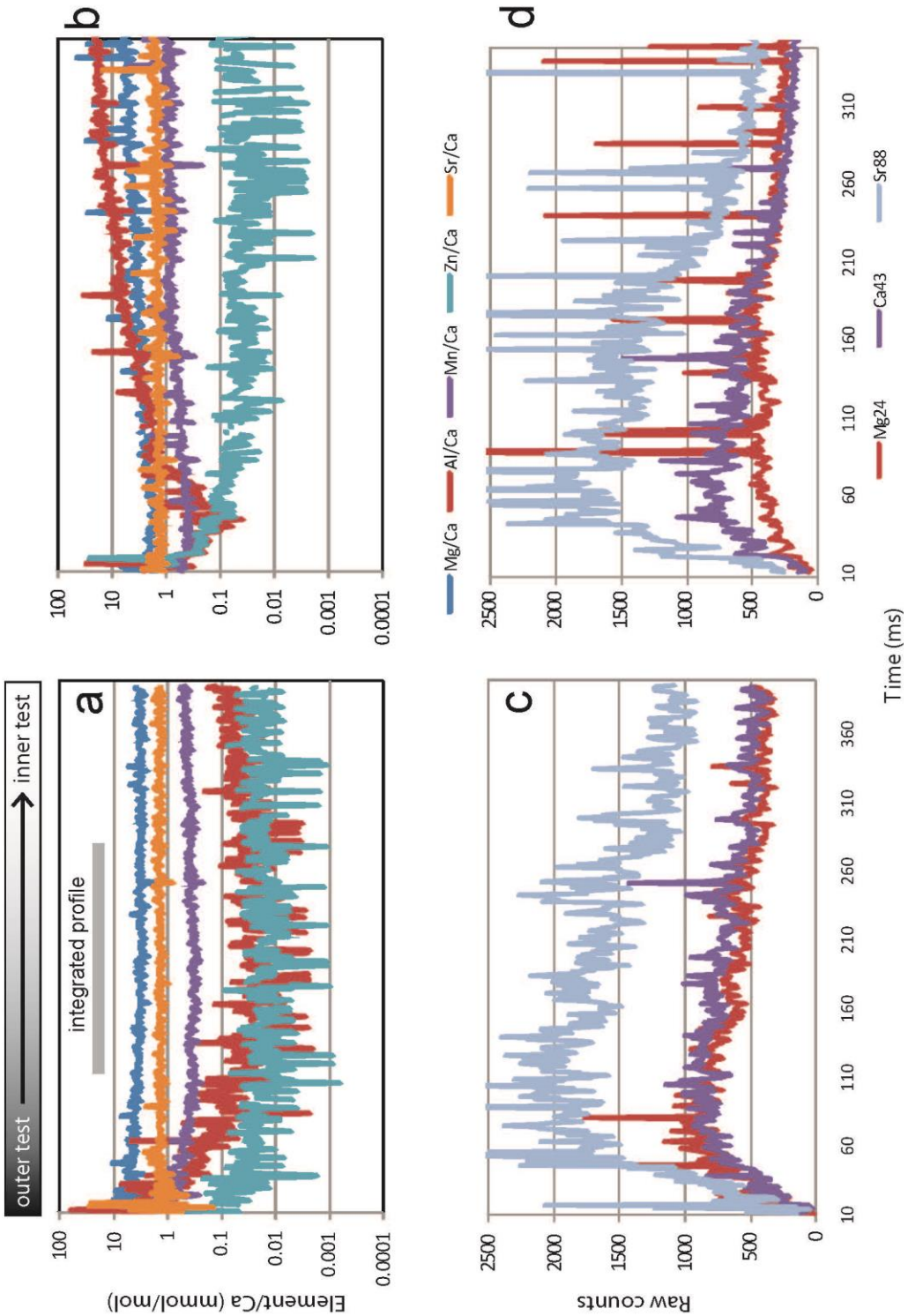

Figure 2.4. Trace element depth profiles [a,b] and their corresponding raw count plots used to determine when the test is being ablated [c,d]. a, Example of a typical profile with grey bar indicating data integrated into final measurement, excluding both the outer enriched surface veneer and section of the inner test where Al/Ca increases indicating ablation of a clay phase. b, Example of a discarded profile with elevated Al/Ca. c, raw count plot for profile a above. Where counts begin to decrease significantly the inside of the test has been reached, and the integrated section ends. d, raw count plot for profile b above.

The *in situ* LA-ICPMS technique has two main advantages over conventional solution-based ICPMS techniques for analysing Mg/Ca in foraminiferal calcite:

(1) Foraminifera specimens do not need to be crushed and undergo vigorous cleaning procedures such as oxidative or reductive techniques [*e.g., Barker et al*., 2003] to remove trace element-rich surface veneers, adhering clays, and sediment filling inner test cavities, which all have the potential to bias calculated paleo-ocean temperatures [*Eggins et al.*, 2003]. Elimination of the effects of these contaminants can be achieved through examination of LA-ICPMS trace element depth profiles through the foraminifera test wall.

(2) Intra- and inter-individual variations in foraminifera geochemistry potentially related to factors such as ontogeny, seasonality and diagenetic effects can be identified and examined and, where appropriate, excluded from mean sample data [*Bolton et al.*, 2011; *Marr et al.*, 2011]

2.6 Calculation of Mg/Ca-derived paleo-ocean temperatures

Mg incorporation into foraminiferal calcite follows an exponential endothermic relationship with a temperature sensitivity of *ca*. 10 ± 1% change in Mg/Ca per degree Celsius temperature change [*e.g*., *Eggins et al.*, 2003; *Nürnberg et al.*, 1996; *Rosenthal et al.*, 1997]. This sensitivity is about three times more than observed in experiments of Mg partitioning into inorganic calcite, suggesting that some factor other than temperature, probably of biological origin, also affects Mg incorporation into foraminiferal calcite. Furthermore, this effect has

been shown to be species-specific [*e.g., Eggins et al.*, 2003 and 2004; *Lea et al.*, 1999; *Rosenthal*, 2007]. Secondary controls on Mg incorporation into foraminifera calcite such as salinity and pH have also been demonstrated [*Lea*, 2003], however, temperature is most likely to be the first order control of average Mg incorporation into foraminiferal calcite for the two species [*Gg. bulloides* and *Gs. ruber*] analysed in this thesis [*Bolton et al.*, 2011; *Marr et al.*, 2011].

Mg incorporation into foraminiferal calcite has a relationship with temperature, which is expressed as:

$$\text{Mg/Ca [mmol/mol]} = A \exp^{[BT]}$$

where T is temperature and A and B are species-specific constants derived by calibrations from analyses of modern foraminifera that lived in known environmental conditions [*e.g., Anand et al.*, 2003; *Bolton et al.*, 2011; *Eggins et al.*, 2003; *Elderfield and Ganssen,* 2000; *Marr et al.*, 2011]. Such calibrations are ideally established by making multiple analyses of a single species of modern "core top" foraminifera from several localities in close proximity with known environmental conditions [*e.g., Anand et al.,* 2003*; Bolton et al.,* 2011*; Elderfield and Ganssen*, 2000; *Marr et al.*, 2011]. These data are then plotted on a log-linear graph with known temperature on the x-axis and Mg/Ca [mmol/mol] on the y-axis, with the intercept and slope yielding the constants A and B, respectively. When a calibration is derived it can then be applied to fossil

foraminifera of the same species from the same region to obtain paleo-ocean temperatures.

Species-specific calibrations are necessary for Mg/Ca paleo-ocean thermometry, as *Lea et al.* [1999] have shown with culturing experiments that different species of planktonic foraminifera incorporate differing amounts of Mg by up to a factor of two [this range is larger if benthic foraminifera are included]. Multi-species calibrations can be applied, but may lead to the introduction of systematic errors, and therefore multi-species calibrations should only be employed when no species-specific calibration exists such as for the analysis of an extinct species [*Anand et al.*, 2003; *Creech et al.*, 2010; *Lea*, 2003].

This study utilizes the calibration derived by *Marr et al.* [2011] for *Gg. bulloides* [Fig. 1.9]:

$$\text{Mg/Ca [mmol/mol]} = 0.952 \times e^{0.068 \times T} \; [r^2 = 0.95]$$

and the calibration derived by *Bolton et al.* [2011] for *Gs. ruber* [Fig. 1.9]:

$$\text{Mg/Ca [mmol/mol]} = 0.891 \times e^{0.067 \times T} \; [r^2 = 0.89]$$

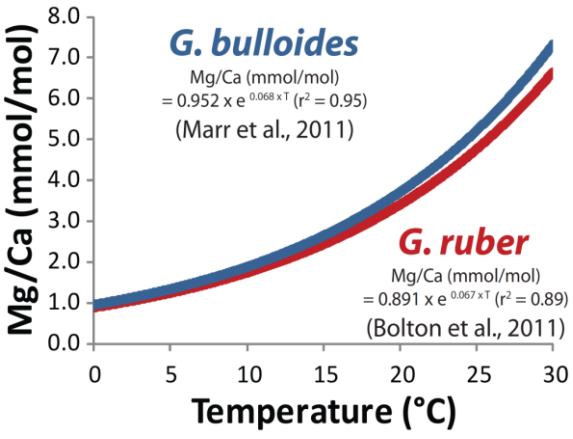

Figure 2.5. Exponential relationship between Mg/Ca [mmol/mol] and temperature [°C] for *Gg. bulloides* and *Gs. ruber*, derived from multiple foraminiferal analyses of modern core top samples of known temperatures for the offshore New Zealand region. Figure taken from *Marr et al.* [in prep].

These calibrations are specific to the analytical methodology applied in this study, as well as being derived from a similar location in the Southwest Pacific Ocean. For analysis of *Gg. bulloides,* the antepenultimate chamber [*f-2*] measurement was used to calculate paleo-ocean temperatures as this chamber has been shown to display the least intra-specimen variability and appears to record the 'average' growth conditions [*Marr*, 2009] in the shallow ocean [depth preference 50 to 200m, *Hemleben et al*., 1985]. For *Gs. ruber, Bolton et al*. [2011] found no statistically distinguishable difference between the penultimate and antepenultimate chambers [*f-1* and *f-2,* respectively] and so for this species either chamber was analysed.

2.7 Scanning electron microscopy [SEM] imaging

As noted previously, measurement of SNW revealed that test weights were lower than expected for the Mg/Ca-derived paleo-ocean temperatures following the SNW calibration of *Marr et al*. [2011], particularly during MIS 11. Given this, after LA-ICPMS trace element analysis, selected samples were transferred to a metal stub and carbon coated for SEM imaging on a JEOL JSM 6500F Scanning Electron Microscope at Victoria University of Wellington. The resultant high-resolution images were then examined for signs of diagenetic recrystallisation and dissolution.

2.8 Stable isotope analysis

High-resolution stable isotope analysis of *Gg. bulloides* and the benthic genus *Uvigerina* spp. was previously carried out on a sample subset by *Federici et al,* [*unpubl. data*]. For each analysed sample, between three and six individuals

were picked from the > 150 μm size fraction. The samples were dissolved in three drops of phosphoric acid [H_3PO_4] at 75°C and analyses were carried out on a Finnigan MAT 252 mass spectrometer equipped with an automated individual carbonate reaction "Kiel Device" at the National Institute of Water and Atmospheric Research [NIWA], Wellington. Internal precision was determined by running carbonate standards [NBS-19] as ± 0.06‰ for $\delta^{18}O$ and ± 0.03‰ for $\delta^{13}C$ and external precision [between runs] of ± 0.03‰ for $\delta^{18}O$ and ± 0.02‰ for $\delta^{13}C$. All values are normalized to Standard Mean Ocean Water [SMOW].

Chapter 3: Results

3.1 Trends in foraminiferal trace element/Ca ratios during MIS 12 to 11

Although two planktonic foraminifera species were analysed only the trace element/Ca data for *Gg. bulloides* are plotted and discussed in this section, due to the sporadic occurrence of *Gs. ruber* through the record [429-395 ka]. *Gs. ruber* is considered in Sections 3.2.4, 4.1.2 and 4.1.4 with reference to this species susceptibility to dissolution and comparison with the modern day temperature-depth relationship with *Gg. bulloides*.

Mg/Ca ratios for *Gg. bulloides* are highest in the interglacial showing the greatest magnitude of change [~1.25–2.75 mmol/mol; mean glacial and interglacial values, respectively] through the deglacial transition from 437 to 424 ka [Fig. 3.1a]. In general, chamber *f-2* of *Gg. bulloides* shows consistently slightly higher Mg/Ca values relative to chamber *f*, [Fig. 3.1a]. The percent difference between Mg/Ca values for chamber *f-2* and *f* during MIS 11 is 5% and during MIS 12 is 7% [Table 3.1]. The relatively higher Mg/Ca values of chamber *f-2* over *f* is consistent with modern core-top values obtained from the New Zealand region [*Marr*, 2009]. Offsets in Mg/Ca [Fig. 3.1a] between the two chambers most likely indicate migration with ontogeny to relatively cooler deeper water, apart from MIS 12, when this relationship appears reversed, and again during the interval *ca*. 400–405 ka, which may indicate enhanced thermal mixing of the upper water column encompassing the entire depth range of *Gg. bulloides*. During the deglacial transition the two chambers show only a small difference in Mg/Ca which may indicate either changes in the behaviour of *Gg.*

bulloides [minimal downward migration with ontogeny], or mixing and collapse in the upper water column thermal structure.

Al/Ca values in *Gg. bulloides* are generally slightly elevated in chamber *f-2* compared with *f* and show no clear changes over the studied time period, oscillating around 0.15 ± 0.05 mmol/mol [Fig. 3.1b]. The percent difference between Al/Ca values for chamber *f-2* and *f* during MIS 11 is 7% and in MIS 12 is 36% [Table 3.1]. Al/Ca is analysed as a contamination indicator for the presence of clay phases.

Mn/Ca values in *Gg. bulloides* exhibit a strong shift between average glacial and interglacial ratios [~0.08 and 0.23 mmol/mol, respectively], and the variability about these mean values is greater in the interglacial period [Fig. 3.1c]. During MIS 11, Mn/Ca values are consistently higher in chamber *f* relative to *f-2* by an average of 0.10 ± 0.05 mmol/mol [i.e., 22 and 25% during MIS 11 and the deglacial transition, respectively]. The greatest difference between the Mn/Ca values of the two chambers occurs intermittently throughout the time period, but most notably during MIS 12 [51%; Table 3.1].

Zn/Ca values in *Gg. bulloides* also show a strong shift between average glacial and interglacial ratios [~0.007 and 0.035 mmol/mol, respectively], with more variability observed during the interglacial [Fig. 3.1d]. This decreased variability during the glacial period may potentially reflect differences in sampling resolution between the glacial and interglacial periods. Like Mn/Ca values, Zn/Ca ratios show consistently higher values in chamber *f* relative to f2 of approximately 0.07 ± 0.04 mmol/mol, with the greatest difference between the two chambers characterising MIS 12 [48%; Table 3.1]. During MIS 11 and

the deglacial transition the percent difference in Zn/Ca ratios between chambers *f-2* and *f* was 22 and 24% respectively; Table 3.1.

Mn and Zn/Ca ratios [Fig. 3.1c and d] show conflicting results, with Zn/Ca converging in the two chambers at 435 to 420 ka, and Mn/Ca remaining more or less consistently offset, converging at 398 ka. This suggests that the process[es] which control the distribution and bio-availability of these trace elements in the upper water column differ.

Sr/Ca values in *Gg*. *bulloides* show little variability throughout the record [~1.37 ± 0.06 mmol/mol]. Sr/Ca is measured for analytical control and is expected to be uniform throughout profiles due to the long residence times and efficient mixing of both elements in seawater.

	MIS 11 interglacial [374–427 ka]	**Deglacial [428-434 ka]**	**MIS 12 glacial [435-453 ka]**	**Total % difference**
Mg/Ca	**5**	**4**	**7**	**4**
Al/Ca	**7**	**3**	**36**	**3**
Mn/Ca	**22**	**25**	**51**	**25**
Zn/Ca	**22**	**24**	**48**	**24**
Sr/Ca	**1**	**1**	**3**	**1**

Table 3.1 Percent difference in the trace element/Ca ratio between chambers *f-2* and *f* of *Gg. bulloides.* The larger percent differences during MIS 12 may, in part, reflect the smaller number of samples analysed for MIS 12 than for MIS 11 [n=8 and 60, respectively].

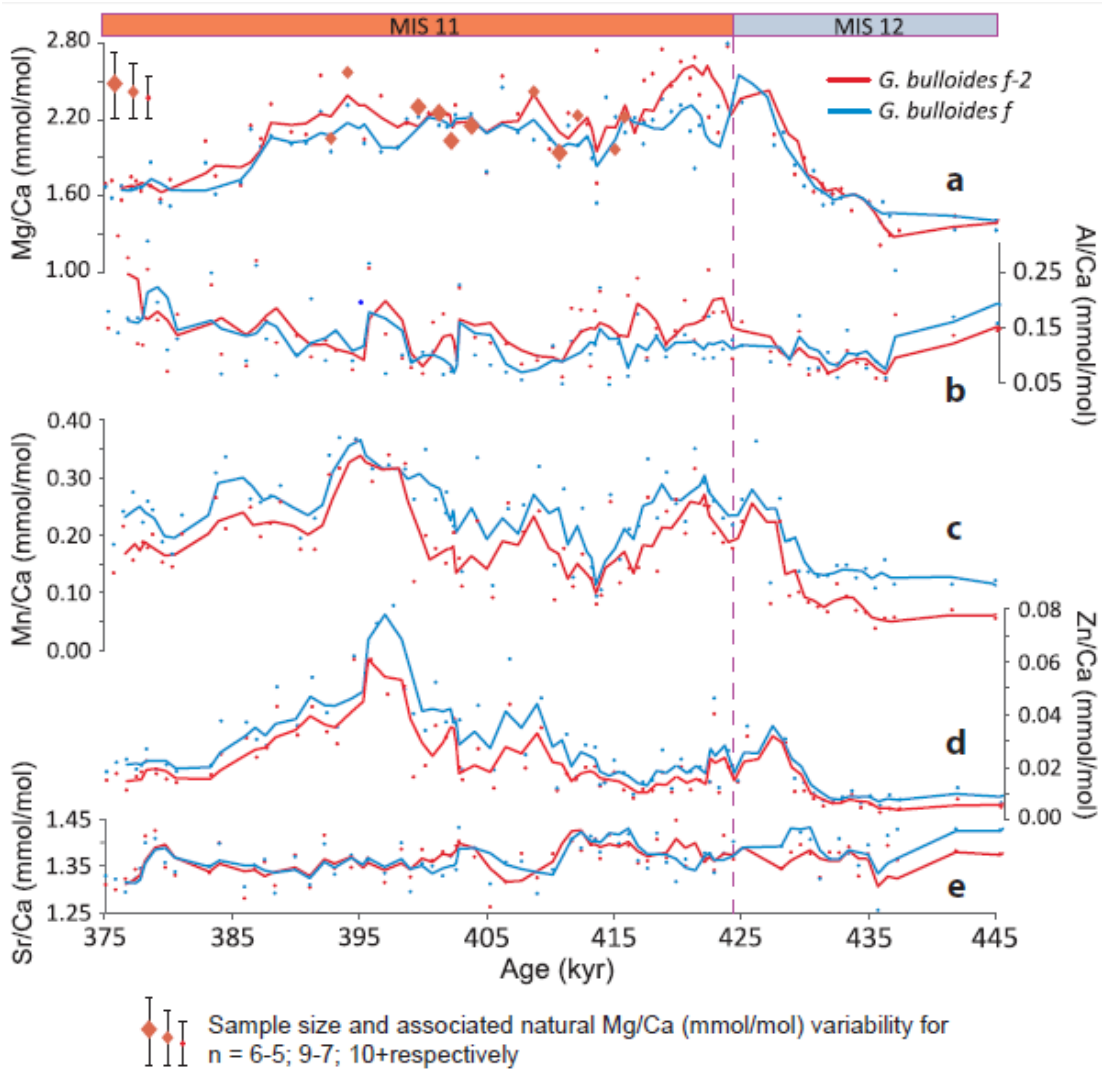

Figure 3.1. Nested trace element/Ca [mmol/mol] graphs for *Gg. bulloides* showing data for the antepenultimate chamber [*f-2*; red line] and final chamber [*f;* blue line]. The range of error in Mg/Ca [mmol/mol] for varying sample sizes is shown as different sized red diamonds.

3.2 Stable isotope data

Stable oxygen isotope data were previously acquired [*Federici et al., unpubl. data*] on a high-resolution sample subset of planktonic *Gg. bulloides* and benthic *Uvigerina spp.* [Fig. 3.2]. $\delta^{18}O$ begins to increase first in *Gg. bulloides* at *ca*. 431 kyr, followed 3 ka later by *Uvigerina spp*. The absolute change between glacial and interglacial values is similar for both species; ca. 2.4 ‰ for *Gg. bulloides* and 2.2 ‰ for *Uvigerina spp*. The early interglacial $\delta^{18}O$ record [431-402 ka] of *Gg.*

bulloides is characterised by *ca*. 10 kyr oscillations, which become more rapid on the order of several thousand years during the late interglacial. Such oscillations are not clearly observed in the benthic record.

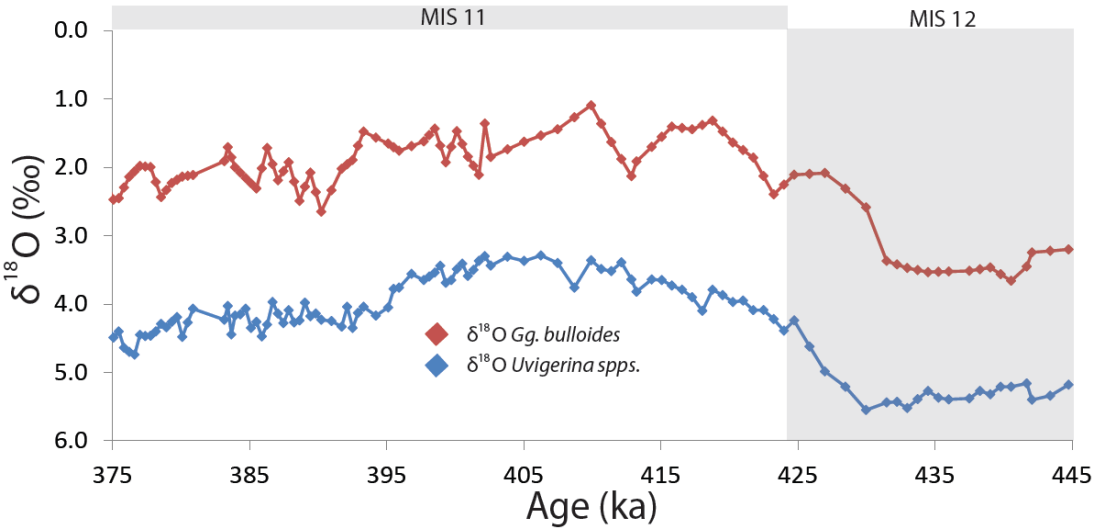

Fig. 3.2. $\delta^{18}O$ data for planktonic *Gg. bulloides* and benthic *Uvigerina spp*. [*Federici et al., unpubl. data*].

3.3 Size normalised test weights

Gg. bulloides samples were weighed and individual foraminifera were measured along the long axis, to determine the mean sample size-normalised test weight [SNW]. All samples appeared abnormally light for their size, with the MIS 11 interglacial samples up to 65 % lighter than expected for their size fraction, according to the calibration of *Marr et al*. [2011]. The MIS 12 glacial samples were less different to modern subantarctic samples compared with the differences between MIS 11 and modern subtropical samples [Fig. 3.3d].

3.4 Mg/Ca and size-normalised weight-derived temperatures

In *Gg. bulloides*, mean foraminiferal weight has been thought to be primarily controlled by CO_3^{-2} concentration where the availability of carbonate ions in the surface and deep ocean, controls the growth and preservation of $CaCO_3$ [*e.g., Barker and Elderfield*, 2002]. Calcification temperature is a secondary control and follows an inverse relationship with mean sample SNW in pristine unaltered specimens, with samples associated with warmer temperatures weighing less than those that calcified in cooler waters, as expressed by the relationship of *Marr et al*. [2011] for modern core-top assemblages [Fig 3.3d].

Mg/Ca-derived paleo-ocean temperatures calculated for MIS 12-11 and SNW-predicted temperatures show a large offset of 3 to 10°C i.e., the foraminiferal tests were lighter than they should be considering the Mg/Ca-derived temperatures [Fig. 3.3a]. The maximum difference of 65% occurred after the initial interglacial optimum warm period at 415 ka, while the remainder of MIS 11 is characterised by a ~50% difference**.** The minimum difference between SNW-predicted temperatures and Mg/Ca-derived temperatures occurred during MIS 12 and the deglacial transition [~30%; Fig. 3.3b].

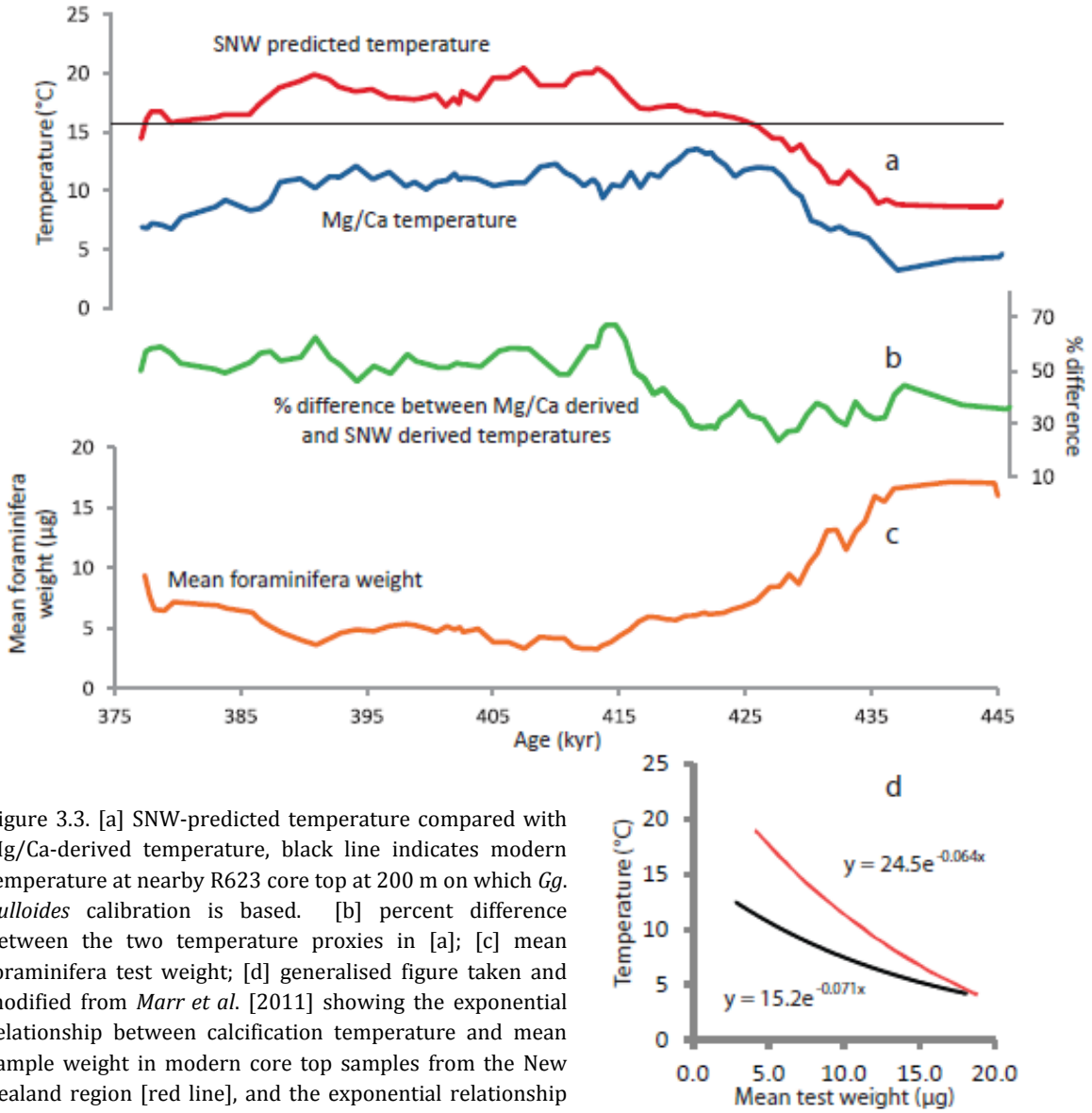

Figure 3.3. [a] SNW-predicted temperature compared with Mg/Ca-derived temperature, black line indicates modern temperature at nearby R623 core top at 200 m on which *Gg. bulloides* calibration is based. [b] percent difference between the two temperature proxies in [a]; [c] mean foraminifera test weight; [d] generalised figure taken and modified from *Marr et al.* [2011] showing the exponential relationship between calcification temperature and mean sample weight in modern core top samples from the New Zealand region [red line], and the exponential relationship between calcification temperature and mean sample weight in the samples analysed in this study [black line]. This indicates that the cooler samples analysed in this study are more similar to modern specimens, whereas samples from the warm MIS 11 period are considerably lighter [ca. 50-60 %] than expected.

3.5 Trace element/Ca error determination

Errors for natural Mg/Ca sample heterogeneity [i.e., inter-individual variations] were estimated by randomly selecting several samples throughout the MIS 12-11 to provide baseline Mg/Ca ranges [*e.g., Sadekov et al.*, 2008]. These baseline ranges for each sample were used to generate twenty random numbers and then the average standard deviation on a range of simulated sample sizes [n = 1-15; i.e., the number of foraminifera in a sample] was calculated to ascertain the size of the error [2 sd] associated with varying sample sizes. The 2sd follows a power law distribution [Appendix 3; Fig. 3.4]. These Mg/Ca [mmol/mol] errors can then be converted to a paleo-ocean temperature error, so the data obtained from smaller samples could be included in the final dataset, albeit with larger associated errors [Fig. 3.1a]. Errors for natural sample variability in the other trace elements measured were not calculated because the absolute concentrations of these other trace elements are much lower than Mg, and natural sample variability is not resolvable from analytical uncertainty. However Sr/Ca is present in sufficient levels, but inter-individual variability is low and therefore calculating errors is not necessary. Temperature errors for *Gg. bulloides* range from ± 5˚C where n = 2; ± 4˚C where n= 4; and ± 2˚C where n = 15.

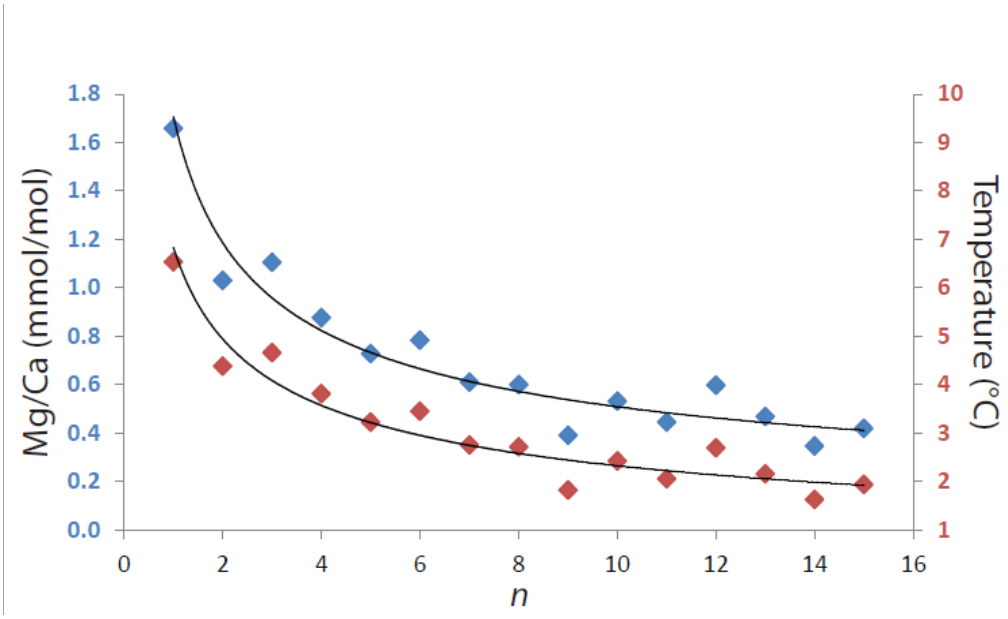

Figure 3.4. The associated error on natural intra-sample variability of *Gg. bulloides* with various sample sizes. Calculation details are described in the text and Appendix 3. Scales have been deliberately offset for ease.

3.6. Scanning electron microscopy images

If the modern SNW-paleo-ocean temperature calibration of *Marr et al*. [2011] holds for *Gg. bulloides* during MIS 12-11 at ODP 1123, the SNW-predicted and the Mg/Ca-derived paleo-ocean temperatures should be similar, however, this is not the case [Fig. 3.3.a]. Thus, during MIS 12-11 some other factors may have influenced the SNW or Mg/Ca ratios, such as low CO_3^{-2} concentration or post-mortem dissolution and recrystallisation. In that context, SEM imaging of a subset of *Gg. bulloides* tests was undertaken, examples of which are shown in Fig. 3.5. The surface textures appear to indicate that these samples have been affected by either unsatisfactory growth conditions and/or post-depositional alteration. The occurrence of one or both of these two phenomena has the potential to affect the geochemical proxies utilised in this thesis and this is discussed further in Section 3.5.2.

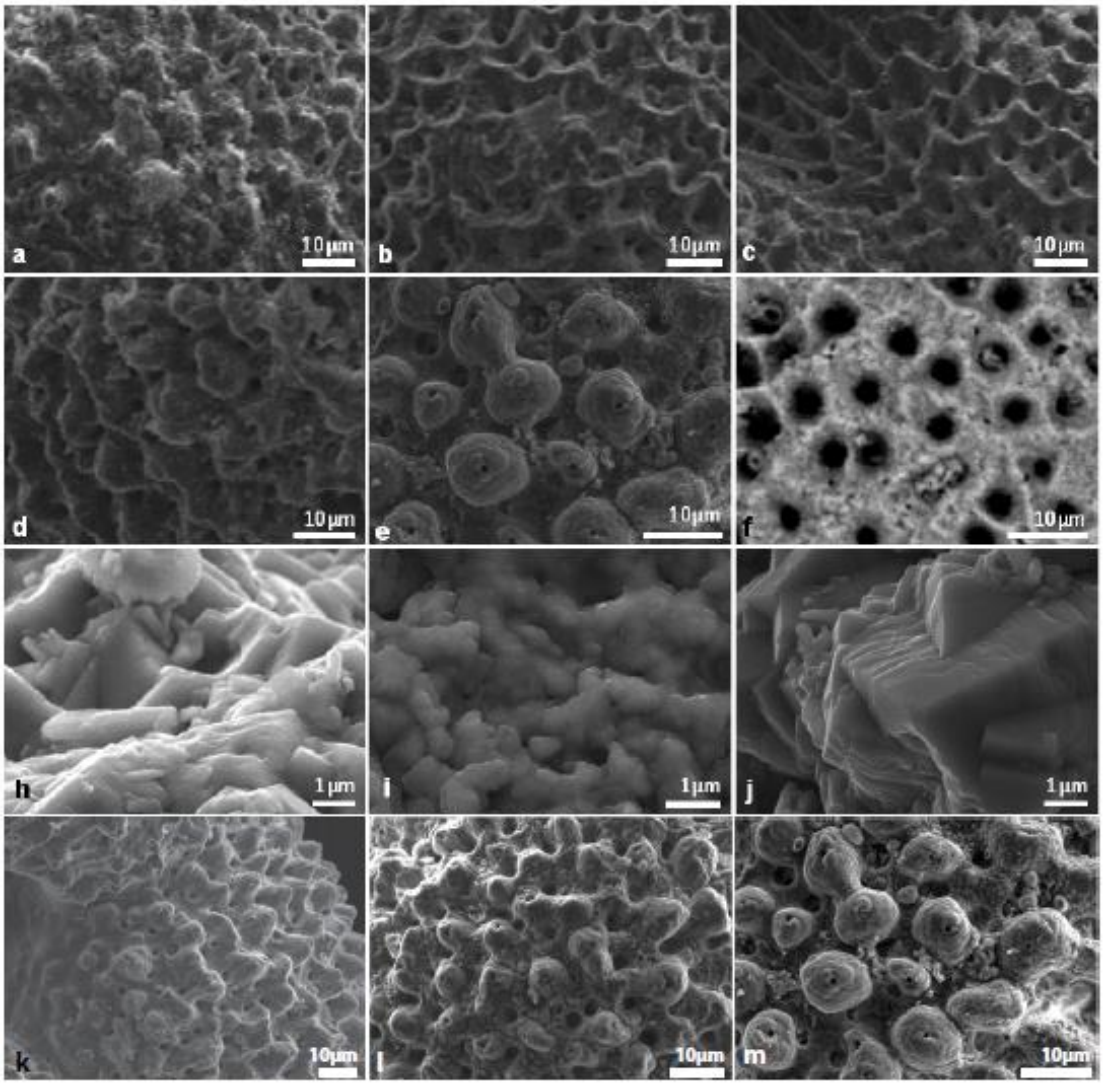

Figure 3.5. Ontogenetic variability in surface ultrastructure associated with the gametogenic and pre-gametogenic calcification of *Gg. bulloides* from NIWA plankton tow material [U2322] [**a-d**] and ODP 1123 core [**e-m**]. Images **a-c** show the textural progression of surface ultrastructures on a single *Gg. bulloides* foraminifera from youngest to oldest chamber [*f*; *f-2* & *f-3; f-1* omitted]. The preservation of well defined spines and hexagonal pore pits in **C** shows that this specimen has not been affected by diagenetic change [dissolution or post-mortem crystallisation], and has likely not yet undergone reproduction as the pseudo-cancellate surface ultra-structure is a primary feature associated with test growth. The lack of minute holes associated with re-absorption of spines at the tips of the pustules also supports the interpretation that this specimen has not undergone gametogenesis. Each successively older chamber has more well defined pseudo-cancellate ultrastructures reflecting the secretion of additional calcite layers to the entire test with the growth of each new chamber. **d:** *f-1* chamber shows the globular appearance of gametogenic calcite associated with reproduction at the end of the foraminifera's lifecycle, where a layer of secondary calcite is sourced from absorption of spines and secreted over the entire test having a smoothing effect on the primary surface ultrastructure. Image **e** is an *f-1* chamber from ODP 1123 [16.61 m – 413.6 ka] showing good preservation with well defined spine holes. The pustulose [globular] appearance is associated with the addition of gametogenic calcite, however in older chambers the pustules partially fuse and form a poorly developed anastomosing pustulose-ultrastructure. Images **f** and **j** are from different

specimens in the same sample [15.67 m – 386.7 ka], with **f** showing dissolution with enlarged primary pore spaces, and **j** showing crystallisation where the surface ultrastructure is composed of well-developed interlocking crystallites, with euhedral crystal faces. Images **h** and **i** also belong to two different individuals from a single sample [16.61 m – 413.6 ka], with **h** again showing euhedral crystals and **i** showing etched textures associated with partial dissolution and recrystallisation. **k-m**: three typical examples of *Gg. bulloides* test surface ultrastructure [**k**: 15.67m – 386.7 ka – good preservation; **l**: 16.46 m – 407.5 ka – moderate preservation; **m**: 16.16 m – 398.8 ka – moderate preservation].

3.7 Timing of changes in geochemical proxies

Irrespective of any diagenetically induced effects on the absolute values of Mg/Ca and $\delta^{18}O$, the timing and sequence of changes observed during the deglacial transition are still likely to be robust and significant. Figure 3.6 shows MIS 12-11 changes as portrayed by Mg/Ca-derived paleo-ocean temperatures, Zn/Ca and Mn/Ca measurements from the same *Gg. bulloides* individuals, and $\delta^{18}O$ measurements of *Gg. bulloides* specimens from the same sediment samples.

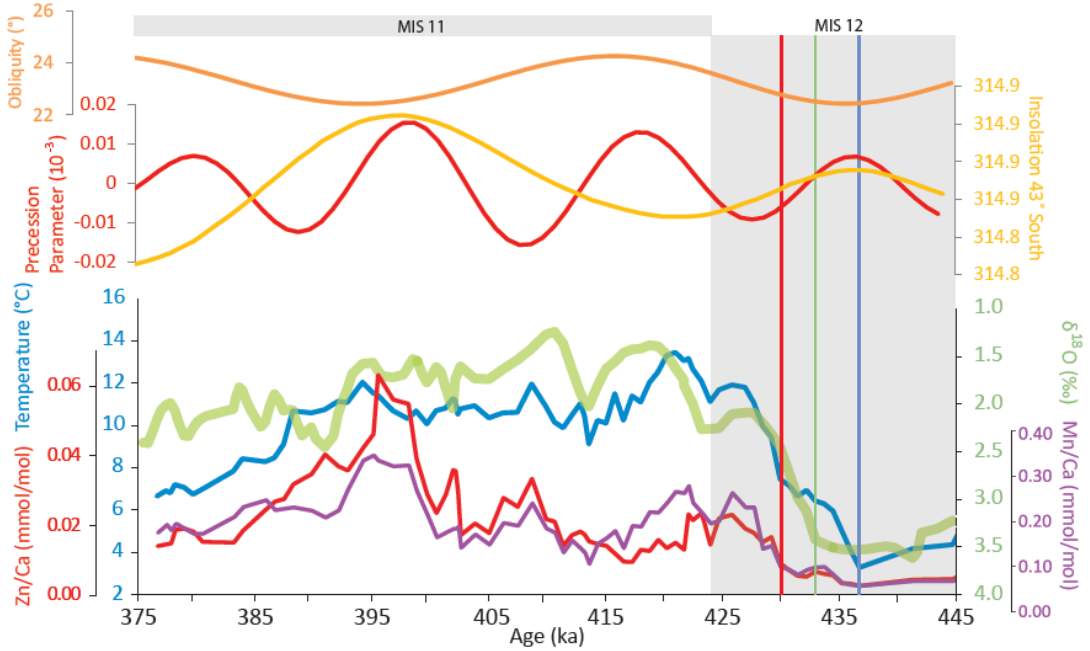

Figure 3.6. Orbital solutions, and timing and magnitude of changes in geochemical proxies during MIS12-11 at ODP 1123. Obliquity [orange curve] after Paillard et al., [1996], precession [red curve] after Lasker [2004] and insolation at 43°S [yellow curve] generated by Peter Huybers. Green curve represents $\delta^{18}O$, blue curve represents Mg/Ca-derived paleo-ocean temperatures, red curve represents Zn/Ca and purple curve represents Mn/Ca all on the same *Gg. bulloides* samples. Vertical coloured bars are referred to in the

text and represent events associated with the sequence of deglaciation at this site. Shaded grey box indicates MIS 12 based on the global benthic stack [*Lisiecki and Raymo*, 2005].

The deglacial transition is first noticeable at 437 ka when *Gg. bulloides* Mg/Ca ratios increase, [blue bar; Fig 3.6], rise steadily for 2.5 kyr then slow slightly until 430 ka. $\delta^{18}O$ values begin to lighten from 433 ka [green bar] until 425 ka. Finally Zn/Ca and Mn/Ca ratios begin to increase at 430 ka [red bar], concomitant with a rapid rise of Mg/Ca ratios. From 430 ka onwards, all three proxies change coherently until an abrupt and pronounced ACR – like event [cf., *Carter et al*., 2008], is observed at the MIS 12-11 boundary [424 ka; *Lisiecki and Raymo*, 2005] in all three proxies.

After this event at 424 ka, Mg/Ca ratios and $\delta^{18}O$ values continue to change again, with Mg/Ca leading $\delta^{18}O$ at 420 ka by 2 kyr. From 418 ka until 395 ka, $\delta^{18}O$ oscillates around an interglacial mean of 1.6‰, with the exception of another excursion to lower Mg/Ca ratios and heavier $\delta^{18}O$ values at 413 ka. For the remainder of MIS 11, $\delta^{18}O$ increases to *ca*. 2.2‰. After reaching maximum values at 420 ka, Mg/Ca ratios record a cooling event at 413 ka, accompanied by increased $\delta^{18}O$ values, followed by relatively stable conditions until 388 ka when Mg/Ca ratios begin to decrease markedly from paleo-ocean temperatures of 11° to 7°C. Zn/Ca and Mn/Ca ratios reached initial maxima at *ca*. 426 ka and then slowly increase to a strong peak at 395 ka, before gradually decreasing through the rest of the record. However, the youngest part of the Zn/Ca and Mn/Ca record [376–384 ka] still has higher Zn/Ca and Mn/Ca ratios than MIS 12.

Superimposed on these relatively long-term trends are small scale perturbations where Mg/Ca, Zn/Ca and Mn/Ca show small increases, accompanied by reductions in $\delta^{18}O$ at 413, 402, 396 and 378 ka.

Chapter 4: Discussion

4.1 Southwest Pacific Ocean marine carbonate system during MIS 11

In the modern Southwest Pacific Ocean, SNW of *Gg. bulloides* follows a predictable exponential inverse relationship with calcification temperature [Fig. 3.3d], with foraminifera that calcify in warmer waters consistently having lower SNW than those that calcify in cooler waters [*Marr et al*., 2011]. SNW has been utilised as a CO_3^{-2} concentration proxy [*de Villiers et al.,* 2005 *and references therein*] and test weight appears to be, in part, strongly controlled by CO_3^{-2} concentration in some foraminifera species including *Gg. bulloides* [*Barker and Elderfield*, 2002; *Bijma et al.*, 2002]. However, measured SNW of *Gg. bulloides* in this study showed that its tests were on average ~35% lighter during the MIS 12 glacial period and ~60% lighter than expected during the MIS 11 interglacial period, compared with modern *Gg. bulloides*.

In addition to normal background glacial-interglacial variation in preservation of foraminifera, the varying preservation states [Fig. 3.5] throughout MIS 12-11 from ODP 1123 may result from one or some combination of three different factors occurring in different oceanic and sedimentary environments:

(1) Non-ideal or marginal growth conditions in the upper ocean and/or during transport to the sea floor may mean that foraminifers were calcifying at the edge of their tolerance range to form thinner tests [*Bijma et al*., 2002; *Spero et al.,* 1997]. Enhanced global marine carbonate production and storage in shallow neritic environments such as coral

reefs during MIS 11, might have lowered the CO_3^{-2} concentration of ambient surface ocean water [*Droxler et al*., 2003; *Zeigler et al*., 2003], meaning that foraminifera ontogeny was taking place in conditions unsatisfactory for healthy unimpeded calcification. This could result in thinner test walls and therefore lower test mass overall as has been shown in laboratory experiments and modern natural environments [*Barker and Elderfield,* 2002; *Zhong and Mucci*, 1989; *Zuddas and Mucci*, 1998]. Furthermore, low CO_3^{-2} concentration impedes Mg incorporation into the test, so not only would the tests be anomalously light, but they may also record erroneously low temperatures [*Regenberg et al*., 2006; *Russell et al*., 2004] and an anomalous $\delta^{13}C$ signature. However, low CO_3^{-2} concentration in the surface ocean should be detectable in the EDC ice core record as corresponding high atmospheric CO_2 concentrations relative to pre-industrial levels [*ca*. 280 ppm for interglacials of the past 850 kyr], and this is not the case [*EPICA Community Members,* 2004]. *Barker et al*. [2006] were able to model the same CO_3^{-2} concentration lowering in the surface ocean during MIS 11 via coccolithophorid blooms without requiring excessive atmospheric CO_2 levels relative to the pre-industrial level. A similar rise in atmospheric CO_2 and associated lowering in ocean CO_3^{-2} concentration is being observed in the modern ocean where excessive anthropogenic atmospheric CO_2 concentrations are being absorbed by ventilation in surface and intermediate waters [*ACE CRC*, 2008; *Bindoff et al*., 2007; *Orr et al*., 2005]. This is likely to cause shoaling of the aragonite and calcite saturation horizons in the coming decades [*Feely et al*., 2002; *Orr et al*., 2005] narrowing the

environment where uninhibited test calcification can occur free from dissolution [*Feely et al*., 2002]. Based on measurements from the WOCE/JGOFS global CO_2 survey [1991 to 1996] and previous studies, *Feely et al*. [2004] estimated that of the $CaCO_3$ produced in the upper Pacific Ocean, 60-80% is dissolved in the top 1000 m of the water column before reaching the sea floor.

Atmospheric pCO_2 levels during MIS 11 do not suggest that the CO_3^{-2} concentration of the upper ocean was significantly different from the modern ocean. This means that unless the atmosphere and ocean carbon system operated rather differently to modern times and were decoupled during MIS 11, the lower surface ocean CO_3^{-2} concentration is unlikely to be the cause of the consistently low SNW measured in *Gg. bulloides*.

(2) Dissolution of foraminiferal tests can occur at the sea floor when cold, corrosive bottom waters are relatively enriched in dissolved CO_2 and have a corresponding low CO_3^{-2} concentration. In this case, even if the organisms were able to calcify large, heavy thick-walled tests in the shallow ocean, they may experience dissolution in the benthic environment. ODP 1123 lies in 3290 m water depth, just below the modern calcite saturation horizon [~3100 m], beneath which ocean water becomes under-saturated with respect to calcite [*Feely et al*., 2002]. The modern lysocline and carbonate compensation depths are 4300 and 4600 m, respectively, although dissolution is known to occur at much shallower depths and is likely to be closer to the calcite saturation horizon [*Bostock et al*., 2011]. On the basis of some of the highest benthic

$\delta^{13}C$ values during the MIS 11 interglacial for the last 1 Ma at ODP 1123, *Hall et al*. [2001] suggested that the enhancement of $\delta^{13}C$ values reflected increased NADW production. It was argued that more NADW was delivered to the core site entrained within lower Circumpolar Deep Water [2800 to 3900 m water depth; *McCave et al.*, 2008]. This influx of old CO_2-rich waters could have displaced the calcite saturation horizon leading to corrosion and diagenetic alteration of the foraminiferal tests.

In this case, diagenetically unaltered test weights in *Gg. bulloides* reflect CO_3^{-2} concentration and other second-order influencing factors such as nutrient bio-availability during calcification, whereas descent in the water column with ontogeny or pre-burial, post-mortem diagenetic alteration would cause secondary overprinting by the deep water CO_3^{-2} signal [*Barker and Elderfield,* 2002]. For this study, the foraminifera have clearly experienced a degree of secondary alteration. However, without knowing the initial test mass and calcification conditions the ability to accurately quantify the amount of dissolution is not possible, except to note that when compared to the fragmentation ratio of *Crundwell et al*. [2008] on the same samples, the low degree of fragmentation [< 10%] suggests dissolution was not sufficiently pronounced to facilitate extensive test breakage.

(3) Diagenetic alteration can be a post-burial process affecting foraminiferal preservation due to increasing pressure and temperature with increasing burial depth and anaerobic decomposition of organic matter producing an acidic environment causing *in situ* dissolution of $CaCO_3$.

$CaCO_3$ is less stable at higher pressures, so with increasing burial in the appropriate lithology [e.g., carbonate ooze is more susceptible than more impermeable clay] *in situ* localised dissolution and recrystallisation can occur [*Lea*, 2003]. Previous studies on the ODP 1123 core extend back to 1.2 Ma, and do not show increasing influence of this diagenetic effect, suggesting that diagenesis in the sediment column after burial may not be important [*Bolton*, 2011; *Crundwell et al*., 2008; *Elderfield et al*., 2010; *Hall et al*. 2001]. In fact, traditional dissolution proxies such as foraminiferal fragmentation indices and planktonic/benthic ratios applied to the whole 1.2 Ma sediment column, do not identify dissolution to be either increasing down core or significant in MIS 11 [*Crundwell et al*., 2008].

Decomposition of organic matter is also unlikely to be significant during MIS 11 as suggested by the findings of *Lean and McCave* [1998] who measured percent carbonate, percent carbon and magnetic susceptibility for the period MIS 6-1 on the CHAT 1K core which is close to ODP 1123 [Fig. 1.3]. *Lean and McCave* [1998] showed that during interglacials MIS 1 and 5e, the biogenic carbonate burial flux declined but this occurred in the presence of a low flux of organic carbon and elevated magnetotactic bacteria indicative of oxic conditions. Such an environment would not be favourable for reducing the benthic pH through decomposition of organic material. In contrast, glacial periods MIS 2 and 6 were accompanied by an elevated organic burial flux, low biogenic carbonate and less oxic conditions [*Lean and McCave*, 1998] that potentially favoured carbonate dissolution. Furthermore, as the organic carbon flux

declined over the MIS 2-1 and MIS 6-5 transitions, the carbonate flux peaked. Similar observations were made at DSDP 594 on the Campbell Plateau by *Kowalski and Meyers* [1997]. This leads to the conclusion that post-depositional dissolution under reduced pH instigated by decaying organic material was not likely to be a prominent post-depositional process during MIS 11.

4.2 Dissolution and its potential effect on geochemical proxies

Recognition of some alteration of foraminiferal tests [e.g., Fig. 3.5; Section 4.1.1] has possible implications for the geochemical proxies utilised in this study, as Mg/Ca and $\delta^{18}O$ are thought to be affected by dissolution and recrystallisation [*Lea*, 2003]. $\delta^{18}O$ in foraminiferal calcite is principally controlled by the calcification temperature and the $\delta^{18}O$ of ambient seawater, which in turn reflect global ice volume and local salinity [*Emiliani*, 1955; *Epstein et al.*, 1953]. Dissolution causes $\delta^{18}O$ to bias towards heavier values, erroneously indicating some equivocal combination of lower calcification temperatures, greater global ice volume and/or increased local salinity [*Lea*, 2003].

With regards to Mg/Ca ratios, most species of planktonic foraminifera, to differing degrees, are thought to secrete their calcite test heterogeneously with alternating high- and low-Mg bands [*e.g., Anand and Elderfield*, 2005; *Erez*, 2003; *Sadekov*, 2008]. The presence of the Mg^{2+} cation warps the delicate calcite crystal structure because of the large ionic size difference of Ca^{2+} and Mg^{2+}, making the high-Mg calcite bands within the test inherently more unstable [*Brown and Elderfield*, 1996; *Lohmann*, 1995]. In theory and laboratory dissolution experiments on selected species, preferential dissolution of the

Mg/Ca-rich bands lowers the overall bulk Mg/Ca value, which results in a corresponding lower Mg/Ca-derived paleo-ocean temperature [*Brown and Elderfield*, 1996; *Rosenthal et al.*, 2000]. More recently, using the same micro-analytical technique as used in this study [LA-ICPMS], *Sadekov et al*. [2010] found that two well-banded species, *Globigerinoides sacculifer* and *Orbulina universa,* do not undergo preferential dissolution of the Mg-rich portions of the test. Both of these species are symbiont-bearing and previous studies [*e.g*., *Anand and Elderfield*, 2005; *Erez*, 2003] have shown that such species display more distinct high-Mg bands than non-symbiont-bearing species. Therefore, in theory, symbiont-bearing species are more prone to preferential dissolution [*Sadekov*, 2008]. The degree to which preferential dissolution of Mg-rich portions of the test affects the species analysed in this study [*Gg. bulloides* – non-symbiont bearing and *Gs. ruber* – symbiont bearing] is unclear.

One of the key research questions of this thesis is whether the geochemical data are robust, when recognizing the low SNW in *Gg*. *bulloides*. Multiple lines of evidence suggest that this is the case, and the Mg/Ca-derived paleo-ocean temperatures are accurate and have not been significantly altered by either low CO_3^{-2} concentration or dissolution, and these points are now discussed sequentially.

1, *Comparison with other Quaternary interglacial periods in the ODP 1123 core*.

2, *Natural intra- and inter-test homogeneity in Gg. bulloides and Gs. ruber.*

3, *Failure of traditional dissolution proxies to recognise dissolution during MIS 11*.

4, *Degree of absolute temperature change recorded in Gg. bulloides from MIS 12 to 11*.

5, *Temperature difference between Gs. ruber and Gg. bulloides.*

6, *Greater nutrient availability during MIS 11 and faster calcification rates.*

7, *Comparison of test wall thickness in modern core top and MIS 11 Gg. bulloides.*

8, *Subtle differences in trace element ratios between chambers f-2 and f in Gg. bulloides are preserved*.

1, *Comparison with other Quaternary interglacial periods in the ODP 1123 core*. Mg/Ca and $\delta^{18}O$ values obtained by *Greaves* [2008] on the same species [*Gg. bulloides*] are similar throughout the ODP 1123 core from MIS 12, and 10 to 1. However, the SNW values from MIS 10-1 are not erroneously light [MIS 11 samples were not analysed by *Greaves* [2008] due to a lack of *Gg*. *bulloides* in the 300-355 μm size fraction, interpreted as evidence for dissolution]. Peak interglacial Mg/Ca values for MIS 7 exceed both the modern Mg/Ca value [~ 2.2 mmol/mol; *Marr*, 2009] and the mean MIS 11 Mg/Ca value [2.2 mmol/mol], but do not reach or exceed mean peak MIS 11 optima Mg/Ca values [2.6 mmol/mol *ca*. 422 ka]. MIS 11 stands out in the context of the *Greaves* [2008] study when compared to subsequent Quaternary interglacials as a prolonged interglacial period, similar or slightly warmer than the later interglacial periods [MIS 9, 7, 5 and 1].

Peak MIS 11 has higher Mg/Ca ratios [2.6 mmol/mol] and if we assume that mean MIS 11 temperatures were only a few degrees warmer than the mean modern temperatures, as indeed our data and that of others suggest [*e.g*.

Crundwell et al., 2008], then this implies that the degree to which dissolution has actually reduced the original Mg/Ca values is likely to be small. Thus the temperature data generated in this study can be taken as a minimum estimate of temperature during MIS 11.

2, *Natural intra- and inter-test heterogeneity in Gg. bulloides and Gs. ruber.*

This in turn suggests that symbiont-barren *Gg. bulloides* may secrete their calcite tests more homogenously than other foraminifera species. The lack of symbionts may be responsible for the lack of alternating high and low-Mg bands [*Sadekov*, 2008], and thus any dissolution may not have significantly altered the original Mg/Ca values, as discussed in section x.

Anand and Elderfield [2005] measured Mg/Ca ratios by element mapping on an electron microprobe in transects across chamber walls in three *Gg. bulloides* specimens. These authors found some evidence of heterogeneous intra-chamber Mg/Ca variability in *Gg. bulloides*, but this was not as pronounced as other species such as symbiont-bearing *O. universa* [*Eggins et al*., 2004], *Gs. ruber* and *Globigerinoides sacculifer* [*Sadekov*, 2008], which showed systematic cyclic Mg/Ca variations through the test walls on the order of 4 mmol/mol. The intra-chamber Mg/Ca differences measured in three specimens of *Gg. bulloides* on chamber *f-2* by *Anand and Elderfield* [2005] were variable, ranging from < 1 to 5 mmol/mol. This suggests that natural intra-sample variability is large and any dissolution would serve to homogenise this natural variability. Foraminifera exhibit biological mediation over the incorporation of Mg into their calcite tests, as evinced by a higher temperature sensitivity and around three times less Mg incorporated than the thermodynamic predictions suggest. This biologic control or 'vital effect', is thought to be the main source of this

intra-chamber chemical variation, rather than measuring actual temperature change by vertical migration in the water column [*Erez*, 2003; *Lea et al*., 1999; *Lea*, 2003; *Rosenthal et al*., 1997]. If this is the case, and dissolution only serves to lessen the intra-test heterogeneity, then even the absolute Mg/Ca-derived paleo-ocean temperatures calculated from data obtained in the study for *Gg. bulloides* are relatively robust.

Gs. ruber has a higher dissolution ranking than *Gg. bulloides* [*Berger*, 1968] and displays systematic cyclic high- and low-Mg bands through the test walls [*Sadekov*, 2008]. Thus, even small amounts of dissolution may lower the overall Mg/Ca ratio of *Gs. ruber* if preferential dissolution of the high-Mg bands does in fact occur in nature. This means that the paleo-ocean temperatures derived from Mg/Ca analyses on *Gs. ruber* may be less reliable than those derived for *Gg. bulloides*. However, *Sadekov et al*. [2010] did not observe significant bulk Mg/Ca values change when performing successive acid leaches of two symbiont-bearing species with alternating high- and low-Mg bands similar to *Gs. ruber*. Therefore, it is important to compare other estimates of paleo-ocean temperature generated from the same core to assess if dissolution is a problem for this species.

3, *Failure of traditional dissolution proxies to recognise dissolution during MIS 11*.

While the MIS 11 foraminifera studied in this thesis may be affected by either poor calcification conditions and/or post-mortem alteration as potentially suggested by low SNW and SEM images of tests [Figs. 3.5 and 3.7], traditional proxies used to assess dissolution fail to conclusively show this effect. Percent fragmentation index and planktonic/benthic ratios do not show any significant spikes during MIS 11 or 12 in the ODP 1123 core. Moreover, the percent

carbonate is high, varying between 60–80% [*Crundwell et al*., 2008]. Therefore, faunal assemblage derived SST together with the dissolution proxies provide a robust paleo-environmental framework, if the faunal assemblage has not changed significantly due to dissolution [*Crundwell et al*., 2008]. MIS 11 SST derived via transfer functions from the ODP 1123 MIS 11 faunal assemblages are similar or higher than MIS 11 SST from other, shallower depth cores in the region [*Hayward et al*., 2008; 2012] suggesting that the ODP 1123 assemblages are representative of the paleo-environmental conditions.

4, *Degree of absolute temperature change recorded in Gg. bulloides from MIS 12 to 11.*

In addition, the degree of change in Mg/Ca ratios from MIS 12 to MIS 11 confirms that a significant surface signal is still retained, with a 10°C temperature increase observed, which has not been erased by diagenetic overprinting in the benthic realm [*ca*. 3°C MIS 12-11 change in benthic *Uvigerina spp.* found by *Elderfield et al*. [2010] at ODP 1123]. Furthermore, this 10°C change is similar in magnitude to the paleo-SST change for the same site calculated by *Crundwell et al*. [2008] and at other New Zealand sites [*Hayward et al*., 2008; 2012] all of which used the Artificial Neural Network 25 [ANN_{25}] technique to estimate paleo-ocean temperatures.

5, *Temperature difference between Gs. ruber and Gg. bulloides.*

The difference between the Mg/Ca-derived SSTs from *Gs. ruber* and the ANN_{25} SSTs from *Crundwell et al*. [2008] is variable [0-5°C; Fig. 4.1] providing some indication of the amount of dissolution that may have been experienced by the *Gs. ruber* samples analysed expressed as an absolute temperature difference, if one assumes the ANN_{25} SSTs are robust. However, comparison with the modern

temperature difference between *Gs. ruber* and *Gg. bulloides* at this core site by *Bolton* [2011] is the same as calculated in this study [*ca*. 4°C] suggesting that MIS 11 *Gs. ruber* may in fact be recording accurate paleo-ocean temperatures, and perhaps the ANN_{25} record is over estimating true paleo-ocean temperatures [Fig. 4.1].

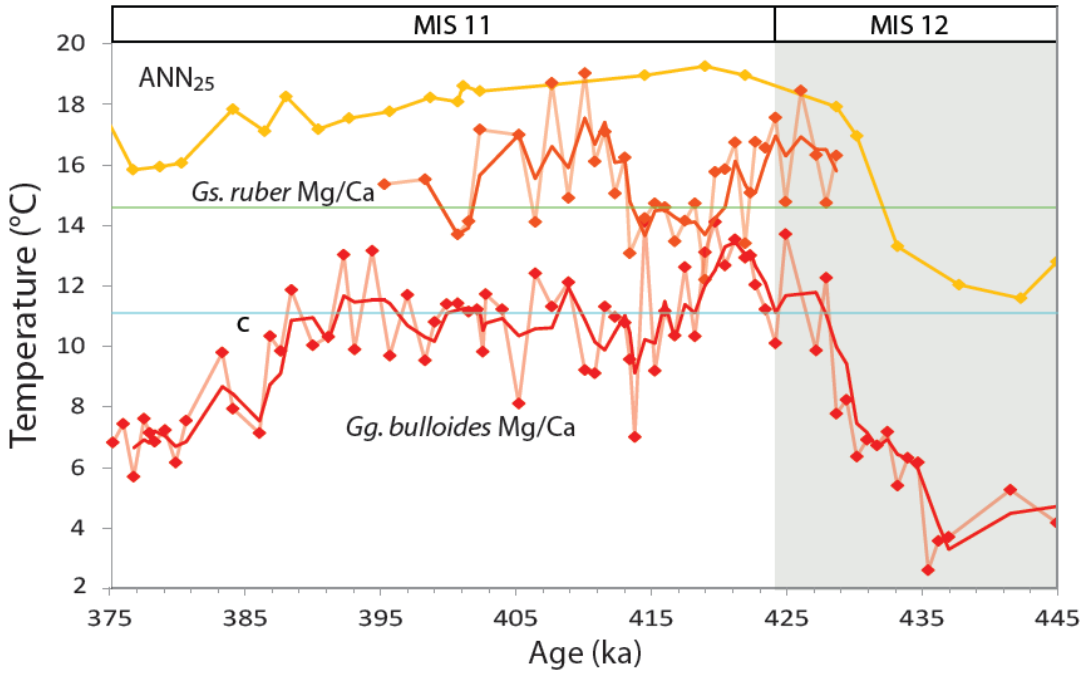

Figure 4.1. Two SST and one sub-SST record from ODP 1123. The offset between the ANN_{25} SST record [*Crundwell et al*., 2008] and the *Gs. ruber* Mg/Ca-derived paleo-ocean temperature record from this study may represent dissolution, which would result in erroneously low SST on the latter record. However, if an assumed depth of 200 m is assigned to *Gg. bulloides*, this suggests that the *Gs. ruber* record may not be erroneously low, as the temperature difference between the two records is similar to modern conditions [*ca*. 4°C], except perhaps for the period 425-415 ka. Green line represents modern SST [mean 0-50 m] at ODP 1123 core top on which *Gs. ruber* calibration is based [*Bolton et al*., 2011]. Blue line indicates modern temperature at nearby R623 core top at 200 m on which *Gg. bulloides* calibration is based [*Marr et al*., 2011]. Solid line for both Mg/Ca records is a three point running mean.

Berger [1968] ranked *Gs. ruber* as the most susceptible species of planktic foraminifera to dissolution. *Gg. bulloides* ranked 6th out of 15, with other subsequent studies more or less in agreement [*e.g., Malmgren*, 1983]. This suggests that if the samples analysed were affected by dissolution, the amount

experienced by *Gg. bulloides* is likely to be less than that of *Gs. ruber*, and the temperature range of the upper 200 m of ocean during MIS 11 between the known modern depth ranges of *Gs. ruber* [0-50 m; *Wilke et al*., 2009] and *Gg. bulloides* [50 - 200 m; *Hemleben et al*., 1985] may be greater than the Mg/Ca record generated in this study implies [e.g., modern temperature at 50 m = 16°C, 100 m = 14°C and 200 m = 12°C; Fig. 4.2; *Schlitzer*, 2002] and the mean Mg/Ca temperature offset in this study between *Gs. ruber* and *Gg. bulloides* is 4°C.

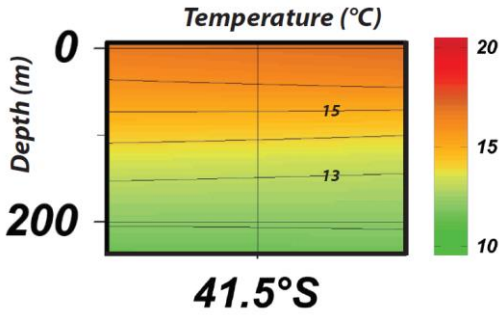

Figure 4.2. Modern upper ocean thermal structure near ODP 1123. Conductivity temperature depth point 41°S, 170°W [*Schlitzer*, 2002].

6, *Greater nutrient availability during MIS 11 and faster calcification rates. Aldridge et al*. [2012] found that macronutrient availability is a strong control on SNW variation in *Gg*. *bulloides*, where greater nutrient availability leads to lower SNW. This implies, not surprisingly, that the eutrophic species respond to greater macronutrient availability, calcifying thinner tests overall at a greater rate. During MIS 11, greater incursion of micronutrient-rich STW at the ODP 1123 led to increased micronutrient availability [Sections 3.5.3 and 3.5.4], which may have resulted in lower SNW in *Gg. bulloides*.

7, *Comparison of test wall thickness in modern core top and MIS 11 Gg. bulloides.* Following on from point 5 above, visual comparison of modern core top *Gg*. *bulloides* from the New Zealand region [*Marr*, 2009] and MIS 11 specimens from ODP 1123, shows that on average MIS 11 specimen test walls were ca. 50 %

thinner but not as a clear result of dissolution. This supports the interpretation that the low SNW encountered in *Gg*. *bulloides* in this study is likely to be a primary feature and has not significantly affected the geochemical proxies.

8, *Subtle differences in trace element ratios between chambers f-2 and f in Gg. bulloides are preserved*.

Had the *Gg*. *bulloides* specimens been influenced by the amount of dissolution needed to remove up to half of their test mass, the subtle differences in chamber *f-2* and *f* trace element ratios would have been homogenised, and this is not the case.

4.3. Implications of unusual Southwest Pacific Ocean chemistry during MIS 11

What are the implications of the low SNW found in *Gg. bulloides* for the chemical characteristics of the ocean during MIS 11 at ODP 1123? It is established that a global-scale dissolution event, the mid-Bruhnes dissolution interval, occurred from 600 to 200 ka with its peak centred on MIS 11 [*e.g., Barker et al*., 2006]. What is uncertain, however, is the cause of the mid-Bruhnes dissolution interval and how the global carbon cycle operated during that interval in order to cause widespread dissolution, without a corresponding rise in atmospheric CO_2 [*EPICA Community Members*, 2004]. Conditions were clearly different to the present and other Quaternary interglacial periods in the Southwest Pacific as evinced by the good preservation of foraminiferal tests and SNW range in line with the modern calibration in the majority of the ODP 1123 core [*e.g., Crundwell et al*., 2008; *Elderfield et al.,* 2010; *Greaves,* 2008; *Hall et al*., 2001]. This raises the question as to whether, in the context of the mid-Bruhnes

dissolution interval, MIS 11 is a suitable analogue for the chemical response of the ocean to future climate warming? In the Pacific Ocean, the lysocline generally appears to follow a pattern of shoaling during interglacials and deepening during glacials [*e.g., Hodell et al*., 2001]. ODP 1123 sits just below the modern calcite saturation horizon and has been used to generate reliable geochemical paleoclimate proxy data in other studies [*e.g., Bolton et al.,* 2011; *Elderfield et al.,* 2010; *Greaves,* 2010]. However, intermittently throughout the ODP 1123 record, dissolution has occurred indicating possible episodic shoaling of the calcite saturation horizon [*Greaves*, 2008; *Elderfield et al*., 2010].

4.4 Mn and Zn/Ca records

Both Mn/Ca and Zn/Ca ratios have been shown to be higher in foraminifers from modern Southwest Pacific core top assemblages located in STW, north of the STF, as compared with assemblages located in SAW to the south [*Marr,* 2009]. Furthermore, a surface water mass transect across the Chatham Rise also shows Zn to be enriched in STW relative to SAW [Fig. 4.3; *Ellwood*, pers. comm., unpubl. data]. Although the exact pathway by which these elements are biomineralised into foraminiferal calcite is not well understood, there is a clear difference between foraminifera that calcified in STW and SAW. Moreover, the absolute Mn/Ca and Zn/Ca values obtained in this study are similar to the modern unaltered core top values obtained by *Marr* [2009] by the same LA-ICPMS method [Fig. 4.4]. This indicates that these trace elements may be homogeneously distributed throughout the test as a single phase and any dissolution does not lower the overall Mn/Ca and Zn/Ca values.

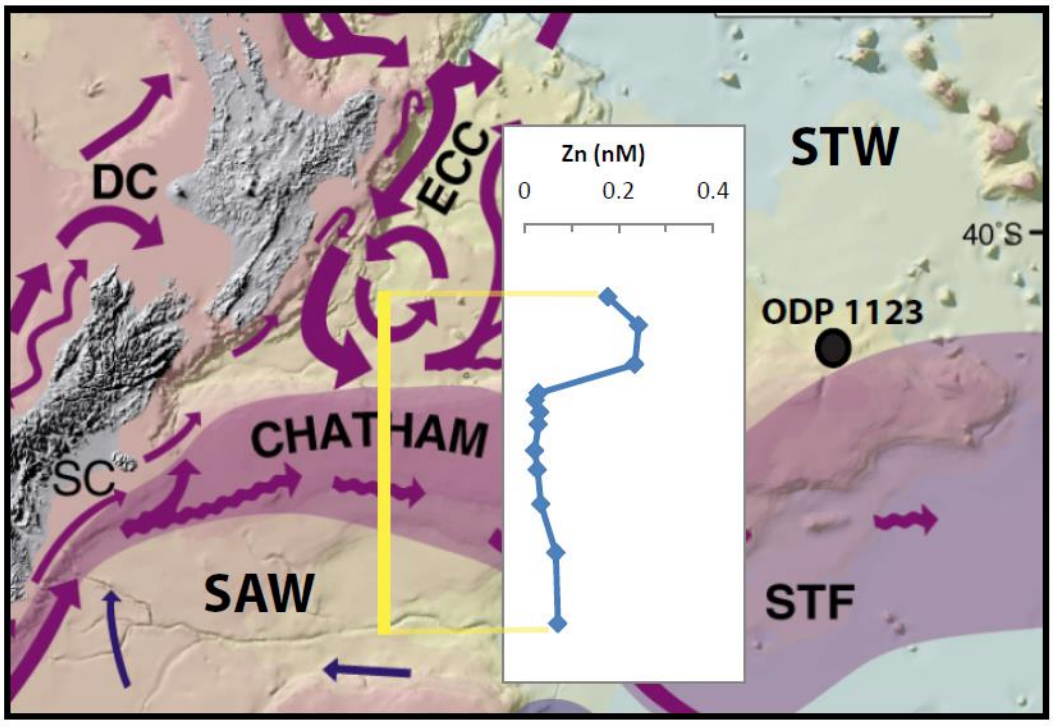

Figure 4.3. Yellow vertical bar indicates transect of surface Zn concentrations measured southeast of New Zealand, which show enrichment in STW and a marked depletion across the high productivity zone of the Chatham Rise and in SAW. ODP 1123 core site is marked for reference. Unpublished Zn data were provided by Dr Michael Ellwood of Australia National University. Map taken and modified from *Carter et al.* [1998].

Figure 4.4. Zn and Mn/Ca data for *Gg. bulloides* chamber *f-2* generated in this study, compared with modern mean subtropical and subantarctic values from a range of core tops around New Zealand [*Marr*, 2009]. Grey shaded box indicates MIS 12 after *Lisiecki and Raymo* [2005].

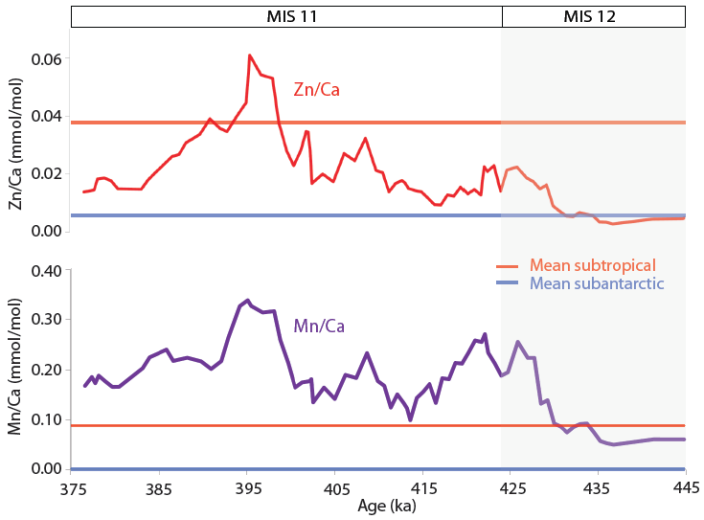

As Mn/Ca and Zn/Ca have been shown to be enriched in foraminiferas that calcified in STW relative to those that calcified in SAW in the New Zealand region [*Marr*, 2009], enrichments in these two trace elements may indicate

greater STW influence at the core site, especially when they coincide with higher Mg/Ca ratios. Zn and Mn are micronutrients [*Anderson et al*., 1978; *Bruland and Lohan*, 2003; *Coale*, 1991; *Sunda et al*., 1983] and both are considered to be productivity indicators. Depth profiles of Zn concentrations in the water column indicate that Zn is a micronutrient in the Tasman Sea [Fig. 4.5]. Thus, in addition to acting as a water mass tracer at ODP 1123, these micronutrients are also likely recording a productivity signal. Moreover, the significant positive anomaly in both Zn/Ca and Mn/Ca at *ca*. 398 ka is coincident with an increase in eutrophic species abundance [*Crundwell et al*., 2008]. However as productivity was reduced during MIS 11 relative to MIS 12 [*Kowalski and Meyers*, 1997; *Lean and McCave*, 1998], it is likely that the overall enrichment in these trace elements associated with the MIS 11 interglacial does, in fact, primarily reflect changing water mass influences at ODP 1123, with a secondary superimposed productivity signal.

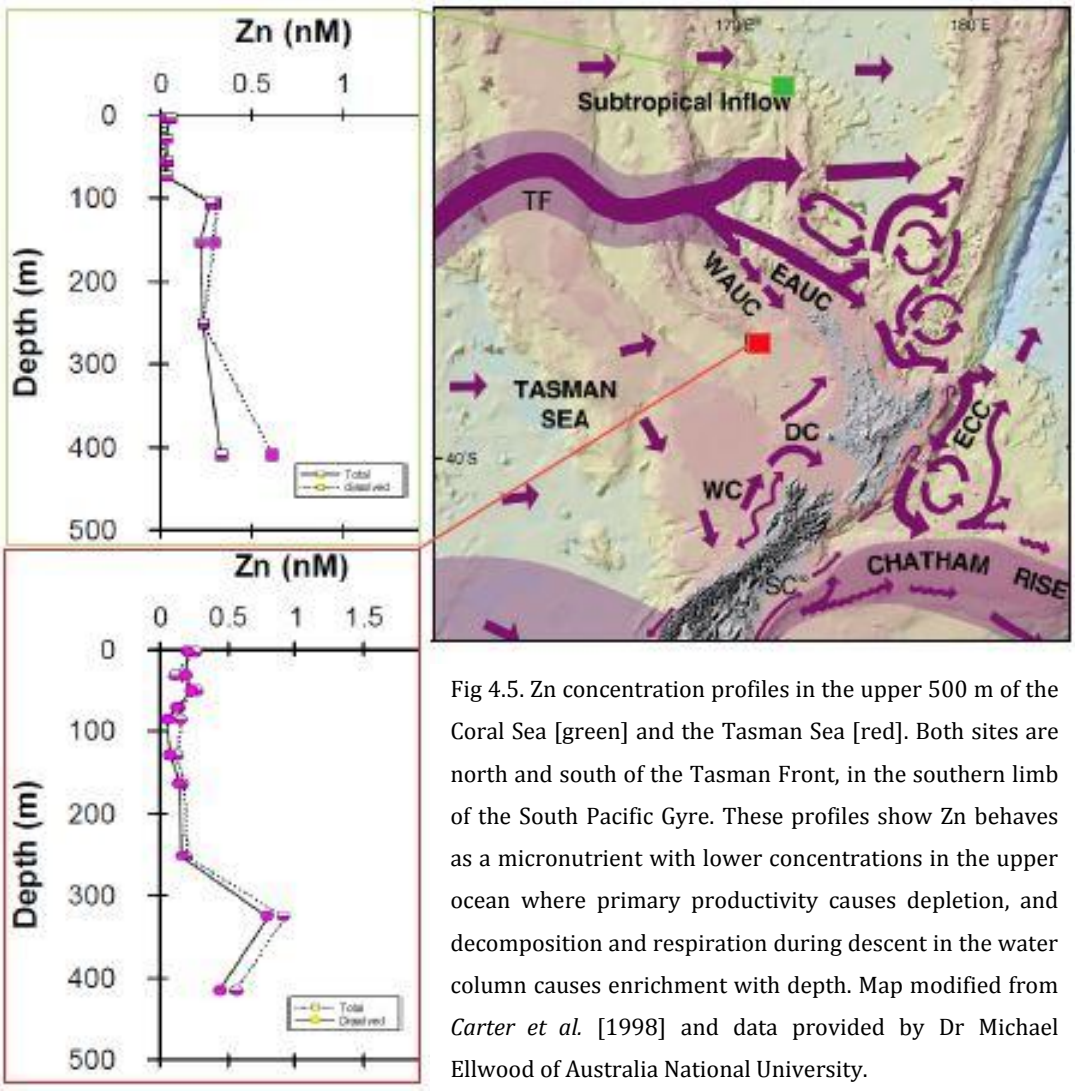

Fig 4.5. Zn concentration profiles in the upper 500 m of the Coral Sea [green] and the Tasman Sea [red]. Both sites are north and south of the Tasman Front, in the southern limb of the South Pacific Gyre. These profiles show Zn behaves as a micronutrient with lower concentrations in the upper ocean where primary productivity causes depletion, and decomposition and respiration during descent in the water column causes enrichment with depth. Map modified from *Carter et al.* [1998] and data provided by Dr Michael Ellwood of Australia National University.

4.5 Paleoclimate reconstruction for MIS 12-11

The earliest noticeable change in the four geochemical proxies [Fig. 3.6] occurred during MIS 12 at 437 ka when obliquity was at a minimum, *Gg. bulloides* Mg/Ca ratios reveal a surface ocean warming. No corresponding planktonic $\delta^{18}O$ response was detected until 433 ka when $\delta^{18}O$ in *Gg. bulloides* became lighter, implying that the initial 2°C warming recorded in the Mg/Ca record was insufficient to destabilise the global cryosphere, or there was a lag in response by the cryosphere, or that this warming was effectively hidden in the

local surface salinity signal. For this reason, the timing relationship between the planktonic $\delta^{18}O$ and Mg/Ca-derived paleo-ocean temperatures is not considered further. In addition to this 4 kyr lag, there is a further delay of 2 kyr between planktonic and benthic foraminiferal $\delta^{18}O$ signals [Appendix 4].

Three thousand years after the $\delta^{18}O$ change, Mg/Ca, Zn/Ca and Mn/Ca ratios [Fig. 3.6] increase to new levels at 430 ka. This change is interpreted to reflect an increasing presence of STW at ODP 1123 as supported by warming SST and changes in foraminiferal assemblages with increasing presence of subtropical and eutrophic species [*Crundwell et al*., 2008].

The Mg/Ca, Mn/Ca and Zn/Ca records show coherent peaks, most notably at the end of the deglacial transition, when the climate semi-stabilises after the ACR-like event at 424 ka, although Mn/Ca stays elevated for a longer duration during this period, and Mg/Ca ratios only show small increases for the last two peaks. Following the ACR-like event, the interglacial is characterised by a series of these warm peaks, where Zn/Ca, Mn/Ca, Mg/Ca-derived paleo-ocean temperatures, and to a lesser extent $\delta^{18}O$, are in phase, suggesting incursions of STW. These incursions are approximately 12 ky apart suggesting half-precessional forcing [*Scott et al*., submitted]. The variability in the Zn/Ca and Mn/Ca record may also in part reflect productivity changes which would be consistent with the mixing of the incoming STW with SAW. The large positive anomaly in both Zn/Ca and Mn/Ca at *ca*. 398 ka is likely to have been productivity driven as it is coincident with an increase in eutrophic species abundance [*Crundwell et al*., 2008].

The occurrence of ACR-like events at the end of the deglacial is not unique to ODP 1123 and appears in other Southern Hemisphere Atlantic records [ODP

1093 and 1094, *Bianchi and Gersonde*, 2004 and *Kunz-Pirrung et al*., 2002; 2004 and ODP 1089, *Cortese et al.,* 2004; 2007] and Pacific records [MD06-2986, *Kolodziej,* 2010*;* MD97-2120; *Pahnke and Zahn*, 2005; 2010; DSDP 594, *Prebble*, 2012; MD97-2121, *Carter et al*., 2008]. These reversals appear to be more pronounced south of the STF, and only appear at the end of Termination I and V in the EDC ice core record [*EPICA Community Members*, 2004; *Jouzel et al*., 2007], confirming that this ACR – like event is forced from the south. The presence of this predominantly Southern Ocean feature in this study confirms that ODP 1123 records both subantarctic and subtropical signals. Furthermore, its widespread occurrence suggests it is likely to be orbitally forced rather than reflect non-linear ice dynamics.

The coupled trace element change [Mg/Ca, Mn/Ca and Zn/Ca] during MIS 11 may reflect a strengthening and southward migration of the South Pacific Gyre, as observed in the modern ocean with a warming climate [*Cai et al*., 2005; *Cai*, 2006; *Oke and England*, 2004; *Roemmich et al*., 2007] and has also been noted in glacial to interglacial cycles in the Tasman Sea [*Martinez*, 1993; *Sikes et al*., 2009]. In that context, the input of STW would be enhanced if the Tasman Front component of the gyre strengthened and migrated south to an optimal position for maximum jetting through the shallow bathymetric constraints northwest of New Zealand, providing more warm, Zn- and Mn-rich STW to the East Cape Current and ODP 1123. Moreover, subtropical species abundance peaks from *ca*. 430 to 396 ka, coincident with the initial increases in both Mn/Ca and Zn/Ca, and a secondary increase in Mg/Ca [Fig 3.6], support the interpretation that increases in these micronutrients do in fact reflect an increase in STW at ODP 1123 [*e.g., Carter et al*., 2008].

Modern observations show that in the last 60+ years the East Australian Current [EAC] has warmed, strengthened and extended south by 350 km [*Cai et al*., 2005; *Ridgway,* 2007]. The Tasman Front is directly fed by the EAC and modern observations indicate that when the EAC intensifies, it potentially reduces the volume transport of the Tasman Front, but this may reflect decadal variability rather than an overall decrease [*Hill et al*., 2011]. *Fernandez* [2012] suggested that rather than declining, the flows associated with the STF and SAF off eastern New Zealand are increasing in response to local winds. Given this, it is hypothesised that during MIS 11, the South Pacific Gyre intensified during the protracted warm period, and this translated into an intensified STF, which underwent a series of flow perturbations that potentially are the result of half precessional forcing of the regional wind-driven ocean circulation as indicated by spectral analysis of the faunal assemblage based SST record from MIS 12-10 at ODP 1123 by *Scott et al*. [submitted]. Evidence from ODP 1089 suggests that during MIS 11 the Agulhas spillage from the Indian to the Atlantic Oceans was intensified, perhaps resulting from a strengthened EAC that fed water warmed in the tropical Pacific and Indian Oceans into the Atlantic, via the southern hemisphere supergyre [*Cortese et al*., 2004; *Ridgway and Dunn*, 2007].

4.6 Intra-test trace element convergence in Gg. bulloides

Two periods occurred when the offset between Mg/Ca in chambers *f-2* and *f* in *Gg. bulloides* significantly diminished [433–436 and 400-407 ka; Fig. 3.1]. This might imply either an ecological change in the depth habitat of *Gg. bulloides*, a shallowing of the thermocline, or periods of enhanced dissolution. If the foraminifera were not migrating downwards through the water column with

ontogeny, and given that both of these periods occur when Mn/Ca and Zn/Ca are steeply increasing, and *Gg. bulloides* is a eutrophic species [*e.g., Crundwell et al.,* 2008], the increased availability of micronutrients may have inhibited migration with ontogeny. However, the secretion of additional layers of calcite associated with the natural progression through the foraminifera's life cycle would serve to decrease buoyancy. If the thermocline shallowed, this could be forced either by enhanced winds or increased upwelling. Such upwelling would bring cooler nutrient-rich waters to shallower depths, which could account for the convergence in Mg/Ca ratios of chambers *f-2* and *f*, and the increased micronutrient content. However, ODP 1123 is not a significant upwelling location as it is a remote deep-water site that is distant from bathymetric features promoting upwelling. Periods of enhanced wind stress are possible when considering the modern observations of *Fernandez* [2012]. The third possibility is preferential dissolution. If dissolution of Mg-rich portions of the test occurred, this would act to homogenize the Mg/Ca ratios in the two analysed chambers, as the *f-2* chamber would likely be more susceptible to dissolution than the *f* chamber due to its originally higher Mg content. A brief convergence between chamber *f-2* and *f* Mg/Ca values also occurs at 387 ka, which happens to coincide with foraminifera that appear to have experienced significant dissolution [Appendix 1; sample 15.67m].

Unequivocally distinguishing whether the convergence in Mg/Ca ratio of chambers *f-2* and *f* is an ecological and/or oceanographic signal is not possible with the data obtained in this study. However, the low SNW that characterise the entire record indicating that dissolution is unlikely to be the primary control.

Chapter 5: Regional overview – MIS 11 paleo-ocean temperatures in the Southwest Pacific Ocean

5.1 Regional oceanographic response to MIS 11

To reconstruct a regional paleo-oceanographic response of the Southwest Pacific Ocean to MIS 11, paleo-SST data have been compiled from seven sites around the New Zealand region including ODP 1123 [Table 5.1; Fig. 5.1]. Comparison between cores from different sites and utilising different proxies [*e.g., Barrows et al.*, 2007; *Sikes et al.*, 2009] such as those for paleo-ocean temperatures incorporates inherent errors associated with different dating methods, different sampling resolutions and the differing proxies themselves. These effects are particularly problematic when comparing short intervals [i.e., millennial changes], as is the case here. With these caveats in mind, MIS 11 interglacial conditions at seven sites around New Zealand [Fig. 5.1] are examined to assess the regional oceanographic response to MIS 11.

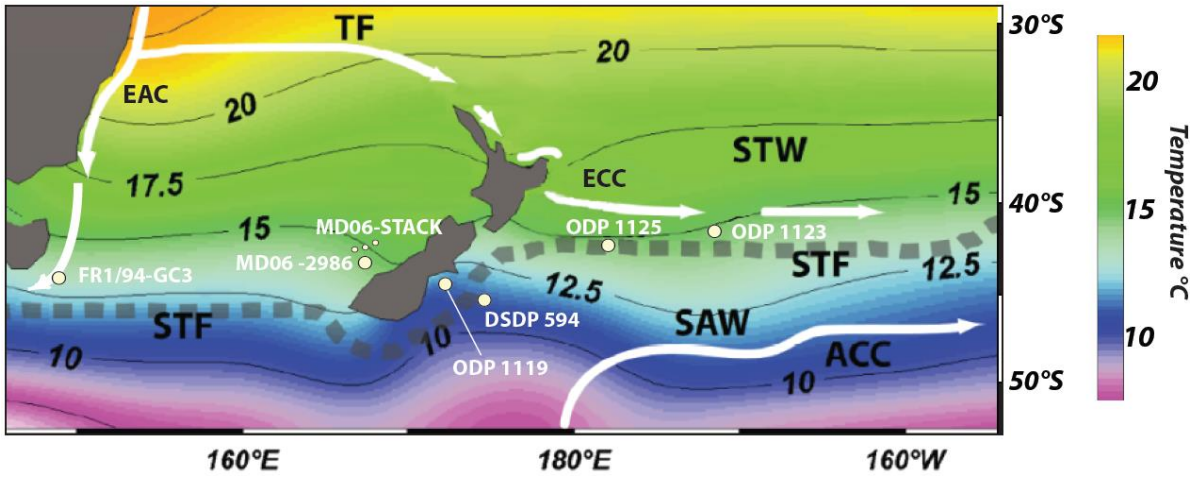

Figure 5.1. Regional modern SST chart with all core sites plotted. MD06-STACK refers to three cores: MD06-2987, MD06-2988 and MD06-2989, which have been presented as a stacked record due to their close proximity to minimise age uncertainty errors after *Prebble* [submitted]. Selected major oceanographic features are represented schematically as follows. The southwestern limb of the South Pacific Gyre is represented by the east Australian Current [EAC], which bifurcates and feeds the Tasman

Front [TF], and then passes northern New Zealand to eventually feed the East Cape Current, bringing STW to ODP 1123. The STF is shown by the dashed grey line and the Antarctic Circumpolar Current [ACC] is also shown, which marks the boundary between SAW and the southern ocean. Figure modified from *Bolton* [2011].

All sites north of the STF [Fig. 5.2 a, b, d and e] record similar SSTs throughout the peak of MIS 11 of between 17.7 and 19.3°C, with the exception of the alkenone record from the South Tasman Sea [FR1/94-GC3], which sits close to the southern extension of the EAC. This alkenone record has peak SSTs that are up to 5˚C lower than the other paleo-SST records, but comparable to modern SSTs at that site. The difference may reflect the more southerly location of FRI/94-GC3 and position proximal to a dynamic STF, which provides the opportunity for the ready exchange of SAW with STW [*e.g*., *Sikes et al*., 2009].

At ODP 1123, ANN_{25} SST from planktic foraminiferal assemblages are similar to other sites, but the *Gg. bulloides* Mg/Ca peak temperatures are *ca*. 6˚C cooler mainly reflecting the depth preference of this species between 50 and 200m deep in the water column [*Hemleben et al.,* 1985; note: the modern temperature at ODP 1123 at 50 m is *ca*. 15°C and at 200 m is *ca*. 12°C, based on *Schlitzer*, 2002]. As such, the temperature record generated by Mg/Ca analyses of *Gg. bulloides* is referred to herein as the sub-surface temperature [sub-SST]. In contrast, *Gs. ruber* SST are *ca*. 2˚C cooler than the ANN_{25} SST, which may reflect the effects of dissolution or may suggest that the ANN_{25} SST are overestimating peak MIS 11 conditions [See section 4.1.2: Dissolution and its potential effect on geochemical proxies]. The two sites south of the STF both show consistently lower SSTs, between 11.7 and 16.4°C as would be expected for core sites bathed mainly in cooler SAW. The warmer 17.5°C reported at DSDP 594 by *Schaefer et al.* [2005] refers to the summer SST for MIS 11 when it is likely that STW

arrived at the site, possibly due to either southward leakage through the Mernoo Saddle or an enhanced SC introducing warm STW from the south.

The two full records from ODP 1123 [this study = Mg/Ca *Gg. bulloides* derived sub-SST; *Crundwell et al*. [2008] = ANN_{25} derived SST] have been depth tuned to the *Lisiecki and Raymo* [2005] global benthic stack age model using the *Uvigerina*-based $\delta^{18}0$ record [*Federici et al., unpubl. data*]. Ignoring the differences in resolution between the two planktonic records, the ANN_{25} SST record appears to begin warming gradually 5 kyr before the sub-SST Mg/Ca record. The ANN_{25} SST plateaus after 429 ka to reach maximum SST of 19.3˚C at 419 ka. In contrast, the *Gg. bulloides* [i] exhibits an ACR-like event during the deglacial transition, [ii] reaches peak temperatures 2 kyr earlier at 421 ka, and [iii] shows a more distinct and prolonged warm period [427–388 ka] before descending into glacial conditions. The ACR-like event is likely to represent a widespread climatic signal. Ocean cooling has been identified in other SST records [*e.g*. *Cortese et al.,* 2004; 2007; *Kolodziej,* 2010; *Prebble*, 2012] as well as occurring the EPICA Dome C ice core record [*EPICA Community Members*, 2004]. The coincidence of a cooler ocean and colder Antarctica is very similar to that observed during the ACR in Termination 1 [*Carter et al*., 2008; *Pahnke and Zahn*, 2005]. At that time, SAW, as identified from faunal assemblages and SSTs, moved northwards at least as far as 40°S off eastern New Zealand. In that context, a similar mechanism is suggested for the cold reversal in Termination V: the fluctuating SSTs reflecting the interaction of SAW with STW. An alternative hypothesis that the fluctuating SSTs resulted from enhancement of the subtropical inflow is at odds with Termination V cooling. The *Gs. ruber* Mg/Ca SST record [Fig. 5.2.b] only covers the peak warm period from 427 to

395 ka, as this species lives in tropical-subtropical environments [*Crundwell et al*., 2008]. The entire *Gs. ruber*-derived SST record is consistently lower [*ca*. 2-4˚C] that the ANN_{25} derived SST suggesting that dissolution may have affected *Gs. ruber*, or the ANN_{25} SST record is erroneously warm [See section 4.2: Dissolution and its potential effect on the geochemical proxies].

The two South Island, West Coast records [Fig. 5.2d and e] display strong similarity, which is not unexpected by virtue of their close proximity. There is also some similarity of the timing of this West Coast deglaciation with the *Gg. bulloides* Mg/Ca-derived sub-SST record at ODP 1123 [Fig. 5.2c] when taking age model uncertainties into account. Nevertheless, small differences are evident that may simply reflect differences in age models. The West Coast records are based on age models where planktonic $\delta^{18}0$ is tuned to the *Lisiecki and Raymo* [2005] benthic stack age model. If we assume the 2-3 kyr offset between planktonic and benthic signals, as observed at ODP 1123 [Appendix 4], is applicable to the West Coast cores, then the deglaciation between the cores west and east of New Zealand begins within about *ca*. 2 kyr of each other. The West Coast SST records both show late peaks at 414 and 389 ka [Figs. 5.2d and 5.2e respectively], as well as a prolonged warm period that is similar to the ODP 1123 *Gg. bulloides* sub-SST [Fig. 5.2c].

The two records from DSDP 594 are also tuned using planktonic $\delta^{18}O$ and the *Lisiecki and Raymo* [2005] age model [*Hayward et al*., 2008, 2012]. Again, this may result in assigned ages being 2-3 kyr younger that the true sediment age, assuming that the relationship between planktonic and benthic isotopes is similar to nearby ODP 1123 where the benthic/planktonic offset is identified. Interestingly, the deglaciation appears to begin earlier in the dinoflagellate

transfer function [DTF; *Prebble*, submitted] record [Fig. 5.2f] than the ANN_{25} record [Fig. 5.2g]. The DTF SST reaches peak temperature early at 426 ka, while the ANN_{25} SST does not reach peak temperatures until 401 ka. The two DSDP 594 records are dissimilar in terms of the timing and length of peak warm period. In addition, the DTF record [Fig. 5.2f] shows an ACR-like event towards the end of the termination, which is not recorded in the ANN_{25} SST record [Fig. 5.2g].

The duration of MIS 11 varies between the different regional sites, from 20 kyr at DSDP 594 [Fig 5.2g] below the STF, to 40 kyr at ODP 1123 [Fig. 5.2c] and the West Coast cores [Fig. 5.2d and e], both located north of the STF. While the amplitude of warming may have been greater south of the STF, this warming was short-lived, which may support the theory of subtropically sourced water episodically breaching the Chatham Rise during the prolonged warm period [*e.g., Schaefer et al*., 2005] or being introduced from the south by a STW-dominant SC. This is also consistent with the elevated Mn/Ca and Zn/Ca ratios of *Gg*. *bulloides* at ODP 1123 at this time, together with a higher proportion of subtropical faunal assemblages noted by *Crundwell et al*. [2008] and interpreted to represent a strengthened South Pacific Gyre.

The largest glacial-interglacial amplitude temperature change occurred south of the STF in the DSDP 594 records, with both proxies showing >10°C difference for Termination V [Figs. 5.2.f. and 5.2.g]. This is consistent with the findings of *Schaefer et al.* [2005] that the temperature gradient across the Chatham Rise likely decreased during MIS 11 due to a greater STW influence. The *Gg. bulloides* sub-SSTs [Fig. 5.2c] at ODP 1123 also show a large amplitude change between peak glacial and interglacial conditions of 10°C, compared with an 8°C change

recorded in the ANN_{25} SST record at the same site. This difference in absolute temperature change may also, in part, indicate a change in the habitat depth of *Gg. bulloides*, with a change in nutrient availability or thermocline depth. The two West Coast records are similar to the ANN_{25} SST ODP 1123 record and show a temperature change of 6 to 8˚C between peak glacial and interglacial conditions.

A potential Antarctic influence is also evident north of the STF at ODP 1123 and in the West Coast stack. At *ca*. 424 ka, an ACR-like event occurs in the sub-SST ODP 1123 record, and can be observed *ca*. 2 kyr later in the West Coast record. This implies that although both of these sites are primarily bathed in subtropically sourced water they are both still influenced by polar waters and climate.

Core	Location	Proxy	Surface watermass	Mean MIS 11 T°C [427-397 ka]	Modern T°C	Reference	Notes
ODP 1123	41°47.17'S, 171°29.94' W	Mg/Ca SST	STW*	16.0	15.5	*This study; Gs. ruber*	May be artificially low due to dissolution, see section 3.5.2
ODP 1123	41°47.17'S, 171°29.94' W	ANN_{25} SST	STW*	18.7	15.5	*Crundwell et al,* [2008]	May be artificially high, see section 3.5.2
ODP 1125	42°32.98'S, 178°09.99' W	MAT	STW*	18.0^{x}	14.5	*Schaefer et al,* [2005]	Not included in Figure 4.2
ODP 1125	42°32.98'S, 178°09.99' W	ANN_{25} SST	STW*	16.0	14.5	*Hayward et al,* [2008]	Not included in Figure 4.2
MD06-2986	43°26.91'S, 167°54.00'E	ANN_{25} SST	STW	16.8	14.0	*Kolodziej,* [2010]	
M606-STACK	3 core stack, see caption	DFT ANN_{25} SST	STW	15.0	14.5	*Prebble, submitted*	Dinoflagelate transfer function
FR1/94-GC3	44°15'S, 149°59'E	U^{K}_{37}	STW	13.3	13.0	*Pelejero et al,* [2006]	Not included in Figure 4.2
ODP 1119	44°45.33'S, 172°23.60'E	ANN_{25} SST	SAW^{o}	9.5	11.0	*Hayward et al,* [2008]	
DSDP 594	45°31.41'S, 174°56.88'E	ANN_{25} SST	SAW	10.5	11.0	*Hayward et al,* [2008]	
DSDP 594	45°31.41'S, 174°56.88'E	DTF ANN_{25} SST	SAW	13.0	11.0	*Prebble, submitted*	
DSDP 594	45°31.41'S, 174°56.88'E	MAT	SAW	10.5^{x}	11.0	*Schaefer et al,* [2005]	Not included in Figure 4.2

Table 5.1. Compilation of SST records spanning 427 to 397 ka for the New Zealand region. * Northern tip of STF, ^{o} Southern tip of STF, ^{x} Summer SST. Certain records have not been included in Figure 4.2 as indicated in the final column as a means of simplicity. All SST records of *Schaefer et al.* [2005] are excluded as these

are summer SSTs. The ODP 1125 and 1119 records of *Hayward et al.* [2008] are excluded as they are either of very low or patchy resolution. The alkenone record from the south Tasman Sea reported by *Pelejero et al.* [2006] is excluded due to its distal position.

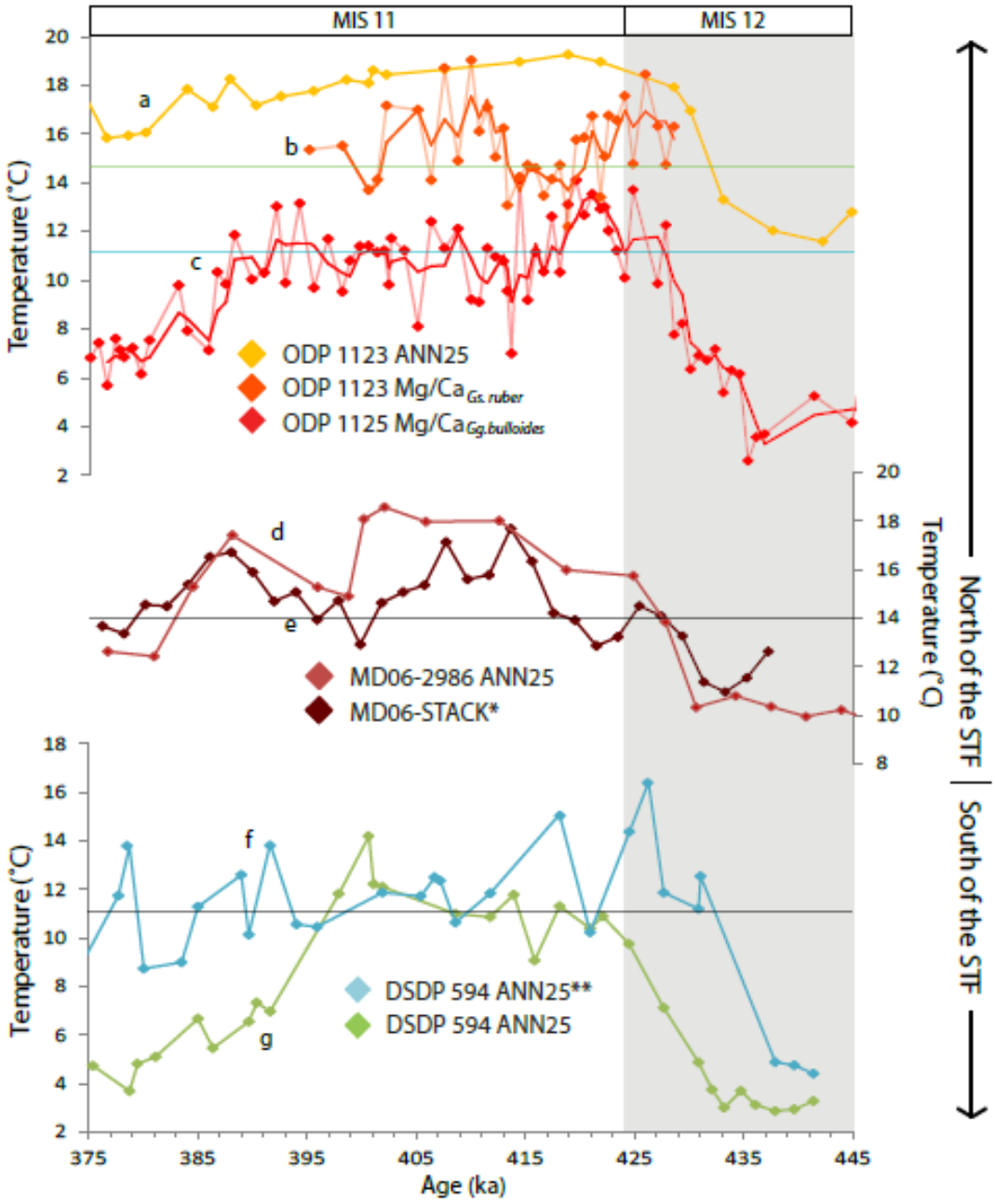

Fig 5.2. SST records and one sub-SST record [c] from the New Zealand region from ODP 1123 [a – c], west coast cores MD06–2986 [d] and the three core stack of MD06-2987, 2988 and 2989 denoted by * [e], and finally DSDP 594 [f & g]. MDO6-STACK* and DSDP 594 ANN25** records are dinoflagellate transfer function. Author details for all data can be found in Table 4.1. All temperature axes are on the same scale to facilitate simple comparison between records. The relative position of the STF is shown on the right hand side [black arrows]. Green line in [b] represents modern SST [mean 0-50 m] at ODP 1123 core top on which *Gs. ruber* calibration is based [*Bolton et al.*, 2011]. Blue line in [c] indicates modern temperature at nearby R623 core top at 200 m on which *Gg. bulloides* calibration is based [*Marr et al.*, 2011]. Horizontal solid dark lines show modern SST at each core site, which are located on Figure 4.1. Shaded grey box denotes MIS 12 glacial period after *Lisiecki and Raymo* [2005].

These data show that the STF likely operated in a similar way during MIS 11 to the modern oceanic setting, wrapping around the base of the South Island consistent with the interpretation of *Hayward et al*. [2012]. In addition, the DSDP 594 records also indicate a southerly incursion of subtropical waters between 422 and 399 ka. DSDP 594 is located near the southern end of the Mernoo Saddle that separates the Chatham Rise from the South Island. Modern observations reveal periodic southward incursions of STW towards DSDP 594 [*Greig and Gilmour*, 1992; *Shaw and Vennell*, 2000], which the MIS 11 microfaunal assemblages and SSTs suggest was a phenomenon that was sufficiently pronounced to leave its mark. However, as noted earlier, the introduction of warm water from the south via the SC with an enhanced STW content is not discounted.

In summary, comparison of the climatic/oceanic expression of MIS 11 from several ocean sediment cores around New Zealand is limited by the inherent difficulties associated with different age models and sampling resolution. This effect is compounded when comparing multiple different proxies, as is the case here. With this in mind, the deglacial transition into MIS 11 began at 443 ka in the ANN_{25} ODP 1123 record, but was not recorded in the *Gg. bulloides* Mg/Ca-derived paleo-ocean sub-SST until 6 kyr later at 437 ka. The deglaciation occurred over a period of *ca*. 10 kyr and the MIS 11 interglacial warm period lasted from *ca*. 425 to 388 ka, north of the STF. South of the STF, peak interglacial warmth appeared to last from *ca*. 423 to 400 ka and is likely to be associated with incursions of warm subtropically sourced water across the Chatham Rise, and/or via the SC. Mean MIS 11 SST was perhaps 2 - 4˚C warmer than present SST north of the STF, and similar to modern SST south of the STF.

Chapter 6: Conclusions

6.1 Concluding remarks

The main aim of this thesis was to reconstruct the ocean and climate of MIS 11 in the Southwest Pacific Ocean at ODP 1123. Two species of planktonic foraminifera [*Gs. ruber*, which dwells at *ca*. 0-50 m and *Gg. bulloides,* which dwells at *ca*. 50 – 200 m] were analysed using laser ablation-inductively coupled plasma mass spectrometry [LA-ICPMS] to determine trace element chemistry and hence identify paleo-ocean temperature, upper ocean thermal stratification and circulation. Size-normalised weight [SNW] was measured in *Gg. bulloides*, to determine if the modern relationship between SNW and Mg/Ca-derived paleo-ocean temperature holds for MIS 11, and the implications of this for ocean chemistry.

Six key findings generated from this thesis research are presented:

Finding 1: Determine the timing and pattern of the MIS 11 interglacial

The sub-surface temperature [sub-SST] record generated by LA-ICPMS of *Gg. bulloides,* shows a long and well defined warm period, lasting approximately 40 kyr, from 428 to 387 ka [Fig. 4.2.c].

The MIS 12-11 deglacial transition manifested more than 10 kyr earlier than the global benthic $\delta^{18}O$ stack [*Lisiecki and Raymo*, 2005; Fig. 4.2.a and c] in the Southwest Pacific Ocean. At ODP 1123, the sub-SST record shows rapid warming beginning at *ca*. 437 ka [Fig. 3.5]. The end of the deglacial transition is characterised by an ACR - like cooling event, close to the MIS 12-11 boundary at 424 ka. This event is also noted by *EPICA Community Members* [2004] in the EDC ice core δD record. The occurrence of this event in MIS 11 as well as MIS 1

may suggest that the associated incursion of SAW may be a feature of deglaciations and hence is potentially orbitally driven rather than being a non-linear response of ice dynamics. Following the cooling, MIS 11 reached its optimum at *ca*. 420 ka, after which the interglacial period is characterised by relatively stable warm conditions until *ca*. 387 ka, when the climate began to cool into MIS 10.

Finding 2: Determine a paleo-ocean temperature record for MIS 11 using Mg/Ca-based thermometry

The geochemical data show the MIS 12 – 11 deglacial transition was large. *Gg. bulloides* sub-SST record a change of 10°C, which is similar to the ANN_{25}-based SST change of 8°C of *Crundwell et al*. [2008]. This large amplitude temperature change at the MIS 12 – 11 deglacial transition is also observed in other studies around the New Zealand region, north and south of the STF. Mean optimum SST during MIS 11 [Mg/Ca derived SSTs on *Gs. ruber*] were up to 2°C warmer than modern mean annual SST of 15.5°C

Finding 3: Identify changes in water masses and ocean structure from peak glacial MIS 12 conditions to the end of MIS 11 using trace element foraminiferal test chemistry

Four trace elements [Al, Mn, Zn and Sr/Ca] were analysed in addition to Mg/Ca. Of these four trace elements, Mn/Ca and Zn/Ca ratios increase greatly in concentration in the interglacial period reflecting an increase in the influence of STW at ODP 1123, as STW is enriched in these trace elements relative to SAW in the same foraminiferal species. This influx of STW is interpreted as a

strengthening of the South Pacific Gyre during MIS 11, which is consistent with modern observations.

The difference between measured Mg/Ca in chambers *f-2* and *f* in *Gg*. *bulloides* appears to represent the species migration down through the water column with ontogeny and hence provides information about the thermal stratification of the upper 200 m of the ocean. Periods of low stratification occurred at 436–433 and 407–400 ka suggesting deeper mixing and marked shallowing of the thermocline under presumed windiness of these cool periods. In contrast, warm periods are characterised by well defined thermal stratification. However, it is possible that ecological factors such as changes in migration and depth habitat of *Gg*. *bulloides* may influence these results.

Finding 4: Investigate the ocean carbon response to MIS 11 via size normalised weight [SNW] of foraminiferal tests

Gg. *bulloides* samples from MIS 12-11 were found to have anomalously low SNW, implying that if the modern SNW-Mg/Ca temperature calibration of *Marr et al*. [2011] holds, then [i] calcification temperatures were up to 10˚C warmer than indicated by the Mg/Ca-derived paleo-ocean temperatures or [ii] if these paleo-ocean temperatures are robust, then *Gg*. *bulloides* samples have on average 50% lower SNW than expected.

Regardless of the cause of the low SNW in *Gg. bulloides*, any potential effects on the geochemical proxies have been explored. Several lines of evidence suggest that the low SNW has not artificially lowered Mg/Ca ratios or biased stable isotope data.

1) When comparison is drawn with the earlier part of the ODP 1123 core [*Greaves*, 2008], MIS 11 Mg/Ca values and $\delta^{18}O$ are not unusually low, as would be expected if they had been dramatically affected by low CO_3^{-2} concentration or dissolution.
2) Traditional dissolution proxies applied to ODP 1123 [*Crundwell et al*., 2008], do not indicate significant dissolution and instead show normal background levels when compared with the rest of the core.
3) The degree of absolute temperature change in *Gg. bulloides* from the MIS 12 glacial to the MIS 11 interglacial is *ca*. 10˚C, which clearly has not been overprinted in the benthic realm. Moreover, at this core site bottom water changes recorded by benthic foraminiferal during MIS 12 to 11 are on the order of 3˚C [*Elderfield et al*., 2010].
4) The temperature difference between *Gs. ruber* and *Gg. bulloides* [*ca*. 4˚C] during MIS 11 is similar to the modern temperature difference between these two species at ODP 1123 [*Bolton*, 2011]. *Gs. ruber* is more susceptible to dissolution than *Gg. bulloides*, and so if dissolution had affected these samples, the temperature difference between these two species would be erroneously low, which is not the case.
5) Other trace elements acquired during LA-ICPMS analysis show greater concentrations during MIS 11, when eutrophic species *Gg. bulloides* has anomalously low SNW. Evidence suggests that these foraminifera may calcify faster when nutrient availability is high, and faster calcification is likely to result in lower test mass overall [*Aldridge et al*., 2012].
6) Visual comparison of SEM images of MIS 11 and modern core top *Gg. bulloides* from the New Zealand region reveals that test walls are on

average around 50 % thinner during MIS 11, implying that poor calcification environment may be the reason for the low SNW. However, Mg/Ca-derived paleo-ocean temperatures are slightly warmer than modern SST at the ODP 1123, similar to other studies, confirming the robustness of the geochemical proxies.

Finding 5: Determine the New Zealand oceanic regional response to MIS 11

The regional oceanic response to MIS 11 was assessed by comparing seven ocean sediment cores. Caution is necessary in considering these results, as the accuracy of this comparison is limited to comparing different paleo-ocean thermometry techniques, sampling resolutions and age model determinations. However, with this caveat in mind, MIS 11 manifested as a rapid warming to temperatures that are similar or slightly warmer than present both north and south of the STF both to the east and west of New Zealand.

Finding 6: Compare MIS 11 and MIS 1 to assess suitability of the former as an analogue for the future

Ocean chemistry was fundamentally different during MIS 11 as compared with the Holocene. Specifically, the ocean carbon cycle operated in a different way causing the mid-Bruhnes dissolution interval with no associated detectable rise in atmospheric CO_2 relative to pre-industrial levels [*Barker et al.*, 2006]. However, the data generated in this study implies that a 2°C warming at southern mid-latitudes is sufficient to significantly affect marine calcifying organisms, and this change in the ocean carbon cycle is manifested in *Gg. bulloides* with its abnormally low SNW. While the MIS 11 and 1 orbital

parameters were similar during the terminations, orbits now differ; in the next few thousand years projected insolation will be low, compared with second insolation peak during MIS 11, for 65°N July insolation. In addition, a natural dissolution cycle occurred in the ocean. This implies that MIS 11 may not be the most suitable recent Quaternary interglacial analogue to MIS 1.

6.2 Suggestions for future work

A comparison study between solution-based and laser ablation-based Mg/Ca paleothermometry is needed, if long term, high-resolution temperature records are to be generated. Mg/Ca values complement routine $\delta^{18}O$ measurements by providing an unequivocal temperature signal, uncomplicated by global ice volume. Obtaining such data by LA-ICPMS, while providing much more information than traditional solution-based-ICPMS, is a time consuming process. The resolution, length of the record, time available for analytical work and type of information sought must be considered first before choosing which method to employ. When certainty of comparable measurements between the two techniques can be assured, much finer resolution data may be acquired via solution-based-ICPMS providing more information about centennial-scale climate events, core resolution permitting.

The low SNW encountered in *Gg. bulloides* in this study indicates that the MIS 11 ocean was chemically different to modern ocean conditions, in the Southwest Pacific region. Successive acid leaches and weight measurements on modern core top specimens may quantify the amount of dissolution required to generate the low SNW. However, this approach assumes that the source of the low SNW is in fact post-mortem dissolution. If the low SNW is caused by low

CO_3^{-2} concentration in the surface ocean, this could be quantified by applying paleo-pH proxies to the samples to determine CO_3^{-2} concentration required to cause anomalously low SNW. This can be achieved using boron isotopes and B/Ca ratios, and a calibration for this needs to be developed for *Gg. bulloides*.

Presuming the low SNW is either caused by low CO_3^{-2} concentration during calcification or post-morten, a simple way to assess the cause is to compare MIS 11 data in samples from different water depths in the region. This would determine if the dissolved appearance of the foraminifera is due to low CO_3^{-2} concentration in the surface ocean, or due to corrosive bottom water conditions. However, the relationship between nutrient availability and growth rates, and their effect on SNW needs to be quantified in the Southwest Pacific region, as has been carried out in the North Atlantic. This would require taking modern samples of live specimens, while conducting measurements to accurately determine in situ CO_3^{-2} concentration and nutrient concentrations. East of New Zealand, north and south of the STF is an area that provides an ideal natural laboratory for this due to the very different nutrient characteristics of the subtropical and subantarctic water masses.

In this study, I have shown that MIS 11 was warmer than present in the South-West Pacific Ocean, and natural dissolution occurred. This poses the question as to the validity of MIS 11 as an analogue to the Holocene, especially when considering the orbital similarities between these two time periods, previously hailed as one of the reasons for the MIS 11 analogue theory. In regards to the MIS 11 natural dissolution cycle, what are the implications of this, when applied to the modern warming climate? Will we see marine calcifying organisms affected in the future in the same way, and is MIS 11 a natural analogue for

anthropogenic ocean acidification? And if the case, what are the wider implications for the marine food web?

Reference List

ACE CRC (2008), Position analysis: CO_2 and climate change: ocean impacts and adaptation issues. Prepared by Howard, W., Sandford, R., Haward, M. and T. TruII. PA02--D80516.

Aldridge, D., C. J. Beer, and D. A. Purdie (2012), Calcification in the planktonic foraminifera *Globigerina bulloides* linked to phosphate concentrations in surface waters of the North Atlantic Ocean, Biogeosciences, 9, 1725–1739, doi:10.5194/bg-9-1725-2012.

Alexander, I., M. S. Andres, C. J. R. Braithwaite, J. C. Braga, P. J. Davies, H. Elderfield, M. A. Gilmour, R. L. F. Kay, D. Kroon, J. A. Mckenzie, L. F. Montaggioni, A. Skinner, R. Thompson, C. Vasconcelos, J. Webster, and P. A. Wilson (2001), New constraints on the origin of the Australian Great Barrier Reef: Results from an international project of deep coring, *Geology*, *29*, 483-486.

Anand, P., and H. Elderfield (2005), Variability of Mg/Ca and Sr/Ca between and within the planktonic foraminifers Globigerina bulloides and Globorotalia truncatulinoides, *Geochemistry Geophysics Geosystems*, *6*, Q11D15, doi:10.1029/2004GC000811.

Anand, P., H. Elderfield, and M. H. Conte (2003), Calibration of Mg/Ca thermometry

in planktonic foraminifera from a sediment trap time series, *Paleoceanography*, *18*, 1050, doi:1010.1029/2002PA000846.

Anderson, M. A., F. M. M. Morel, and R. R. L. Guillard (1978), Growth limitation of a coastal diatom by low zinc ion activity, *Nature, 276*, 70–71.

Barker, S., and H. Elderfield (2002), Foraminiferal calcification response to glacial-interglacial changes in atmospheric CO_2, *Science, 297,* 833–836, doi:10.1126/science.1072815.

Barker, S., M. Greaves, and H. Elderfield (2003), A study of cleaning procedures used for foraminiferal Mg/Ca paleothermometry, *Geochemistry Geophysics Geosystems, 4*, 1-20.

Barker, S., D. Archer, L. Booth, H. Elderfield, J. Henderiks, and R. E. M. Rickaby (2006), Globally increased pelagic carbonate production during the Mid-Brunhes dissolution interval and the CO_2 paradox of MIS 11, *Quaternary Science Reviews*, *25*, 3278-3293.

Barrows, T. T., S. Juggins, P. De Deckker, E. Calvo, and C. Pelejero (2007), Long-term sea surface temperature and climate change in the Australian–New Zealand region, *Paleoceanography*, 22, PA2215, doi:10.1029/2006PA001328.

Berger, A., and M. F. Loutre (2002), An exceptionally long interglacial ahead?, *Science*, *297*, 1287-1288, doi:10.1126/science.1076120.

Berger, W. H. (1968), Planktonic foraminifera: Selective solution and paleoclimatic interpretation, *Deep Sea Research, 15*, 31-43.

Bianchi, C., and R. Gersonde (2002), The Southern Ocean surface between Marine Isotope Stages 6 and 5d: Shape and timing of climate changes, *Palaeogeography Palaeoclimatology Palaeoecology, 187*, 151– 177.

Bianchi, C., and R. Gersonde (2004), Climate evolution at the last deglaciation: The role of the Southern Ocean, *Earth and Planetary Science Letters, 228,* 407–424.

Bijma, J., B. Hönisch, and R. E. Zeebe (2002), The impact of the ocean carbonate chemistry on living foraminiferal shell weight, (Discussion of Broecker, W. S., and E. Clark (2002), Carbonate ion concentration in glacial-age deep waters of the Carribbean Sea, *Geochemistry Geophysics Geosystems, 3*, 1021), *Geochemistry Geophysics Geosystems, 3*(11), 1064.

Bindoff, N., J. Willebrand, V. Artale, A. Cazenave, J. Gregory, S. Gulev, K. Hanawa, C.L. Quéré, S. Levitus, Y. Nojiri, C.K. Shum, L. Talley and A. Unnikrishnan, 2007: Observations: oceanic climate change and sea level, *in Climate Change 2007:*

The Physical Science Basis. Working Group I Contribution to the Intergovernmental Panel on Climate Change Fourth Assessment Report, S. Solomon, D. Qin, M. Manning, Z. Chen, M. Marquis, K. B. Averyt, M. Tignor and H. L. Miller, Eds., Cambridge University Press, 385-432.

Bolton, A. (2011), LA-ICP-MS Trace element analysis of planktonic foraminifera and application to Marine Isotope Stage 31 in the Southwest Pacific Ocean, PhD thesis, Victoria University of Wellington, Wellington.

Bolton, A., J. A. Baker, G. B. Dunbar, L. Carter, E. G. C. Smith, and H. L. Neil (2011), Environmental versus biological controls on Mg/Ca variability in *Globigerinoides ruber* (white) from core top and plankton tow samples in the southwest Pacific Ocean, *Paleoceanography*, *26*, PA2219, doi:10.1029/2010PA001924.

Boning, C. W., A. Dispert, M. Visbeck, S. R. Rintoul, and F. U. Schwarzkopf (2008), The response of the Antarctic Circumpolar Current to recent climate change, *Nature Geoscience*, *1*, 864-869, doi:10.1038/ngeo362.

Bostock, H. C., B. W. Hayward, H. L. Neil, K. I. Currie, and G. B. Dunbar (2011), Deep-water carbonate concentrations in the southwest Pacific, *Deep Sea Research Part I, 58*, 72-85, doi:10.1016/j.dsr.2010.11.010.

Bowen, D. Q. (2010), Sea level ~400 000 years ago (MIS 11): Analogue for present and future sea-level?, *Climate of the Past*, *6*, 19-29.

Boyd, P. W., and E. R. Abraham (2001), Iron-mediated changes in phytoplankton photosynthetic competence during SOIREE, *Deep Sea Research Part II, 48*, 2529–2550.

Boyd, P. W., J. LaRoche, M. Gall, R. Frew, and R. M. L. McKay (1999), The role of iron, light and silicate in controlling algal biomass in sub-Antarctic water southeast of New Zealand, *Journal of Geophysical Research, 104,* 13,395 13,408.

Boyd, P. W., G. McTainsh, V. Sherlock, K. Richardson, S. Nichol, M. Ellwood, and R. Frew (2004), Episodic enhancement of phytoplankton stocks in New Zealand subantarctic waters: Contribution of atmospheric and oceanic iron supply, *Global Biogeochemical Cycles*, *18*, GB1029.

Broecker, W (2002), The glacial world according to Wally, *Eldigo Press*.

Broecker, W., and T.-H. Peng (1987), The role of $CaCO_3$ compensation in the glacial to interglacial atmospheric CO2 change, *Global Biogeochemical Cycles, 1*, 15-29.

Brown, S. J., and H. Elderfield (1996), Variations in Mg/Ca and Sr/Ca ratios of planktonic foraminifera caused by postdepositional dissolution: Evidence of shallow Mg-dependent dissolution, *Paleoceanography*, *11*, 543-551.

Bruland, K. W., and M. C. Lohan (2003), Controls on trace metals in seawater, *Treatise on Geochemistry,* 23-44, Elsevier**.**

Cabioch, G., L. Montaggioni, N. Thouveny, N. Frank, T. Sato, V. Chazottes, H. Dalamasso, C. Payri, M. Pichon, and A.-M. Semah (2008), The chronology and structure of the western New Caledonian barrier reef tracts, *Palaeogeography, Palaeoclimatology, Palaeoecology, 268*, 91-105.

Cai, W. (2006), Antarctic ozone depletion causes an intensification of the Southern Ocean super-gyre circulation, *Geophysical Research Letters*, 33, L03712, doi:10.1029/2005GL024911.

Cai, W., G. Shi, T. Cowan, D. Bi, and J. Ribbe (2005), The response of the Southern Annular Mode, the East Australian Current, and the southern mid-latitude ocean circulation to global warming, *Geophysical Research Letters*, 32, L23706, doi:10.1029/2005GL024701.

Candy, I. (2009), Terrestrial and freshwater carbonates in Hoxnian interglacial deposits, UK: micromorphology, stable isotopic composition and

palaeoenvironmental significance, *Proceedings of the Geologists' Association*, *120*, 49-57.

CANZ Group (Carter, L., Cook, J.D., Foster, G.A., Garlick, R.D., Lichfield, N.J., Mitchell, J.S., Wright, I.C.), 1996. Undersea New Zealand. New Zealand region physiography, 1:4,000,000. *NIWA Chart Miscellaneous Series* 74.

Caron, D. A., O. Roger Anderson, J. L. Lindsey, J. Faber, W. W., and E. E. Lin Lim (1990), Effects of gametogenesis on test structure and dissolution of some spinose planktonic foraminifera and implications for test preservation, *Marine Micropaleontology*, *16*, 93 - 116.

Carter, L., and I. N. McCave (1994), Development of sediment drifts approaching an active plate margin under the SW Pacific Deep Western Boundary Current, *Paleoceanography*, *9*, 1061-1085.

Carter, L. and J, Wilkin (1999) Abyssal circulation around New Zealand – a comparison between observations and a global circulation model, *Marine Geology* 159, 221–239.

Carter, L., J. D. Cook, G. A. Foster, R. D. Garlick, N. J. Lichfield, J.S. Mitchell, and I. C. Wright (1997), New Zealand region bathymetry (3rd edition), 1:4,000,000. *NIWA Chart, Miscellaneous Series* 73.

Carter, L., R. D. Garlick, and P. Sutton (1998), Ocean Circulation New Zealand, *NIWA Chart Miscellaneous Series*, *76*.

Carter, R.M., I. N. McCave, C. Richter, and L. Carter et al., (1999), *Proceedings of the Ocean Drilling Program, Initial Reports,* 181: Ocean Drilling Program, College Station, Texas, doi:10.2973/odp.proc.ir.181.2000.

Carter, L., I. N. McCave, and M. J. M. Williams (2008), Chapter 4 Circulation and Water Masses of the Southern Ocean: A Review, in *Developments in Earth and Environmental Sciences*, Eds F. Fabio and S. Martin, pp. 85-114, Elsevier.

Carter. L., B. Manighetti, G. Ganssen, and L. Northcote (2008), Southwest Pacific modulation of abrupt climate change during the Antarctic Cold Reversal Younger Dryas, *Palaeogeography, Palaeoclimatology, Palaeoecology,* 260, 284–298.

Chiswell, S. M. (1994), Variability in sea surface temperature around New Zealand from AVHRR images, *New Zealand Journal of Marine and Freshwater Research*, *28*, 179-192.

Chiswell, S. M. (2002), Temperature and salinity mean and variability within the

subtropical front over the Chatham rise, New Zealand, *New Zealand Journal of Marine and Freshwater Research*, *36*, 281-298.

Clarke, F. W., and W. C. Wheeler (1922), The inorganic constituents of marine invertebrates, *USGS Professional Paper*, *124*, 55.

Coale, K. H (1991), Effects of iron, manganese, copper and zinc enrichments on productivity and biomass in the subarctic Pacific, *Limnology and oceanography, 36*, 1851-1864.

Cortese, G., A. Abelmann, and R. Gersonde (2004), A glacial warm water anomaly in the subantarctic Atlantic Ocean, *Earth and Planetary Science Letters, 222*, 767– 778.

Cortese, G., A. Abelmann, and R. Gersonde (2007), The last five glacial-interglacial transitions: A high-resolution 450,000-year record from the subantarctic Atlantic, *Paleoceanography, 22*, PA4203, doi:10.1029/2007PA001457.

Creech, J. B., J. A. Baker, C. J. Hollis, H. E. G. Morgans, and E. G. C. Smith (2010), Eocene sea temperatures for the mid-latitude southwest Pacific from Mg/Ca ratios in planktonic and benthic foraminifera, *Earth and Planetary Science Letters, 299*, 483-495.

Crundwell, M., G. H. Scott, T. R. Naish, and L. Carter (2008), Glacial-interglacial

ocean climate variability from planktonic foraminifera during the Mid-Pleistocene transition in the temperate Southwest Pacific, ODP Site 1123, *Palaeogeography, Palaeoclimatology, Palaeoecology*, *260*, 202-229.

Dickson, A. J., C. J. Beer, C. Dempsey, M. A. Maslin, J. A. Bendle, E. L. McClymont, and R. D. Pancost (2009), Oceanic forcing of the Marine Isotope Stage 11 interglacial, *Nature Geoscience*, *2*, 428-433.

Doney, S. C., V. J. Fabry, R. A. Feely, and J. A. Kleypas (2009), Ocean acidification: The other CO_2 problem*, Annual Reviews in Marine Science, 1*, 169-192.

Droxler, A. W., and J. W. Farrell (2000), Marine Isotope Stage 11 (MIS 11): new insights for a warm future, *Global and Planetary Change*, *24*, 1-5.

Droxler, A. W., R. B. Alley, W. R. Howard, R. Z. Poore, and L. H. Burckle (2003), Unique and exceptionally long interglacial marine isotope stage 11: window into earth warm future climate, *in Earth's Climate and Orbital Eccentricity: The Marine Isotope Stage 11 Question, Geophysical Monograph Series, 137*, 1-14.

Eggins, S., P. De Deckker, and J. Marshall (2003), Mg/Ca variation in planktonic foraminifera tests: implications for reconstructing palaeo-seawater temperature and habitat migration, *Earth and Planetary Science Letters*,

212, 291-306.

Eggins, S., A. Sadekov, and P. De Deckker (2004), Modulation and daily banding of Mg/Ca in *Orbulina universa* tests by symbiont photosynthesis and respiration: a complication for seawater thermometry?, *Earth and Planetary Science Letters*, *225*, 411-419.

Eldefield, H., and G. Ganssen (2000), Past temperature and $\delta^{18}O$ of surface ocean waters inferred from foraminiferal Mg/Ca ratios, *Nature, 405*, 442-445.

Elderfield, H., C. J. Bertram, and J. Erez (1996), A biomineralization model for the incorporation of trace elements into foraminiferal calcium carbonate, *Earth and Planetary Science Letters, 142*, 409-423.

Elderfield, H., M. Vautravers, and M. Cooper (2002), The relationship between shell size and Mg/Ca, Sr/Ca, $\delta^{18}O$, and $\delta^{13}C$ of species of planktonic foraminifera, *Geochemistry geophysics geosystems, 3*, doi: 10.1029/2001GC000194.

Elderfield, H., M. Greaves, S. Barker, I. R. Hall, A. Tripati, P. Ferretti, S. Crowhurst, L. Booth, and C. Daunt (2010), A record of bottom water temperature and seawater $\delta^{18}O$ for the Southern Ocean over the past 440 kyr based on Mg/Ca of benthic foraminiferal *Uvigerina* spp, *Quaternary Science Reviews*, *29*, 160-169.

Elmejdoub, N., and Y. Jedoui (2009), Pleistocene raised marine deposits of the Cap Bon peninsula (N-E Tunisia): Records of sea-level highstands, climatic changes and coastal uplift, *Geomorphology*, *112*, 179-189.

Emiliani, C. (1955), Pleistocene temperatures, *Journal of Geology*, *63*, 538-578.

EPICA Community Members (2004), Eight glacial cycles from an Antarctic ice core, *Nature*, *429*, 623-628.

Epstein, S., R. Buchsbaum, H. A. Lowenstam, and H. C. Urey (1953), Revised carbonate-water isotopic temperature scale, *Bulletin of the Geological Society of America*, *64*, 1315-1326.

Erez, J. (2003), The source of ions for biomineralization in foraminifera and their implications for paleoceanographic proxies, *Reviews in Mineralogy and Geochemistry*, *54*, 115-149.

Farrell, J. W., and W. L. Prell (1989), Climatic change and $CaCO_3$ preservation: An 800,000 year bathymetric reconstruction from the central equatorial Pacific Ocean, *Paleoceanography*, *4*, 447-466.

Feely, R. A., C. L. Sabine, K. Lee, F. J. Millero, M. F. Lamb, D. Greeley, J. L. Bullister, R. M. Key, T.-H. Peng, A. Kozyr, T. Ono, and C. S. Wong (2002), In situ calcium carbonate dissolution in the Pacific Ocean, *Global Biogeochemical Cycles, 16*, 1144.

Feely, R. A., C. L. Sabine, K. Lee, W. Berelson, J. Kleypas, V. J. Fabry, and F. J. Millero (2004), Impact of anthropogenic CO_2 on the $CaCO_3$ system in the oceans, *Science, 305*, 362-366, doi:10.1126/science.1097329.

Ferguson, J. E., G. M. Henderson, M. Kucera, and R. E. M. Rickaby (2008), Systematic change of foraminiferal Mg/Ca ratios across a strong salinity gradient, *Earth and Planetary Science Letters, 265*, 153-166, doi:10.1016/j.epsl.2007.10.011.

Fernandez, D (2012), Do winds control the confluence of subtropical and subantarctic surface waters east of New Zealand? MSc thesis, Victoria University of Wellington, Wellington.

Fyke, J. G., A. J. Weaver, D. Pollard, M. Eby, L. Carter, and A. Mackintosh (2011), A new coupled ice sheet/climate model: description and sensitivity to model physics under Eemian, Last Glacial Maximum, late Holocene and modern climate conditions, Geoscientific Model Development, *4*, 117-136, doi:10.5194/gmd-4-117-2011.

Greaves, M. (2008), Trace Elements in Marine Biogenic Carbonates: Analysis and Application to Past Ocean Chemistry, PhD thesis, University of Southampton, Southampton.

Greig, M. J., and A. E. Gilmour (1992), Flow through the Memoo Saddle, New Zealand, *New Zealand Journal of Marine and Freshwater Research, 26,* 155-165.

Gupta, B. K. S. (Ed.) (1999), *Systematics of Modern Foraminifera*, 7-36, Kluwer Academic Publishers, Great Britain.

Hall, I. R., I. N. McCave, N. J. Shackleton, G. P. Weedon, and S. E. Harris (2001), Intensified deep Pacific inflow and ventilation in Pleistocene glacial times, *Nature*, *412*, 809-812.

Hays, J. D., J. Imbrie, and N. J. Shackleton (1976), Variations in the Earth's orbit: pacemaker of the ice ages, *Science*, *194*, 1121-1132.

Hayward, B. W., G. H. Scott, M. P. Crundwell, J. P. Kennett, L. Carter, H. L. Neil, A. T. Sabaa, K. Wilson, J. S. Rodger, G. Schaefer, H. R. Grenfell, and Q. Li (2008), The effect of submerged plateaux on Pleistocene gyral circulation and sea-surface temperatures in the Southwest Pacific, *Global and Planetary Change*, *63*, 309-316.

Hayward, B. W., A. T. Sabaa, A. Kolodziej, M. P. Crundwell, S. Steph, G. H. Scott, H. L. Neil, H .C. Bostock, L. Carter, and H. R. Grenfell (2012), Planktic foraminifera-based sea-surface temperature record in the Tasman Sea and history of the Subtropical Front around New Zealand, over the last one million years, *Marine Micropaleontology, 82-83*, 13-27.

Hearty, P. J. (2002), The Ka'ena Highstand of O'ahu, Hawai'i: Further evidence of Antarctic ice collapse during the Middle Pleistocene, *Pacific Science*, *56*, 65-82.

Hearty, P. J., and S. L. Olson (2008), Mega-highstand or megatsunami? (Discussion of McMurtry et al. (2007), Elevated marine deposits in Bermuda record a late Quaternary megatsunami: *Sedimentary Geology, 200*(3-4), 155-165), *Sedimentary Geology*, *203*, 307-312.

Hearty, P. J., P. Kindler, H. Cheng, and R. L. Edwards (1999), A +20 m middle Pleistocene sea-level highstand (Bermuda and the Bahamas) due to partial collapse of Antarctic ice, *Geology*, *27*, 375-378.

Heath, R. (1975), Oceanic circulation and hydrology off the southern half of South Island, New Zealand, *Memoir New Zealand Oceanographic Institute, 72,* 36.

Heath, R. A. (1981), Oceanic fronts around southern New Zealand, *Deep Sea*

Research, 28A, 547-560.

Heath, R. A. (1985), A review of the physical oceanography of the seas around New Zealand - 1982, *New Zealand Journal of Marine and Freshwater Research, 19*, 79-124.

Hemleben, C., M. Spindler, I. Breitinger, and W. G. Deuser (1985), Field and laboratory studies on the ontogeny and ecology of some *Globorotaliid* species from the Sargasso Sea off Bermuda, *Journal of Foraminiferal Research, 15*, 254-272.

Henderson, C. (2006), Ocean acidification: the other CO_2 problem, *New Scientist*, *191,* 45-53.

Hill, K. L., S. R. Rintoul, K. R. Ridgway, and P. R. Oke (2011), Decadal changes in the South Pacific western boundary current system revealed in observations and ocean state estimates, *Journal of Geophysical Research Oceans, 116*, CO1009, doi:10.1029/2009JC005926.

Hillenbrand, C. D., G. Kuhn, and T. Frederichs (2009), Record of a Mid-Pleistocene depositional anomaly in West Antarctic continental margin sediments: an indicator for ice-sheet collapse?, *Quaternary Science Reviews*, *28*, 1147-1159.

Hodell, D. A., C. D. Charles, and F. J. Sierro (2001), Late Pleistocene evolution of the ocean's carbonate system, *Earth and Planetary Science Letters, 192*, 109-124.

Hodell, D. A., S. L. Kanfoush, K. A. Venz, C. D. Charles, and F. J. Sierro (2003), The Mid-BrunhersTransition in ODP Sites 1089 and 1090 (Subantarctic South Atlantic), *in Earth's Climate and Orbital Eccentricity: The Marine Isotope Stage 11 Question, Geophsical monograph series, 137*, 1-14.

Howard, W. R. (1997), Palaeoclimatology: A warm future in the past, *Nature*, *388*, 418-419.

Howard, W. R., and W. L. Prell (1992), Late Quaternary surface circulation of the Southern Indian Ocean and its relationship to orbital variations, *Paleoceanography*, *7*, 79-117.

Huybers, P. (2007), Glacial variability over the last two million years: an extended depth-derived age model, continuous obliquity pacing, and the Pleistocene progression, *Quaternary Science Reviews*, *26*, 37-55.

Huybers, P., and C. Wunsch (2005), Obliquity pacing of the late Pleistocene glacial terminations, *Nature*, *434*, 491-494.

Huybrechts, P. (1993), Glaciological Modelling of the Late Cenozoic East Antarctic Ice Sheet: Stability or Dynamism? *Geografiska Annaler. Series A, Physical Geography*, *75*, 221-238

Imbrie, J. and J. Z. Imbrie (1980), Modeling the climatic response to orbital variations, *Science, 207*, 943-953.

Imbrie, J., A. Berger, E. A. Boyle, S. C. Clemens, A. Duffy, W. R. Howard, G. Kukla, J. Kutzbach, D. G. Martinson, A. McIntyre, A. C. Mix, B. Molfino, J. J. Morley, L.C. Peterson, N.G. Pisias, W. L. Prell, M. E. Raymo, N. J. Shackleton, and J. R. Toggweiler (1993), On the structure and origin of major glaciation cycles 2. The 100,000-year cycle, *Paleoceanography*, *8*, 699-735.

Jouzel, J., V. Masson-Delmotte, O. Cattani, G. Dreyfus, S. Falourd, G. Hoffmann, B. Minster, J. Nouet, J. M. Barnola, J. Chappellaz, H. Fischer, J. C. Gallet, S. Johnsen, M. Leuenberger, L. Loulergue, D. Luethi, H. Oerter, F. Parrenin, G. Raisbeck, D. Raynaud, A. Schilt, J. Schwander, E. Selmo, R. Souchez, R. Spahni, B. Stauffer, J. P. Steffensen, B. Stenni, T. F. Stocker, J. L. Tison, M. Werner, and E.W. Wolff (2007), Orbital and millennial Antarctic climate variability over the past 800,000 Years, *Science*, *317*, 793-796.

Kindler, P., and P. J. Hearty (2000), Elevated marine terraces from Eleuthera (Bahamas) and Bermuda: sedimentological, petrographic and

geochronological evidence for important deglaciation events during the middle Pleistocene, *Global and Planetary Change*, *24*, 41-58.

Kolodziej, A. P. (2010), Planktic Foraminifera-based Sea Surface Temperature Estimates and Late Quaternary Oceanography off New Zealand's West Coast, MSc thesis, Victoria University of Wellington, Wellington.

Kowalski, E. A, and P. A. Meyers (1997), Glacial-interglacial variations in Quaternary production of marine organic matter at DSDP Site 594, Chatham Rise, southeastern New Zealand margin, *Marine Geology, 140*, 249-263.

Kozden, R., T. Ushikubo, N. T. Kita, M. Spicuzza, and J. W. Valley (2009), Intratest oxygen isotope variability in the planktonic foraminifer N. pachyderma: Real vs. apparent vital effects by ion microprobe, *Chemical Geology, 258*, 327-337, doi:10.1016/j.chemgeo.2008.10.032.

Kroopnick, P. M. (1985), The distribution of ^{13}C of ΣCO_2 in the world oceans, *Deep Sea Research Part A. Oceanographic Research Papers*, *32*, 57-84.

Kunz-Pirrung, M., R. Gersonde, and D. A. Hodell (2002), Mid-Brunhes century-scale diatom sea surface temperature and sea ice records from the Atlantic sector of the Southern Ocean (ODP Leg 177, Sites 1093, 1094 and core PS2089-2), *Palaeogeography Palaeoclimatology Palaeoecology, 182*, 305–328.

Lea, D. W. (2003), Elemental and isotopic proxies of past ocean temperatures, *Treatise on Geochemistry,* 365-390, Elsevier.

Lea D. W., T. A. Mashiotta, and H. J. Spero (1999), Controls on magnesium and strontium uptake in planktonic foraminifera determined by live culturing, *Geochimica et Cosmochimica Acta, 63*, 2369–2379.

Lea, D. W., D. K. Pak, and H. J. Spero (2000), Climate impact of Late Quaternary equatorial Pacific sea surface temperature variations, *Science*, *289*, 1719-1724.

Lean, C. M. B., and I. M. McCave (1998), Glacial to interglacial mineral magnetic and palaeoceanographic changes at Chatham Rise, SW Pacific Ocean, *Earth and Planetary Science Letters, 163*, 247–260.

Lear, C. H., H. Elderfield, and P. A. Wilson (2000), Cenozoic deep-sea temperatures and global ice volumes from Mg/Ca in benthic foraminiferal calcite, *Science*, *287*, 269-272.

Levitus, S., J. I. Antonov, J. Wang, T. L. Delworth, K. W. Dixon, and A. J. Broccoli (2001), Anthropogenic warming of Earth's climate system, *Science*, *292*, 267-270.

Lisiecki, L. E., and M. E. Raymo (2005), A Pliocene-Pleistocene stack of 57 globally distributed benthic $\delta^{18}O$ records, *Paleoceanography*, *20*, PA1003.

Locarnini, R. A., A. V. Mishonov, J. I. Antonov, T. P. Boyer, and H. E. Garcia (2006), *World Ocean Atlas 2005, Volume 1: Temperature*, U.S. Government Printing Office, Washington, D.C.

Lohmann, G. P. (1995), A model for variation in the chemistry of planktonic foraminifera due to secondary calcification and selective dissolution, *Paleoceanography, 10*, 445-457.

Loulergue, L., A. Schilt, R. Spahni, V. Masson-Delmotte, T. Blunier, B. Lemieux, J.-M. Barnola, D. Raynaud, T. F. Stocker, and J. Chappellaz (2008), Orbital and millennial-scale features of atmospheric CH_4 over the past 800,000 years, *Nature*, *453*, 383-386.

Loutre, M. F. (2003), Clues from MIS 11 to predict the future climate - a modelling point of view, *Earth and Planetary Science Letters*, *212*, 213-224.

Loutre, M. F., and A. Berger (2003), Marine Isotope Stage 11 as an analogue for the present interglacial, *Global and Planetary Change*, *36*, 209-217.

Lüer, V., C. J. Hollis, and H. Willems (2008), Late Quaternary radiolarian assemblages as indicators of paleoceaonographic changes north of the subtropical front, offshore eastern New Zealand, southwest Pacific, *Micropaleonotology*, *54*, 49-70.

Mackay, A. W., E. Karabanov, M. J. Leng, H. J. Sloane, D. W. Morley, V. N. Panizzo, G. Khursevich, and D. Williams (2008), Reconstructing hydrological variability in Lake Baikal during MIS 11: An application of oxygen isotope analysis of diatom silica, *Journal of Quaternary Science*, *23*, 365-374.

Mackensen, A., M. Rudolph, and G. Kuhn (2001), Late Pleistocene deep-water circulation in the subantarctic eastern Atlantic, *Global and Planetary Change, 30*, 197-229.

Malmgren, B. A. (1983), Ranking of dissolution susceptibility of planktonic foraminifera at high latitudes of the South Atlantic Ocean, *Marine Micropaleontology, 8*, 183-191.

Marr, J. (2009), Ecological, oceanographic and temperature controls on the incorporation of trace elements into *Globigerina bulloides* and *Globoconella inflata* in the Southwest Pacific Ocean, MSc thesis, Victoria University of Wellington, Wellington.

Marr, J. P., J. A. Baker, L. Carter, A. S. R. Allan, G. B. Dunbar, and H. C. Bostock (2011), Ecological and temperature controls on Mg/Ca ratios of *Globigerina bulloides* from the southwest Pacific Ocean, *Paleoceanography*, *26*, PA2209.

Martin, W.R., and F. L. Sayles (1996), $CaCO_3$ dissolution in sediments of the Ceara Rise and western equatorial Atlantic, *Geochimica et Cosmochimica Acta, 60*, 233–263.

Martinez, J. I. R. (1993), Late Pleistocene Paleoceanography of the Tasman Sea, Australian National University.

Mashiotta, T. A., D. W. Lea, and H. J. Spero (1999), Glacial-interglacial changes in Subantarctic sea surface temperature and $\delta^{18}O$-water using foraminiferal Mg, *Earth and Planetary Science Letters*, *170*, 417-432.

Maslin, M. A., and A. J. Ridgwell (2005), Mid-Pleistocene revolution and the 'eccentricity myth', *Geological Society, London, Special Publication*, *247*, 19-34.

Masson-Delmotte, V., G. Dreyfus, P. Braconnot, S. Johnsen, J. Jouzel, M. Kageyama, A. Landais, M. F. Loutre, J. Nouet, F. Parrenin, D. Raynaud, B. Stenni, and E.

Tuenter (2006), Past temperature reconstructions from deep ice cores: relevance for future climate change, *Climate of the Past*, *2*, 145-165.

McCave, I. N., and L. Carter (1997), Recent sedimentation beneath the Deep Western Boundary Current off northern New Zealand, *Deep Sea Research Part I: Oceanographic Research Papers*, *44*, 1203-1237.

McCave, I. N., L. Carter, and I. R. Hall (2008), Glacial-interglacial changes in water mass structure and flow in the SW Pacific Ocean, *Quaternary Science Reviews*, *27*, 1886-1908.

McManus, J., and C. Tzedakis (2006), Global climate during marine isotope stage 11 (MIS 11), *Pages News: Past Global Changes*, *14*, 42-43.

McManus, J. F., D. W. Oppo, and J. L. Cullen (1999), A 0.5-million-year record of millennial-scale climate variability in the North Atlantic, *Science*, *283*, 971-975.

McManus, J., D. W. Oppo, J. J. Cullen, and S. Healy (2003), Marine Isotope Stage 11 (MIS 11): Analog for Holocene and Future Climate?, *in Earth's Climate and Orbital Eccentricity: The Marine Isotope Stage 11 Question, Geophysical monograph series, 137*, 1-14.

McMurtry, G.M., D. R. Tappin, P. N. Sedwick, I. Wilkinson, J. Fietzke, and B, Sellwood (2008), Reply to ‘‘Mega-highstand or megatsunami? (Discussion of McMurtry et al. (2007), Elevated marine deposits in Bermuda record a late Quaternary megatsunami, *Sedimentary Geology, 200*, 155–165) *Sedimentary Geology, 203*, 313–319. doi:10.1016/j.sedgeo.2007.11.008.

Miller, G. H., J. Brigham-Grette, R. B. Alley, L. Anderson, H. A. Bauch, M. S. V. Douglas, M. E. Edwards, S. A. Elias, B. P. Finney, J. J. Fitzpatrick, S. V. Funder, T. D. Herbert, L. D. Hinzman, D. S. Kaufman, G. M. MacDonald, L. Polyak, A. Robock, M. C. Serreze, J. P. Smol, R. Spielhagen, J. W. C. White, A. P. Wolfe, and E.W. Wolff (2010), Temperature and precipitation history of the Arctic, *Quaternary Science Reviews*, *29*, 1679-1715.

Mix, A. C., N. G. Pisas, W. Rugh, J. Wilson, A. Morley, and T. K. Hagelberg (1995), *Proceedings Ocean Drilling Program, Scientific results, 138*, Ocean Drilling Program, College Station, Texas, doi:10.2973/odp.proc.sr.138.120.1995.

Mix, A. C., D. C. Lund, N. G. Pisias, P. Bode´n, L. Bornmalm, M. Lyle, and J. Pike (1999), Rapid climate oscillations in the Northeast Pacific during the last deglaciation reflect Northern and Southern Hemisphere sources, *in Mechanisms of Global Climate Change at Millennial Time Scales, Geophysical Monograph Series, 112*, 127 – 148

Montaggioni, N., G. Cabioch, N. Thouveny, N. Frank, T. Sato, and A.-M. Semah (2011), Revisiting the Quaternary development history of the western New Caledonian shelf system: From ramp to barrier reef, *Marine Geology, 280*, 57-75.

Morris, M., B. R. Stanton, and H. L. Neil (2001), Subantarctic oceanography around New Zealand: preliminary results from an ongoing survey, *New Zealand Journal of Marine and Freshwater Research,* 35, 499-519.

Mortimer, N. (2004), New Zealand's geological foundations, *Gondwana Research*, *7*, 261-272.

Mortyn, P. G., and C. D. Charles (2003), Planktonic foraminiferal depth habitat and $\delta^{18}O$ calibrations: Plankton tow results from the Atlantic sector of the Southern Ocean, *Paleoceanography*, *18*, 1037.

Murphy, R. J., M. H. Pinkerton, K. M. Richardson, J. M. Bradford-Grieve, and P. W. Boyd (2001), Phytoplankton distributions around New Zealand derived from SeaWiFS remotely-sensed ocean colour data, *New Zealand Journal of Marine and Freshwater Research*, *35*, 343-362.

Naish, T., R. Powell, R. Levy, G. Wilson, R. Scherer, F. Talarico, L. Krissek, F. Niessen, M. Pompilio, T. Wilson, L. Carter, R. DeConto, P. Huybers, R. McKay, D.

Pollard, J. Ross, D. Winter, P. Barrett, G. Browne, R. Cody, E. Cowan, J. Crampton, G. Dunbar, N. Dunbar, F. Florindo, C. Gebhardt, I. Graham, M. Hannah, D. Hansaraj, D. Harwood, D. Helling, S. Henrys, L. Hinnov, G. Kuhn, P. Kyle, A. Läufer, P. Maffioli, D. Magens, K. Mandernack, W. McIntosh, C. Millan, R. Morin, C. Ohneiser, T. Paulsen, D. Persico, I. Raine, J. Reed, C. Riesselman, L. Sagnotti, D. Schmitt, C. Sjunneskog, P. Strong, M. Taviani, S. Vogel, T. Wilch, and T. Williams (2009), Obliquity-paced Pliocene West Antarctic ice sheet oscillations, *Nature*, *458*, 322–328, doi:10.1038/nature07867.

Neil, H. L., L. Carter, and M. Y. Morris (2004), Thermal isolation of Campbell Plateau, New Zealand, by the Antarctic Circumpolar Current over the past 130 kyr, *Paleoceanography, 19*, PA4008, doi:10.1029/2003PA000975.

Nelson, C. S., P. J. Cooke, C. H. Hendy, and A. M. Cuthbertson (1993), Oceanographic and climatic changes over the past 160,000 years at Deep Sea Drilling Project Site 594 off southeastern New Zealand, Southwest Pacific Ocean, *Paleoceanography*, *8*, 435 - 458.

Nelson, C. S., I. L. Hendy, H. L. Neil, C. H. Hendy, and P. P. E. Weaver (2000), Last glacial jetting of cold waters through the Subtropical Convergence zone in the Southwest Pacific off eastern New Zealand, and some geological implications, *Palaeogeography, Palaeoclimatology, Palaeoecology*, *156*,

103-121.

Norris, R. J., and A. F. Cooper (2000), Late Quaternary slip rates and slip partitioning on the Alpine Fault, New Zealand, *Journal of Structural Geology, 23*, 507-520.

Nürnberg, D., J. Bijma, and C. Hemleben (1996), Assessing the reliability of magnesium in foraminiferal calcite as a proxy for water mass temperatures, *Geochimica et Cosmochimica Acta*, *60*, 803-814.

Oke, P. R., and M. H. England (2004), Oceanic response to changes in the latitude of the southern hemisphere subpolar westerly winds, *Journal of Climate*, *17*, 1040–1054.

Olson, S. L., and P. J. Hearty (2009), A sustained +21 m sea-level highstand during MIS 11 (400 ka): direct fossil and sedimentary evidence from Bermuda, *Quaternary Science Reviews*, *28*, 271-285.

Orpin, A., L. Carter, A. Goh, E. Mackay, A. Palletin, A. L. Verder, S. Shiswell, and P. Sutton (2008), New Zealand's diverse seafloor sediments, *NIWA Chart Miscellaneous Series* 86.

Orr, J. C., V. J. Fabry, O. Aumont, L. Bopp, S. C. Doney, R. A. Feely, A. Gnanadesikan, N. Gruber, A. Ishida, F. Joos, R. M. Key, K. Lindsay, E. Maier-Reimer, R. Matear, P. Monfray, A. Mouchet, R. G. Najjar, G. -K. Plattner, K. B. Rodgers, C. L. Sabine, J. L. Sarmiento, R. Schlitzer, R. D. Slater, I. J. Totterdell, M. –F. Weirig, Y. Yamanaka, and A. Yool (2005), Anthropogenic ocean acidification over the twenty-first century and its impact on calcifying organisms, *Nature, 437*, 681-686.

Orsi, A. H., T. Whitworth, and W. D. Nowlin (1995), On the meridional extent and fronts of the Antarctic Circumpolar Current, *Deep Sea Research I: Oceanographic Research Papers, 42*, 641-673.

Pahnke, K., and R. Zahn (2005), Southern hemisphere water mass conversion linked with North Atlantic climate variability, *Science, 307*, 1741–1746.

Pearce N. J. G., Perkins W. T., Westgate J. A., Gorton M. P., Jackson S. E., Neal C. R. and Chenery S. P. (1997) A compilation of new and published major and trace element data for NIST SRM 610 and NIST SRM 612 glass reference materials, *Geostandards Newsletter: The Journal of Geostandards and Geoanalysis, 21,* 115–144.

Pearson, P. N., P. W. Ditchfield, J. Singano, K. G. Harcourt-Brown, C. J. Nicholas, R. K. Olsson, N. J. Shackleton, and M. A. Hall (2001), Warm tropical sea surface

temperatures in the Late Cretaceous and Eocene epochs, *Nature*, *413*, 481-487.

Pollard, D., and R. M. DeConto (2009), Modelling West Antarctic ice sheet growth and collapse through the past five million years, *Nature*, *458*, 329-332.

Poore, R. Z., and Dowsett, H. J. (2001). Pleistocene reduction of polar ice caps: Evidence from Cariaco Basin marine sediments, *Geology, 29*(1), 71-74.

Prebble, J. (submitted), Terrestrial and ocean response to a pleistocene warm interglacial as revealed by pollen and dinoflagellates from marine sediment cores, South Island, New Zealand. PhD thesis, Victoria University of Wellington, Wellington

Preece, R. C., S. A. Parfitt, D. R. Bridgland, S. G. Lewis, P. J. Rowe, T. C. Atkinson, I. Candy, N. C. Debenham, K. E. H. Penkman, E. J. Rhodes, J. -L. Schwenninger, H. I. Griffiths, J. E. Whittaker, and C. Gleed-Owen (2007), Terrestrial environments during MIS 11: evidence from the palaeolithic site at West Stow, Suffolk, UK, *Quaternary Science Reviews*, *26*, 1236-1300.

Prokopenko, A. A., E. V. Bezrukova, G. K. Khursevich, E. P. Solotchina, M. I. Kuzmin, and P. E. Tarasov (2010), Climate in continental interior Asia during the longest interglacial of the past 500 000 years: the new MIS 11 records from

Lake Baikal, SE Siberia, *Climate of the Past*, *6*, 31-48.

Purkey, S. G., and G. C. Johnson (2010), Warming of global abyssal and deep southern ocean waters between the 1990s and 2000s: Contributions to global heat and sea level rise budgets, *Journal of Climate, 23*, 6336–6351.

Raymo, M. E., and P. Huybers (2008), Unlocking the mysteries of the ice ages, *Nature*, *451*, 284-285.

Raymo, M. E., and J. X. Mitrovica (2012), Collapse of polar ice sheets during the stage 11 interglacial, *Nature, 438*, 453, doi:10.1038/nature10891.

Raymo, M. E., D. W. Oppo, and W. Curry (1997), The mid-Pleistocene climate transition: A deep sea carbon isotopic perspective, *Paleoceanography, 12*, 546 - 559.

Regenberg, M., D. Nürnberg, S. Steph, J. Groeneveld, D. Garbe-Schönberg, R. Tiedemann, and W.-C. Dullo (2006), Assessing the effect of dissolution on planktonic foraminiferal Mg/Ca ratios: Evidence from Caribbean core tops, *Geochemistry Geophysics Geosystems*, *7*, Q07P15, doi:10.1029/2005GC001019.

Rickaby, R. E. M., E. Bard, C. Sonzogni, F. Rostek, L. Beaufort, S. Barker, G. Rees, and D.P. Schrag, (2007), Coccolith chemistry reveals secular variations in the global carbon cycle?, *Earth and Planetary Science Letters, 253*, 83-93, doi:10.1016/j.epsl.2006.10.016.

Ridgway, K. R. (2007), Long-term trend and decadal variability of the southward penetration of the East Australian Current, *Geophysical Research Letters, 34*, L13613, doi:10.1029/2007GL030393.

Ridgway, K. R. and Dunn, J. (2007), Observational evidence for a Southern Hemisphere oceanic supergyre. *Geophysical Research Letters, 34*, L13612, doi:10.1029/2007GL030392.

Roemmich, D., J. Gilson, R. Davis, P. Sutton, S. Wijffels, and S. Riser (2007), Decadal spinup of the South Pacific subtropical gyre, *Journal of Physical Oceanography, 32*, 162-173.

Rohling, E. J., K. Grant, M. Bolshaw, A. P. Roberts, M. Siddall, Ch. Hemleben, and M. Kucera (2009), Antarctic temperature and global sea level closely coupled over the past five glacial cycles, *Nature Geoscience, 2*, 500–504, doi:10.1038/NGEO557.

Rohling, E. J., K. Braun, K. Grant, M. Kucera, A. P. Roberts, M. Siddall, and G. Trommer (2010), Comparison between Holocene and Marine Isotope

Stage-11 sea-level histories, *Earth and Planetary Science Letters*, *291*, 97-105.

Rohling, E. J., M. Medine-Elizalde, J. G. Shepherd, M. Siddal, and J. D. Stanford (2012) Sea surface and high-latitude temperature sensitivity to radiative forcing of climate over several glacial cycles, *Journal of Climate, 25*, 1635-1656.

Rosenthal, Y. (2007), Elemental proxies for reconstructing Cenozic seawater paleotemperatures, in *Proxies in Late Cenozoic Paleoceanography, Elsevier Science, United States,* 765-793,

Rosenthal, Y., and G. P. Lohmann (2002), Accurate estimation of sea surface temperatures using dissolution-corrected calibrations for Mg/Ca paleothermometry, *Paleoceanography*, *17*, 1044.

Rosenthal, Y., E. Boyle, and N. Slowey (1997), Temperature control on the incorporation of magnesium, strontium, fluorine, and cadmium into benthic foraminiferal shells from Little Bahama Bank: Prospects for thermocline paleoceanography, *Geochimica et Cosmochimica Acta*, *61*, 3633-3643.

Rosenthal, Y., G. P. Lohmann, K. C. Lohmann, and R. M. Sherrell (2000), Incorporation and preservation of Mg in *Globigerinoides sacculifer*: Implications for reconstructing the temperature and $^{18}O/^{16}O$ of seawater,

Paleoceanography, *15*, 135-145.

Rousseau, D. D. (2003), The Continental Record of Stage 11: A Review, *in Earth's Climate and Orbital Eccentricity: The Marine Isotope Stage 11 Question, Geophysical Monograph Series, 137*, 1-14.

Ruddiman, W. F. (2005), Cold climate during the closest stage 11 analog to recent millennia, *Quaternary Science Reviews*, *24*, 1111-1121.

Russell, A. D., B. Hönisch, H. J. Spero, and D. W. Lea (2004), Effects of seawater carbonate ion concentration and temperature on shell U, Mg, and Sr in cultured planktonic foraminifera, *Geochimica et Cosmochimica Acta*, *68*, 4347-4361.

Sadekov, A. Y. (2008), Advancing planktonic foraminifera Mg/Ca thermometry: a microanalytical perspective, PhD thesis, Australian National University, Canberra.

Sadekov, A. Y., S. M. Eggins, P. De Deckker, and D. Kroon (2008), Uncertainties in seawater thermometry deriving from intratest and intertest Mg/Ca variability in *Globigerinoides ruber*, *Paleoceanography, 23,* PA1215, doi:10.1029/2007PA001452.

Sadekov, A., S. M. Eggins, P. De Deckker, U. Ninnemann, W. Kuhnt, and F. Bassinot (2009), Surface and subsurface seawater temperature reconstruction using Mg/Ca microanalysis of planktonic foraminifera *Globigerinoides ruber*, *Globigerinoides sacculifer*, and *Pulleniatina obliquiloculata*, *Paleoceanography*, *24*, PA3201, doi:3210.1029/2008PA001664.

Sadekov, A., S. M. Eggins, G. P. Klinkhammer, and Y. Rosenthal (2010), Effects of seafloor and laboratory dissolution on the Mg/Ca composition of *Globigeriniodes sacculifer* and *Orbulina universa* tests – a laser ablation ICPMS microanalysis perspective, *Earth and Planetary Science Letters, 292*, 312-324, doi:10.1016/j.epsl.2010.01.039.

Schaefer, G., J. S. Rodger, B. W. Hayward, J. P. Kennett, A. T. Sabaa, and G. H. Scott (2005), Planktic foraminiferal and sea surface temperature record during the last 1 Myr across the Subtropical Front, Southwest Pacific, *Marine Micropaleontology*, *54*, 191-212.

Scherer, R. (2003), Quaternary interglacials and the West Antarctic Ice Sheet, *in Earth'sClimate and Orbital Eccentricity: The Marine Isotope Stage 11 Question, Geophysical Monograph Series, 137*, 1-14.

Schlitzer, R. (2002), Ocean Data View, http://www.awi-bremerhaven.de/GEO/ODV,

edited.

Scott, G. H., L. Carter, and G. Cortese (submitted), Interpretation of precession-related warm excursions in the southern hemisphere during MIS 10-11, *Earth and Planetary Science letters*.

Segev, E., and J. Erez (2006), Effect of Mg/Ca ratio in seawater on shell composition in shallow benthic foraminifera, *Geochemistry Geophysics Geosystems*, *7*, Q02P09, doi:10.1029/2005GC000969.

Sexton, P. F., P. A. Wilson, and P. N. Pearson (2006), Microstructural and geochemical perspectives on planktic foraminiferal preservation: Glassy versus frosty, *Geochemistry Geophysics Geosystems*, *7*, Q12P19.

Shackleton, N. J. (1987), Oxygen isotopes, ice volume and sea level, *Quaternary Science Reviews*, *6*, 183-190.

Shaw, A. G. P., and R. Vennell (2000), Variability of water masses through the Mernoo Saddle, South Island, New Zealand, *New Zealand Journal of Marine and Freshwater Research, 34,* 103-116.

Siegenthaler, U., T. F. Stocker, E. Monnin, D. Lüthi, J. Schwander, B. Stauffer, D. Raynaud, J-M. Barnola, H. Fischer, V. Masson-Delmotte, and J. Jouzel (2005),

Stable carbon cycle–climate relationship during the Late Pleistocene, *Science*, *310*, 1313-1317.

Sikes, E. L., W. R. Howard, C. R. Samson, T. S. Mahan, L. G. Robertson, and J. K. Volkman (2009), Southern Ocean seasonal temperature and Subtropical Front movement on the South Tasman Rise in the Late Quaternary, *Paleoceanography*, *24*, PA2201, doi:10.1029/2008PA001659.

Spero, H. J. (1992), Do planktic foraminifera accurately record shifts in the carbon isotopic composition of seawater ΣCO_2?, *Marine Micropaleontology*, *19*, 275-285.

Spero, H. J., J. Bijma, D. W. Lea, and B. E. Bemis (1997), Effect of seawater carbonate concentration on foraminiferal carbon and oxygen isotopes, *Nature, 390*, 497–500.

Stanton-Frazee, C., D. A. Warnke, K. Venz, and D. A. Hodell (1999), The stage 11 problem as seen at the ODP site 982 *in Marine oxygen isotope stage 11 and associated terrestrial records, Workshop report: U.S. Geological Survey Open File Report 99-312*, 75.

Steig, E. J., and A. P. Wolfe (2008), Sprucing up Greenland, *Science, 320*, 1595, doi: 10.1126/science.1160004.

Stephenson, A. E., J. J. DeYoreo, L. Wu, K. J. Wu, J. Hoyer, and P. M. Dove (2008), Peptides enhance magnesium signature in calcite: Insights into origins of vital effects, *Science*, *322*, 724-727.

Sugden, D. E., D. R. Marchant, and G. H. Denton (1993), The Case for a Stable East Antarctic Ice Sheet: The Background, *Geografiska Annaler. Series A, Physical Geography*, 75, 151-154.

Sunda, W. G., S. A. Huntsman, and G. R. Harvey (1983), Photoreduction of manganese oxides in seawater and its geochemical and biological implications, *Nature,* 301, 234–236.

Sutherland, R. (1999), Basement geology and tectonic development of the greater New Zealand region: an interpretation from regional magnetic data, *Tectonophysics*, *308*, 341-362.

Toggweiler, J. R., and J. Russell (2008), Ocean circulation in a warming climate, *Nature*, *451*, 286-288.

Turley, C. (2005), The other CO2 problem, *openDemocracy,* http://www.acamedia.info/sciences/sciliterature/globalw/reference/carol turley.html

Tzedakis, P. C. (2010), The MIS 11-MIS 1 analogy, southern European vegetation, atmospheric methane and the 'early anthropogenic hypothesis', *Climate of the Past*, *6*, 131-144.

Urey, H. C. (1947), The thermodynamic properties of isotopic substances, *Journal of the Chemical Society (Resumed),* 562-581, doi**:** 10.1039/JR9470000562.

de Vernal, A., and C. Hillaire-Marcel (2008), Natural variability of Greenland climate, vegetation, and ice volume during the past million years, *Science*, *320*, 1622-1625.

de Villiers, S. (2005), Foraminiferal shell-weight evidence for sedimentary calcite dissolution above the lysocline, *Deep Sea Research Part I, 52*, 671–680, doi:10.1016/j.dsr.2004.11.014.

Warren, B. A. (1973), Transpacific hydrographic sections at lats. 43°S and 28°S: the SCORPIO expedition - II. deep water, *Deep Sea Research and Oceanographic Abstracts*, *20*, 9-38.

Weaver, P., L. Carter, and H. Neil (1998), Response of surface water masses and circulation to Late Quaternary climate change east of New Zealand, *Paleoceanography*, *13*, 70-83.

Willerslev, E., E. Cappellini, W. Boomsma, R. Nielsen, M. B. Hebsgaard, T. B. Brand, M. Hofreiter, M. Bunce, H. N. Poinar, D. Dahl-Jensen, S. Johnsen, J. P. Steffensen, O. Bennike, J-L. Schwenninger, R. Nathan, S. Armitage, C-J. de Hoog, V. Alfimov, M. Christl, J. Beer, R. Muscheler, J. Barker, M. Sharp, K. E. H. Penkman, J. Haile, P. Taberlet, M. Thomas, P. Gilbert, A. Casoli, E. Campani, and M. J. Collins (2007), Ancient biomolecules from deep ice cores reveal a forested southern Greenland, *Science*, *317*, 111-114.

Wilke, I., H. Meggers, and T. Bickert (2009), Depth habitats and seasonal distributions of recent planktic foraminifers in the Canary Islands region (29°N) based on oxygen isotopes, *Deep Sea Research Part I: Oceanographic Research Papers, 56*, 89-106.

Wu, N., X. Chen, D. D. Rousseau, F. Li, Y. Pei, and B. Wu (2007), Climatic conditions recorded by terrestrial mollusc assemblages in the chinese loess plateau during marine oxygen isotope stages 12-10, *Quaternary Science Reviews*, *26*, 1884-1896.

Zachos, J., M. Pagani, L. Sloan, E. Thomas, and K. Billups (2001), Trends, rhythms, and aberrations in global climate 65 Ma to present, *Science*, *292*, 686-693.

Zachos, J., G. R. Dickens, and R. E. Zeebee (2008), An early Cenozoic perspective on greenhouse warming and carbon-cycle dynamics, *Nature, 451*, 279-283, doi:10.1038/nature06588.

Zazo, C., J. L. Goy, C. J. Dabrio, T. Bardají, C. Hillaire-Marcel, B. Ghaleb, J. Á. González-Delgado, and V. Soler (2003), Pleistocene raised marine terraces of the Spanish Mediterranean and Atlantic Coasts: Records of coastal uplift, sea-level highstands and climate changes, *Marine Geology*, *194*, 103-133.

Zeigler, K. E., J. P. Schwartz, A. W. Droxler, M. C. Shearer, and L. Peterson (2003), Caribbean carbonate crash in Pedro Channel at subthermoclinal depth during marine isotope stage 11: A case of basin-to-shelf carbonate fractionation?, *in Earth's Climate and Orbital Eccentricity: The Marine Isotope Stage 11 Question, Geophysical Monograph Series 137*, 1-14.

Zhong, S., and A. Mucci (1989), Calcite and aragonite precipatation from seawater solutions of various salinities: Precipatation rates and overgrowth compositions, *Chemical Geology*, *78*, 283-299.

Zuddas, P., and A. Mucci (1998), Kinetics of calcite precipation from seawater: II. The influence of ionic strength, *Geochimica et Cosmochimica Acta*, *62*, 757-766, doi.org/10.1016/S0016-7037(98)00026-X.